Distribution Agreement

In presenting this thesis or dissertation as a partial fulfillment of the requirements for an advanced degree from Emory University, I hereby grant to Emory University and its agents the non-exclusive license to archive, make accessible, and display my thesis or dissertation in whole or in part in all forms of media, now or hereafter known, including display on the world wide web. I understand that I may select some access restrictions as part of the online submission of this thesis or dissertation. I retain all ownership rights to the copyright of the thesis or dissertation. I also retain the right to use in future works (such as articles or books) all or part of this thesis or dissertation.

Signature:

_____ _____

Morgan Bair Vaughn Date

Enzyme Dynamics Elucidated via Temperature Jump Fluorescence Spectroscopy

By

Morgan Bair Vaughn
Doctor of Philosophy

Chemistry

Brian Dyer
Advisor

Vincent Conticello
Committee Member

Stefan Lutz
Committee Member

Accepted:

Lisa A. Tedesco, Ph.D.
Dean of the James T. Laney School of Graduate Studies

Date

Enzyme Dynamics Elucidated via Temperature Jump Fluorescence Spectroscopy

By

Morgan Bair Vaughn
B.S., Berry College, 2013

Advisor: Brian Dyer, Ph.D.

An abstract of
A dissertation submitted to the Faculty of the
James T. Laney School of Graduate Studies of Emory University
in partial fulfillment of the requirements for the degree of
Doctor of Philosophy
in Chemistry
2018

Abstract

Enzyme Dynamics Elucidated via Temperature Jump Fluorescence Spectroscopy

By Morgan Bair Vaughn

Enzymes are nature's catalyst. They drastically increase rates of reactions that are necessary for all living organisms. In order to take full advantage of the potential of enzymes to solve medical, environmental, and industrial challenges, we must fully understand how they function. Enzymes are dynamic molecules that move and change conformations, yet many models used to manipulate and predict enzymes treat them as static structures. We must identify motions across all timescales and determine their function so that enzyme dynamics can be incorporated into our models. The microsecond time regime is traditionally difficult to access and thus, has not been well studied. Laser-induced temperature jump fluorescence spectroscopy can measure events occurring on the tens of nanoseconds out to several milliseconds, encompassing the entirety of the microsecond time regime. Herein, we focus on enzyme dynamics on the microsecond timescale such as loop motions and collective motions that impact the search for reactive conformations. We use temperature jump fluorescence spectroscopy to elucidate the dynamics of two enzyme systems: *Escherichia coli* dihydrofolate reductase and *Bacillus stearothermophilus* alcohol dehydrogenase. With dihydrofolate reductase we examined both global and local motions in addition to measuring the transition rates of an important active site loop. With alcohol dehydrogenase we discovered collective motions that are responsible for anomalous temperature dependent behavior. Together, these studies provide a better understanding of enzyme dynamics as well as a framework for future investigations.

Enzyme Dynamics Elucidated via Temperature Jump Fluorescence Spectroscopy

By

Morgan Bair Vaughn
B.S., Berry College, 2013

Advisor: Brian Dyer, Ph.D.

A dissertation submitted to the Faculty of the
James T. Laney School of Graduate Studies of Emory University
in partial fulfillment of the requirements for the degree of
Doctor of Philosophy
in Chemistry
2018

Acknowledgements

To Brian Dyer for guiding me and helping me grow as a scientist.

To my lab-mates, especially Michael Reddish, Erin Schuler, and Brooke Andrews, for commiserating over failed experiments, celebrating beautiful data, and sharing good conversations.

To my husband, Tyler Vaughn, for supporting me throughout this entire process.

Thank you.

Table of Contents

List of Figures and Tables

Chapter 1:

An Introduction to Enzyme Dynamics and Temperature Jump Spectroscopy

Morgan Bair Vaughn

1.1 Enzyme Dynamics and Function

Enzymes are a class of proteins that catalyze reactions. Impressively, reactions that occur independently over days or even years can occur multiple times per second with the help of enzymes.[1] The accelerated rate is crucial for nearly all processes that sustain life. Because of their biological importance, enzymes are often implicated in disease states, making them suitable pharmaceutical targets.[2] In fact, metanalysis of current drugs on the market estimate that 29-50% of them are enzyme inhibitors.[3] One challenge that persists in treating patients is the rise of drug resistant bacterial infections, cancers, and other diseases.[4-5] Society is in need of new pharmaceuticals to circumvent resistance. However, traditional methods for drug development rely heavily on screening large libraries either experimentally or through docking studies and are inefficient, costly, slow, and sometimes ineffective.[6-8] The inability to rationally design drugs is due to our incomplete understanding of how enzymes function.

A general model for how enzymes increase reaction rates comes from transition state theory, in which the enzyme lowers the activation barrier for a given reaction. **Figure 1. 1** is a potential energy diagram showing the reaction coordinate with and without an enzyme catalyst. Several mechanisms for reducing the activation barrier have been postulated. One idea is that enzymes bind tightly to the transition state. Similarly, the transition state can be stabilized by electrostatic interactions within the enzyme active site. In both of these cases, the energy of the transition state is lowered. A third method by which enzymes reduce reactions rates include the reduction of the entropic barrier by pre-organizing the reactants, bringing them close together and in

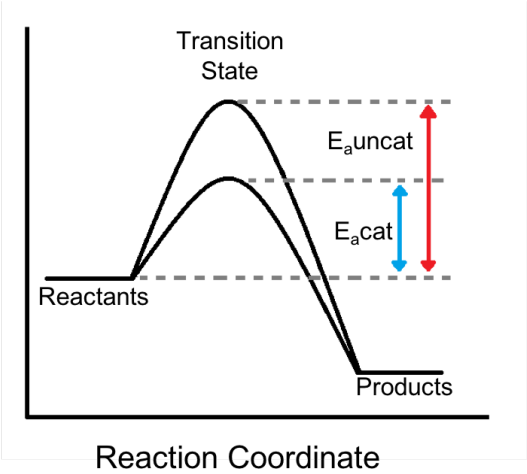

Figure 1. 1 General potential energy diagram of a reaction in solution (uncatalyzed) and with an enzyme (catalyzed). The red and blue arrows show the activation energy of the uncatalyzed and catalyzed reactions, respectively. According to transition state theory, the enzyme accelerates the rate of the reaction by stabilizing the transition state which results in a lower activation barrier.

the proper orientation in the active site. Transition state theory has guided many advances in the field of enzymology, but it does not capture the full catalytic potential of enzymes.[1] This is evident from the limited success of rational *de novo* enzyme design. Structure based programs such as Rosetta have allowed for the rational design of new enzymes by incorporating catalytic residues at the active site of existing scaffolds.[9] This strategy can produce enzymes with the desired functionality, such as the Kemp eliminase[10] and Diels-Alderase[11] rationally designed by Baker et al., but this method has several disadvantages. Often, proposed designs fail to produce an active enzyme, the rate acceleration of the rationally designed enzyme is far lower than naturally evolved enzymes, and subsequent rounds of experimental directed evolution are necessary to increase the rate acceleration several orders of magnitude compared to the computationally designed enzyme.[12] The fact that we can rationally design active enzymes at all, validates that we have a basic understanding of how

enzymes function. Yet, the poor rate acceleration compared to naturally evolved enzymes demonstrates the challenges associated with *de novo* enzyme design. Inherently, the transition state of the reaction must be predicted and a suitable protein structure must be designed to lower the energy of the transition state. Very small structural changes can make a huge difference in energetics, but structural prediction algorithms are only accurate to ~1 Å. Beyond the issue of structural precision, design algorithms are missing a key component: enzyme dynamics. Enzymes are highly flexible molecules that move and interconvert between conformations across all timescales.[1] Despite their dynamic nature, computational tools for designing enzymes have not successfully incorporated protein motions. Pioneers in the field agree that including enzyme dynamics will be necessary for effective enzyme design.[13]

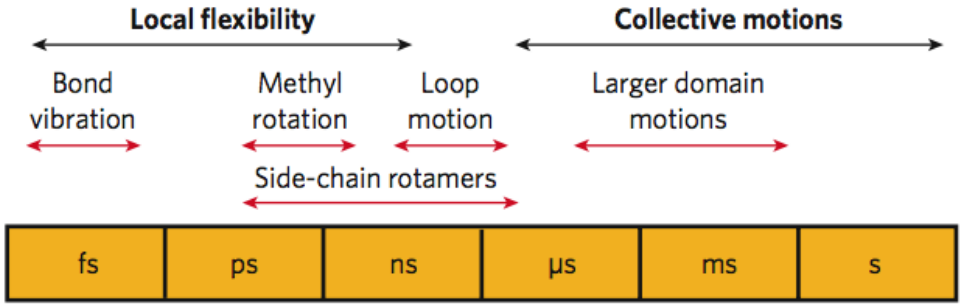

Figure 1. 2 Timeline of enzyme dynamics. Reprinted with permission from Springer Nature: Nature, *450*, 964-972, Dynamic personalities of proteins, Henzler-Wildman, K.; Kearn, D., Copyright 2007.

Understanding enzyme dynamics has been an area of great interest in the biochemistry research community. Enzyme motions and conformational changes occur on a wide range of timescales (**Figure 1. 2**). For example, there are femtosecond promoting vibrations that aide in crossing the barrier of the chemical step, picosecond and nanosecond side chain rotations, microsecond loop motions, millisecond domain motions, and quaternary protein-protein

interactions that occur on seconds or longer timescales.[1, 12, 14] In particular, the microsecond timescale has been poorly studied due to the limitations of techniques that are traditionally used to study enzymes. The work presented here focuses on enzyme dynamics on the order of tens of nanoseconds to a few milliseconds, encompassing the entirety of the microsecond regime. Loop motions and collective motions involved in the search for the reactive conformation are expected to occur on this timescale and each class of motion serves an important role in catalysis.[1, 12, 14] In the following chapters, we present our findings on two model enzyme systems *Escherichia coli* dihydrofolate reductase and *Bacillus stearothermophilus* alcohol dehydrogenase, using temperature jump fluorescence spectroscopy to explore microsecond dynamics.

1.2 Dihydrofolate Reductase

Dihydrofolate reductase (DHFR) is a ubiquitous enzyme that catalyzes the reduction of dihydrofolate to tetrahydrofolate via hydride transfer from an NADPH cofactor. This reaction plays an important role in the nucleic acid biosynthesis pathway. As such, DHFR inhibitors are an important class of drugs that treat cancer, bacterial infections, and other diseases.[15] Due to drug-resistance strains, there is ongoing research for new DHFR inhibitors.[16] In this work we focus on *E. coli* DHFR, which is a small, flexible enzyme composed of four alpha-helices, one 8-stranded beta-sheet, and several loop regions. The Met20 loop (residues 9-24) undergoes large conformational changes throughout the catalytic cycle. The three conformations of the Met20 loop are shown in **Figure 1. 3**. In the reactant bound states, the Met20 loop is in the closed conformation and in the product bound states the Met20 loop is in the occluded conformation, in which the loop protrudes into the active site, sterically hindering the nicotinamide from accessing the binding pocket. The open conformation allows for ligand binding and is observed in various ligand bound states via

crystallography.[17] Additionally, computational simulations predict that the Met20 loop accesses the open conformation at the transition state of hydride transfer.[18]

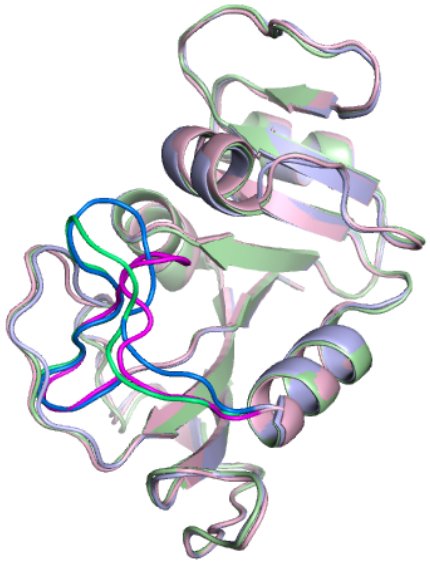

Figure 1. 3 Crystal structure of *E. coli* DHFR. The Met20 loop is highlighted in the three conformations: open (green, PBD:1RA9), closed (blue, PBD:1RX2), and occluded (magenta, PBD:1RX7).

Because of DHFR's flexible nature and the large conformational changes of the Met20 loop, DHFR has been a model enzyme for studying enzyme dynamics. The Met20 loop motions have been postulated to aid with product release, which is the rate limiting step of DHFR catalysis.[19] Increased viscosity decreases k_{cat} at pH 7, but does not affect the hydride transfer rate,[20] which indicates that a conformational change is at least partially rate limiting during steady state turnover. Conformational changes of the Met20 loop are important for overall catalysis, as shown by enzymes with mutations on the Met20 loop. Modification of the Met20 loop by replacing residues 16-19 with glycine causes a 400-fold decrease in the hydride transfer rate.[21] Replacing N23 at the end of the Met20 loop with a double proline sequence prevents the loop from accessing the occluded conformation and results in a 80% reduction of k_{cat}. Nuclear magnetic resonance (NMR)

experiments revealed that the millisecond fluctuations of the Met20 loop are abbrogated in this mutant, suggesting a link between millisecond motions and catalysis.[22] This last point has been hotly debated in the literature,[19, 22-25] though some argue that the difference is just semantics.[26] Certainly, millisecond motions cannot couple directly to barrier crossing of the chemical step, which occurs on the femtosecond timescale, but slower enzyme dynamics can play a role in the search for reactive conformations and ligand binding, which are often the rate limiting steps in enzymatic catalysis.[1]

Protein motions and regions of flexibility throughout the entire DHFR enzyme are necessary for catalysis. Mutations far from the active site can have large impacts on activity. For example, G121 is 15 Å from the active site; mutating this glycine to a valine causes a 200-fold reduction in the hydride transfer rate.[25] Boher et al. used NMR relaxation experiments to compare the conformational exchange of the wildtype enzyme and the G121V mutant.[25] They found that the pico-to-nanosecond and micro-to-millisecond motions of both the FG and Met20 loops were decreased in the mutant. Molecular dynamics simulations and bioinformatic analysis have proposed a network of correlated motions that extends throughout DHFR and includes G121.[27-28] Experimental evidence comes from synergistic effects of select mutations on the temperature dependence of the kinetic isotope effect (KIE). That is, the effect of double mutations is greater than the sum of the effect of the individual mutations, indicating that the two mutated residues are involved in the correlated network. Using this method, G121, F125, M42, and I14 have been confirmed as part of the network of correlated amino acids and W133 has been excluded.[28] Taken together, the effects of mutations far and near to the active site on protein motions and activitiy demonstrate that the entirety of the enzyme plays a necessary role in its function.

DHFR is a well characterized system; there are many studies focused on wildtype and mutant DHFR using a variety of different techniques including single molecule fluorescence, infrared, stopped-flow, and NMR spectroscopies, crystallography, and molecular dynamics

simulations. All of the research discussed above are examples of studies that have focused specifically on the flexibility and dynamics of DHFR. However, the enzyme dynamics of DHFR have yet to be studied on the microsecond timescale. Given the importance of loop motions on DHFR catalysis, the microsecond timescale is a particularly important time regime to study since it is the predicted timescale for enzyme loop motions. The subsequent chapters elucidate microsecond dynamics of DHFR using temperature jump fluorescence spectroscopy.

1.3 Alcohol Dehydrogenase

A family of alcohol dehydrogenases from thermophilic, mesophilic, and psychrophilic organisms have emerged as another useful system to study enzyme dynamics. In particular, the thermophilic alcohol dehydrogenase (ADH) from *Bacillus stearothermophilus* exhibits anomalous

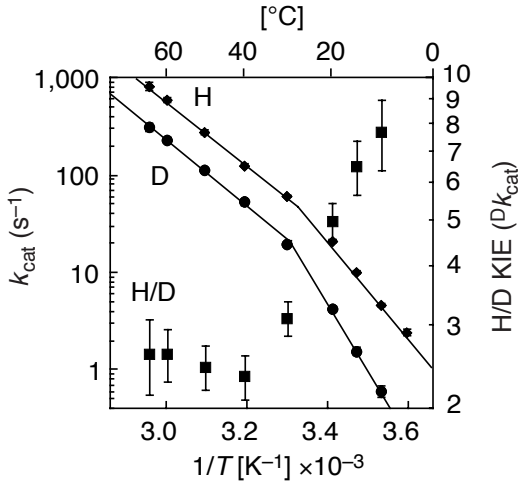

Figure 1. 4 Arrhenius plots of k_{cat} for protonated and deuterated substrates and an Arrhenius plot of their KIE. All plots demonstrate a break in behavior at 30°C. Reprinted with permission from Springer Nature: Nature, 399, 496-499, Enzyme dynamics and hydrogen tunneling in a thermophilic alcohol dehydrogenase, Kohen, A.; Cannio, R.; Bartolucci, S.; Klinman, J. P., Copyright 1999.

temperature dependent trends that are linked to conformational sampling. ADH catalyzes the dehydrogenation of alcohols, transferring a hydride to a NAD^+ cofactor. There is a break in kinetic behaviors at 30°C as shown in **Figure 1. 4**.[29] Below 30°C the activation barrier is increased. One explanation could be that the rate limiting step has changed; however, at all temperatures the rate limiting step is known to be hydride transfer. Additionally, the primary kinetic isotope effect (KIE) is temperature independent above 30°C, but it increases and becomes temperature dependent below 30°C. The hydride transfer step of ADH proceeds via hydride tunneling, which involves wavefunction overlap (**Figure 1. 5**). Because of this, the proper donor-acceptor distance is crucial for activity and could be modulated through conformation sampling.

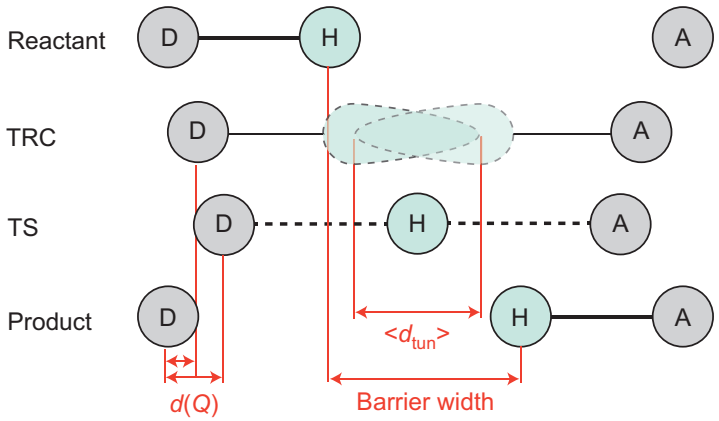

Figure 1. 5 Schematic showing the change in donor-acceptor distance, d(Q), along the reaction coordinate, including the tunneling ready conformation (TRC) and the transition state (TS). The shaded areas of the TRC is where tunneling is most probable due to wavefunction overlap. Reprinted with permission from Springer Nature: Nature Chemistry 4, 161-168, Good Vibrations in Enzyme-catalysed Reactions, Hay, S., and Scrutton, N. S., Copyright 2012.

In an effort to understand the origin of the unusual temperature dependent kinetic properties, ADH protein motions have been investigated. Hydrogen-deuterium exchange (HDX) measurements report on the solvent accessibility and flexibility of enzyme backbones. HDX experiments are performed over long time periods of up to several hours allowing the protein to sample a large range of conformations, a subset of which includes those accessed on the shorter timescale of catalysis. Overall, ADH showed an increase in exchange rate with increasing temperature, which is fairly typical. However, the region of ADH from the substrate binding pocket out to the exterior of the enzyme showed a significant increase in flexibility at temperatures above 30°C.[30] The spatially defined region of increased flexibility suggests that there is a network of protein motions that could be involved with modulating the hydride donor-acceptor distance. Possible origins for the interesting kinetic behavior were investigated further by using single tryptophan mutants to measure fluorescence lifetimes and Stokes shifts, gaining information about motions on the picosecond to nanosecond timescale. However, there was not a correlation between the observed fluorescence and kinetics behaviors.[31] The lack of correlation could be because the motions that are responsible for donor-acceptor distance sampling occur more slowly than pico- to nanoseconds. **Figure 1. 6** shows the timescales that have been interrogated for ADH. Notably, there have been no direct measurements of protein motions on catalytically relevant timescales that demonstrate a break in behavior at 30°C similar to the kinetics.[32] Chapter 5 explores this further by filling in the microsecond time gap using temperature jump Forster resonance energy transfer (FRET) spectroscopy.

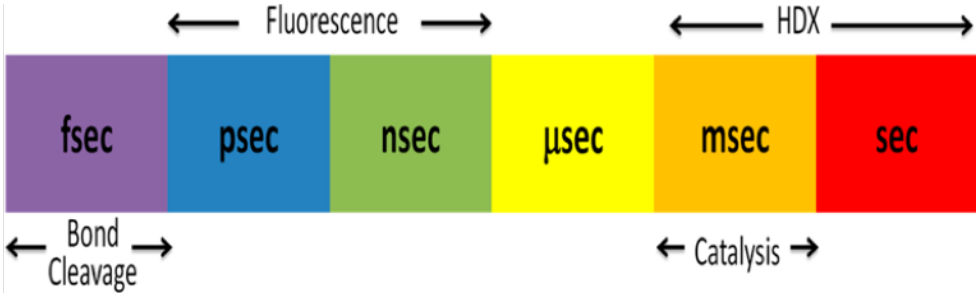

Figure 1. 6 Time frames examined by experimental methods for alcohol dehydrogenase. Reproduced with permission from reference 32.*

*(https://pubs.acs.org/doi/abs/10.1021%2Far5003347) This is an unofficial adaptation of an article that appeared in an ACS publication. ACS has not endorsed the content of this adaptation or the context of its use. Further permissions relating to this material should be directed to the ACS.

1.4 Temperature Jump Spectroscopy

Enzymes do not exist as a single stable folded structure. Instead, they are best described by an ensemble of interconverting conformations across all timescales.[1] Thus, a 2-D energy diagram (potential energy vs the reaction coordinate) as discussed above is a rather simplistic model. It is now understood that a multi-dimensional energy landscape is a better model, incorporating additional dimensions to describe the conformational space.[33] Studying the kinetics of the interconversion between conformational states can be difficult, particularly when studying microsecond enzyme motions. Two commonly used techniques to study enzymes, stopped-flow and protein NMR spectroscopies, do not have the time resolution necessary for monitoring microsecond dynamics. Although stopped-flow instruments have improved, only the fastest instruments can measure signals on the order of hundreds of microseconds and the majority of stopped-flow set-ups are limited by millisecond deadtimes.[34] NMR has the capability of measuring both slower (microsecond to millisecond) and faster (picosecond to nanosecond) dynamics, but is limited by an

inaccessible gap between 10s of nanoseconds and hundreds of microseconds.[35] Beyond identifying conformational changes, another challenge of understanding enzyme dynamics is linking motions to function.[36] Time-resolved experiments have been used to establish the connection between enzyme dynamics and function; for ensemble measurements this necessitates the use of fast initiation methods.[37] Laser-induced temperature jump spectroscopy offers a solution to these temporal and initiation challenges.

Temperature jump spectroscopy is a type of relaxation method. Relaxation methodologies work by poising a system at equilibrium, perturbing the conditions i.e. temperature, pH, pressure, etc., and probing the system as it relaxes to a new equilibrium under the new conditions. In the case of laser-induced temperature jump spectroscopy, a short laser pulse is used to rapidly heat the sample, often by pumping the infrared solvent absorbance. The perturbation to the system relies on a difference in enthalpy between the initial and final states. This technique has been used extensively to study protein folding, but has been used much less to study enzymes.[38] A basic model for an enzyme system includes a single step for ligand binding:

$$E + S \underset{k_{-1}}{\overset{k_1}{\leftrightarrow}} ES \qquad (1)$$

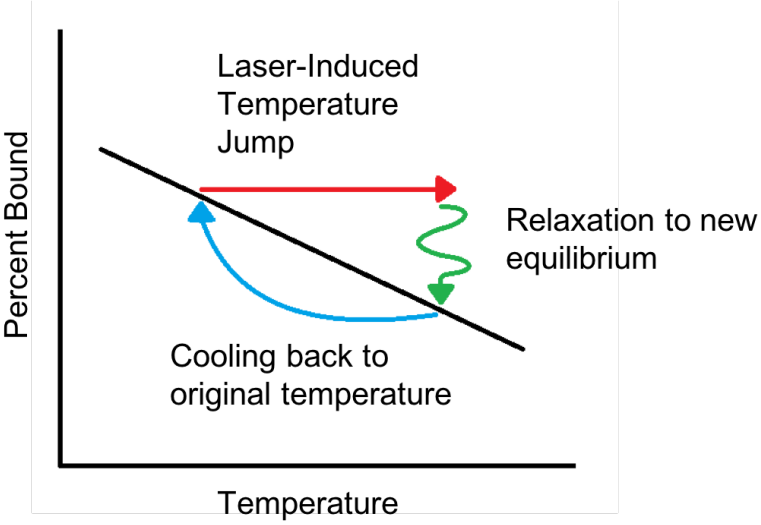

Figure 1. 7 Temperature jump scheme for a simple enzyme – ligand system. At the lower temperature the equilibrium is biased towards binding. The red arrow demonstrates a laser-induced temperature jump. At the higher temperature the equilibrium is biased toward unbound ligand and enzyme. The system must relax to the new equilibrium, as shown by the green arrow. Finally, the system cools back to the original temperature, and the original equilibrium is restored.

Generally, ligand binding is an exothermic process. **Figure 1. 7** demonstrates a temperature jump with a simple enzyme – ligand system. At the lower temperature, the system is at equilibrium. Upon a laser-induced temperature jump, the system must relax to a new equilibrium, which results in a net ligand dissociation. On the order of approximately ten milliseconds, the system cools back down to the original temperature, which allows for averaging multiple "jumps" during a single experiment . The observation window of the temperature jump set up used here extends from the tens of nanoseconds to several milliseconds. It is important to note that even though there is a net ligand dissociation, the system is actually proceeding in both the reverse and forward directions. For simple linear systems as discussed here, the number of observed relaxation rates corresponds to one less than the number of states.[37] In this model (equation 1), there are two states, so there is one

relaxation rate. The observed relaxation rate ($1/\tau$) can be expressed in terms of the microscopic rate constants and equilibrium concentrations of free enzyme and free ligand:[39]

$$1/\tau = k_1(E_{eq} + S_{eq}) + k_{-1} \qquad (2)$$

Unlike mixing methodologies in which the system is far from equilibrium and proceeds primarily in one direction, relaxation methodologies are capable of observing all steps regardless of the order of fast and slow events as long as there is a sufficient population and signal change.[38] A slightly more complicated model is ligand binding followed by an associated conformational change also known as the induced fit model:

$$E + S \underset{k_{-1}}{\overset{k_1}{\leftrightarrow}} ES \underset{k_{-2}}{\overset{k_2}{\leftrightarrow}} E^*S \qquad (3)$$

where E*S denotes a different conformation of the enzyme with ligand bound. With the induced fit model, there are three states, which means there are two relaxation rates. Since the two steps are coupled, the resulting relaxation rates are a complex combination of the all of the microscopic rate constants and the free concentrations, making both of them concentration dependent.[39] Although gaining information about the forward and reverse properties is advantageous, it becomes difficult to analytically solve for the microscopic rate constants when the model contains several states and the data exhibit multiple relaxation times. Nonetheless, laser-induced temperature jump spectroscopy has the advantage of fast initiation and spans the entirety of the microsecond time regime, making this method a particularly suitable technique for studying loop motions and collective motions of enzymes. Temperature jump fluorescence spectroscopy, in which fluorescence is the probing method of choice, is used through the entirety of this dissertation to elucidate the dynamics of the model enzyme systems DHFR and ADH.

1.5 References

1. Callender, R.; Dyer, R. B., The dynamical nature of enzymatic catalysis. *Acc Chem Res* **2015,** *48* (2), 407-13.

2. Loveridge, E. J.; Allemann, R. K., Pinpointing dynamic coupling in enzymes for efficient drug design. *Future Sci OA* **2016,** *2* (1), FSO95.

3. Bull, S. C.; Doig, A. J., Properties of protein drug target classes. *PLoS One* **2015,** *10* (3), e0117955.

4. Schwartz, K. L.; Morris, S. K., Travel and the Spread of Drug-Resistant Bacteria. *Curr Infect Dis Rep* **2018,** *20* (9), 29.

5. Hamis, S.; Nithiarasu, P.; Powathil, G. G., What does not kill a tumour may make it stronger: In silico insights into chemotherapeutic drug resistance. *J Theor Biol* **2018,** *454*, 253-267.

6. Mandal, S.; Moudgil, M.; Mandal, S. K., Rational drug design. *Eur J Pharmacol* **2009,** *625* (1-3), 90-100.

7. Huggins, D. J.; Sherman, W.; Tidor, B., Rational approaches to improving selectivity in drug design. *J Med Chem* **2012,** *55* (4), 1424-44.

8. Do, P. C.; Lee, E. H.; Le, L. T., Steered Molecular Dynamics Simulation in Rational Drug Design. *J Chem Inf Model* **2018**.

9. Richter, F.; Leaver-Fay, A.; Khare, S. D.; Bjelic, S.; Baker, D., De novo enzyme design using Rosetta3. *PLoS One* **2011,** *6* (5), e19230.

10. Rothlisberger, D.; Khersonsky, O.; Wollacott, A. M.; Jiang, L.; DeChancie, J.; Betker, J.; Gallaher, J. L.; Althoff, E. A.; Zanghellini, A.; Dym, O.; Albeck, S.; Houk, K. N.; Tawfik, D. S.; Baker, D., Kemp elimination catalysts by computational enzyme design. *Nature* **2008,** *453* (7192), 190-5.

11. Siegel, J. B.; Zanghellini, A.; Lovick, H. M.; Kiss, G.; Lambert, A. R.; St Clair, J. L.; Gallaher, J. L.; Hilvert, D.; Gelb, M. H.; Stoddard, B. L.; Houk, K. N.; Michael, F. E.; Baker, D., Computational design of an enzyme catalyst for a stereoselective bimolecular Diels-Alder reaction. *Science* **2010,** *329* (5989), 309-13.

12. Osuna, S.; Jimenez-Oses, G.; Noey, E. L.; Houk, K. N., Molecular dynamics explorations of active site structure in designed and evolved enzymes. *Acc Chem Res* **2015,** *48* (4), 1080-9.

13. Preiswerk, N.; Beck, T.; Schulz, J. D.; Milovnik, P.; Mayer, C.; Siegel, J. B.; Baker, D.; Hilvert, D., Impact of scaffold rigidity on the design and evolution of an artificial Diels-Alderase. *Proc Natl Acad Sci U S A* **2014,** *111* (22), 8013-8.

14. Henzler-Wildman, K.; Kern, D., Dynamic personalities of proteins. *Nature* **2007,** *450* (7172), 964-72.

15. Schweitzer, B. I.; Dicker, A. P.; Bertino, J. R., Dihydrofolate reductase as a therapeutic target. *FASEB J* **1990,** *4* (8), 2441-52.

16. Srinivasan, B.; Rodrigues, J. V.; Tonddast-Navaei, S.; Shakhnovich, E.; Skolnick, J., Rational Design of Novel Allosteric Dihydrofolate Reductase Inhibitors Showing Antibacterial Effects on Drug-Resistant Escherichia coli Escape Variants. *ACS Chem Biol* **2017,** *12* (7), 1848-1857.

17. Sawaya, M. R.; Kraut, J., Loop and subdomain movements in the mechanism of Escherichia coli dihydrofolate reductase: crystallographic evidence. *Biochemistry* **1997,** *36* (3), 586-603.

18. Fan, Y.; Cembran, A.; Ma, S.; Gao, J., Connecting protein conformational dynamics with catalytic function as illustrated in dihydrofolate reductase. *Biochemistry* **2013,** *52* (12), 2036-49.

19. Luk, L. Y.; Loveridge, E. J.; Allemann, R. K., Protein motions and dynamic effects in enzyme catalysis. *Phys Chem Chem Phys* **2015,** *17* (46), 30817-27.

20. Loveridge, E. J.; Tey, L. H.; Allemann, R. K., Solvent effects on catalysis by Escherichia coli dihydrofolate reductase. *J Am Chem Soc* **2010,** *132* (3), 1137-43.

21. Li, L.; Falzone, C. J.; Wright, P. E.; Benkovic, S. J., Functional role of a mobile loop of Escherichia coli dihydrofolate reductase in transition-state stabilization. *Biochemistry* **1992,** *31* (34), 7826-33.

22. Bhabha, G.; Lee, J.; Ekiert, D. C.; Gam, J.; Wilson, I. A.; Dyson, H. J.; Benkovic, S. J.; Wright, P. E., A dynamic knockout reveals that conformational fluctuations influence the chemical step of enzyme catalysis. *Science* **2011,** *332* (6026), 234-8.

23. Pisliakov, A. V.; Cao, J.; Kamerlin, S. C.; Warshel, A., Enzyme millisecond conformational dynamics do not catalyze the chemical step. *Proc Natl Acad Sci U S A* **2009,** *106* (41), 17359-64.

24. Glowacki, D. R.; Harvey, J. N.; Mulholland, A. J., Taking Ockham's razor to enzyme dynamics and catalysis. *Nat Chem* **2012,** *4* (3), 169-76.

25. Boehr, D. D.; Schnell, J. R.; McElheny, D.; Bae, S. H.; Duggan, B. M.; Benkovic, S. J.; Dyson, H. J.; Wright, P. E., A distal mutation perturbs dynamic amino acid networks in dihydrofolate reductase. *Biochemistry* **2013,** *52* (27), 4605-19.

26. Kohen, A., Role of dynamics in enzyme catalysis: substantial versus semantic controversies. *Acc Chem Res* **2015,** *48* (2), 466-73.

27. Ramanathan, A.; Agarwal, P. K., Evolutionarily conserved linkage between enzyme fold, flexibility, and catalysis. *PLoS Biol* **2011,** *9* (11), e1001193.

28. Singh, P.; Francis, K.; Kohen, A., Network of remote and local protein dynamics in dihydrofolate reductase catalysis. *ACS Catal* **2015,** *5* (5), 3067-3073.

29. Kohen, A.; Cannio, R.; Bartolucci, S.; Klinman, J. P., Enzyme dynamics and hydrogen tunnelling in a thermophilic alcohol dehydrogenase. *Nature* **1999,** *399* (6735), 496-9.

30. Liang, Z. X.; Lee, T.; Resing, K. A.; Ahn, N. G.; Klinman, J. P., Thermal-activated protein mobility and its correlation with catalysis in thermophilic alcohol dehydrogenase. *Proc Natl Acad Sci U S A* **2004,** *101* (26), 9556-61.

31. Meadows, C. W.; Ou, R.; Klinman, J. P., Picosecond-resolved fluorescent probes at functionally distinct tryptophans within a thermophilic alcohol dehydrogenase: relationship of temperature-dependent changes in fluorescence to catalysis. *J Phys Chem B* **2014,** *118* (23), 6049-61.

32. Klinman, J. P., Dynamically achieved active site precision in enzyme catalysis. *Acc Chem Res* **2015,** *48* (2), 449-56.

33. Klinman, J. P.; Kohen, A., Hydrogen tunneling links protein dynamics to enzyme catalysis. *Annu Rev Biochem* **2013,** *82*, 471-96.

34. Roder, H.; Maki, K.; Cheng, H., Early events in protein folding explored by rapid mixing methods. *Chem Rev* **2006,** *106* (5), 1836-61.

35. Rovo, P.; Linser, R., Microsecond Timescale Protein Dynamics: a Combined Solid-State NMR Approach. *Chemphyschem* **2018,** *19* (1), 34-39.

36. Otten, R.; Liu, L.; Kenner, L. R.; Clarkson, M. W.; Mavor, D.; Tawfik, D. S.; Kern, D.; Fraser, J. S., Rescue of conformational dynamics in enzyme catalysis by directed evolution. *Nat Commun* **2018,** *9* (1), 1314.

37. Callender, R.; Dyer, R. B., Advances in time-resolved approaches to characterize the dynamical nature of enzymatic catalysis. *Chem Rev* **2006,** *106* (8), 3031-42.

38. Callender, R.; Dyer, R. B., Probing protein dynamics using temperature jump relaxation spectroscopy. *Curr Opin Struct Biol* **2002,** *12* (5), 628-33.

39. Bernasconi, C. F., *Relaxation Kinetics*. Academic Press: New York, 1976.

Chapter 2:

Ligand-Dependent Conformational Dynamics of Dihydrofolate Reductase

Reproduced with permission from

Reddish, M. J.*; Vaughn, M. B*.; Fu, R.; Dyer, R. B., Ligand-Dependent Conformational Dynamics of Dihydrofolate Reductase. *Biochemistry* **2016**, *55* (10), 1485-93.

Copyright 2018 American Chemical Society

*Authors M. J. Reddish and M. B. Vaughn contributed equally.

2.1 Abstract

Enzymes are known to change among several conformational states during turnover. The role of such dynamic structural changes in catalysis is not fully understood. The influence of dynamics in catalysis can be inferred, but not proven, by comparison of equilibrium structures of protein variants and protein−ligand complexes. A more direct way to establish connections between protein dynamics and the catalytic cycle is to probe the kinetics of specific protein motions in comparison to progress along the reaction coordinate. We have examined the enzyme model system dihydrofolate reductase (DHFR) from *Escherichia coli* with tryptophan fluorescence-probed temperature-jump spectroscopy. We aimed to observe the kinetics of the ligand binding and ligand induced conformational changes of three DHFR complexes to establish the relationship among these catalytic steps. Surprisingly, in all three complexes, the observed kinetics do not match a simple sequential two-step process. Through analysis of the relationship between ligand concentration and observed rate, we conclude that the observed kinetics correspond to the ligand binding step of the reaction and a noncoupled enzyme conformational change. The kinetics of the conformational change vary with the ligand's identity and presence but do not appear to be directly

related to progress along the reaction coordinate. These results emphasize the need for kinetic studies of DHFR with highly specific spectroscopic probes to determine which dynamic events are coupled to the catalytic cycle and which are not.

2.2 Introduction

It is well established that protein motions are critical for enzymatic catalysis.[1-2] Studies have demonstrated when key motions are knocked out by mutations, the activity of the enzyme is affected.[3-6] However, the exact role of enzyme dynamics in the catalytic cycle is not fully understood and continues to be an active area of research.[7-17] Enzyme dynamics can be split into two categories: motions on the time scale of the chemistry step that may be coupled to crossing the transition state and slower motions related to bringing the enzyme to active conformations, particularly relating to substrate binding and activation. In this study, we focus on the latter class of enzyme dynamics by examining the protein motions of *Escherichia coli* dihydrofolate reductase (*E. coli* DHFR), an archetype for enzyme dynamics. A previous study of DHFR found there are protein motions on the millisecond time scale that are uncorrelated to the chemistry step;[18] the focus of this study is on protein motions that occur on a time scale faster than what has been measured previously. The hydride transfer (crossing the transition state) actually occurs on the picosecond time scale, so it is the search for reactive structures that ultimately determines the time scale of the chemical step. Furthermore, the overall rate-determining step is product release, so steady state measurements on the millisecond time scale are dominated by this slow process. Using temperature-jump methods, we have probed protein motions on a time scale significantly shorter than the overall turnover rate, which allows us to probe all of the motions involved in cofactor and substrate binding and the search for reactive conformations. Thus, this study is also related to fundamental questions of substrate and transition state binding, i.e., induced fit or conformational selection models.[19]

DHFR is a ubiquitous enzyme that catalyzes the reduction of dihydrofolate (DHF) to tetrahydrofolate (THF) via a nicotinamide adenine dinucleotide phosphate (NADPH) cofactor. The crystal structure of *E. coli* DHFR is shown in **Figure 2. 1** with its native fluorophore tryptophans highlighted. DHFR has three flexible loops: the Met20 loop, the FG loop, and the GH loop. The Met20 loop is known for its distinct conformational changes during the reaction. In reactant-like states, such as the holoenzyme (DHFR·NADPH) and the Michaelis complex (DHFR·NADPH·DHF), the Met20 loop exists in the "closed" state where it closes over the active site. The closed conformation seals the active site from solvent and assists the positioning of the nicotinamide ring through hydrogen bonding interactions.[20] The product-bound states (DHFR·$NADP^+$·THF, DHFR·THF, and DHFR·NADPH· THF) exist in the "occluded" conformation, where the Met20 loop protrudes into the active site, preventing the nicotinamide ring of the cofactor from accessing the active site.[20]

Figure 2. 1 Crystal structure of *E. coli* DHFR (blue) in complex with the cofactor $NADP^+$ (yellow) and the substrate folate (green). The five native tryptophans are colored pink (PDB entry 1RX2).

Protein crystallography, NMR, hydrogen−deuterium exchange, ultraviolet photodissociation, and molecular dynamics studies have provided useful insights into the regions of flexibility in DHFR and how that flexibility changes depending on which ligands are bound and which enzyme variants are studied.[3, 21-30] While these studies combine to improve the understanding of DHFR catalysis, these techniques are limited to equilibrium fluctuations. They are not capable of directly observing the coupling of motion to the catalytic cycle. There are two main challenges associated with solving this problem. The first is how to initiate the catalytic cycle on a time scale that is fast enough to observe all of the relevant steps and associated protein motions. The second challenge is that critical fast steps can be "hidden" by a slower step, such as substrate diffusion. However, laser-induced temperature-jump spectroscopy is able to overcome both of these obstacles.

Temperature-jump spectroscopy is a relaxation method that uses a laser pulse to rapidly heat the system. Relaxation methods measure the response to a shift in equilibrium of a reversible reaction caused by some environmental change such as temperature. The observed relaxation rates are actually a complex combination of all of the microscopic rate constants involved in reestablishing the equilibrium. An important consequence of this complexity is that even though a rise in temperature shifts the equilibrium toward one side of the reaction, the relaxation data include information about rate constants for both forward and reverse processes.[31-32] Thus, while it is clear that an increase in temperature shifts the cofactor and substrate binding equilibria of DHFR toward the unbound state (this is certain on the basis of the thermodynamics determined from ITC data), the relaxation kinetics cannot be interpreted solely in terms of ligand release but have some contribution from the binding kinetics. Additionally, the temperature-jump method allows for observation of any related protein conformational changes. Herein, we examine ligand binding pathways of three complexes, DHFR·folate, DHFR·$NADP^+$, and DHFR·$NADP^+$·folate, which are models for the binary product complex, the holoenzyme, and the Michaelis complex, respectively.[20]

We observe two kinetic events in the temperature-jump transients of each of the three complexes. A simple model is applied to analyze the transients that includes a reversible ligand binding step followed by a protein conformational change, as is implied by crystallographic studies.[20] By analyzing the correlation between the rates of these events and ligand concentration, we are able to determine that this model does not fit the data and that these rates represent two unrelated reaction pathways. This study highlights the need for kinetic studies of enzyme systems that directly establish the relationships between dynamics and the catalytic cycle instead of inferring dynamics from equilibrium studies.

2.3 Experimental Procedures

Protein Expression and Purification

The C-terminal six histidine-tagged *E. coli* DHFR was cloned and expressed in *E. coli* strain BL21(DE3) with Luria-Bertani (LB) medium containing 100 μg/mL ampicillin. A single ampicillin-resistant colony was picked and inoculated into 20 mL of LB medium at 30°C overnight. This starter culture of 1 mL was then inoculated into 1000 mL of LB medium, and the bacteria were allowed to grow until the OD_{600} reached 0.6−0.8 at 37°C. Next, isopropyl β-D-thiogalactopyranoside (IPTG) was added to a final concentration of 1 mM, and the culture was allowed to grow overnight at 30°C on a shaking incubator at 200 rpm. The bacteria were harvested by centrifugation at 5000g for 15 min at 4°C and stored at −80°C.

The pellets of bacteria were thawed and resuspended in 50 mM Tris, 150 mM NaCl, 5 mM β-mercaptoethanol (pH 8.0), 1 tablet of protease inhibitor/50 mL of cell lysis buffer, and 1 mg/mL lysosome, stirred on ice for 1 h, and finally sonicated on ice (Sonic Dissemble model 500, Fisher Scientific, Pittsburgh, PA). Insoluble debris was removed by centrifugation at 13000 rpm for 30 min at 4°C. The supernatant was further filtered through a 0.22 μm filter and applied to a HisPrep

affinity column on an AKTA FPLC system (GE Healthcare, Pittsburgh, PA). The column was equilibrated with 50 mM Tris-HCl, 150 mM NaCl, 10 mM imidazole, and 5 mM β-mercaptoethanol (pH 8.0). The DHFR protein was eluted through a gradient to 25% elution buffer [50 mM Tris-HCl, 150 mM NaCl, 500 mM imidazole, and 5 mM β- mercaptoethanol (pH 8.0)] over 15 column volumes. The eluted protein was pooled and concentrated using an Amicon concentrator with a 10000 Da molecular weight cutoff (Millipore, Billerica, MA). The concentrated DHFR was exchanged into 50 mM sodium phosphate, 100 mM NaCl, 5 mM DTT, and 5% glycerol (pH 7.0) using a HiPrep Desalting column (GE Healthcare). Protein purity was determined by sodium dodecyl sulfate−polyacrylamide gel electrophoresis followed by staining with Coomassie blue.

Equilibrium Fluorescence

Fluorescence measurements were taken with a Horiba (Kyoto, Japan) Dual-Fl fluorometer of four complexes: apoenzyme, DHFR·folate, DHFR·$NADP^+$, and DHFR·$NADP^+$·folate. In all samples, the DHFR concentration was 3 μM. In the binary complexes, the folate and $NADP^+$ concentrations were 6 μM. In the tertiary complex, the folate concentration was 6 μM and the $NADP^+$ concentration was 300 μM. The buffer used is the same as for the temperature-jump experiments [50 mM sodium phosphate and 100 mM NaCl (pH 7)]. The data collection parameters were as follows: 1.16 nm resolution, fixed 5 nm slits, a CCD gain setting of "medium", an integration time of 0.5 s, average of five scans, and an excitation wavelength of 280 nm. Temperature dependent spectra were recorded from 12 to 60°C in 3°C increments. To determine the temperature dependent trends of each complex, the tryptophan fluorescence was integrated from 327 to 353 nm, normalized to 1 at the lowest temperature, and then corrected for tryptophan's temperature dependent quantum yield by subtracting the normalized integrated fluorescence of 3 μM tryptophan.

Temperature-Jump Kinetic Methods

Fluorescence temperature-jump relaxation experiments were conducted on a custom-built instrument. A similar instrument has been described previously;[33] the major difference here is the source of the heating pulse. The temperature-jump pump pulse is created by a Q-switched, Tm:fiber-pumped Ho:YAG laser, run at 50 Hz to create a 7 mJ, ~10 ns pulse of 2090 nm light (AQS- Ho-YAG, IPG Phototonics Corp., Oxford, MA). The repetition rate of these pulses is further reduced to 12.5 Hz by an optical chopper (Thorlabs, Newton, NJ). The probing method is tryptophan emission excited around 280 nm. The excitation source is the quasi-continuous frequency-tripled output of a Mira 900 Ti:sapphire laser (845 nm) pumped by a Verdi V12 DPSS high-power laser (Coherent, Santa Clara, CA). The sample emission is focused through an appropriate bandpass filter (Semrock, Rochester, NY) before being measured on a Hamamatsu R7518 photomultiplier tube (Hamamatsu Pho- tonics K. K., Hamamatsu, Japan). The signal is collected, digitized, and averaged (2000 shots) using a Teledyne LeCroy (Chestnut Ridge, NY) Wavesurfer 62Xs-B oscilloscope. Data collection is managed by an in-house routine using the LabVIEW computer program (National Instruments, Austin, TX). The sample thickness is 250 μm. To maintain an even transmittance of the pump pulse through this spacer thickness, the pump beam is split using a 50/50 beamsplitter (Thorlabs) and oriented to heat the sample from both sides. The temperature change in all of our samples shown here is from 29 to 36°C. The initial temperature of the sample is maintained by contact with the sample stage that is temperature-controlled by a recirculating water bath.

All of the temperature-jump experiments described utilized a sample containing 100 μM DHFR and appropriate ligand in a 50 mM sodium phosphate and 100 mM NaCl D_2O buffer at pD 7 (uncorrected pH meter reading). The ligand concentrations were varied from 100 to 200 μM to

determine the concentration dependence of the observed rates. The DHFR·$NADP^+$·folate samples contained an excess of $NADP^+$ to favor cofactor binding and encourage release of substrate from the ternary complex during the temperature jump. DHFR·$NADP^+$·folate has been used previously as a mimic for the Michaelis complex of the enzyme.[20] The rebinding of folate to the oxidized cofactor-bound complex allows us to examine the pathway of binding of substrate to the holoenzyme present in the natural DHFR reaction cycle.

The observed temperature-jump transients include two types of responses to the heating pulse: the sample re-equilibration after heating and the intrinsic fluorescence change of the fluorophore tryptophan due to temperature change. The intrinsic fluorescence change does not report on conformational dynamics and, thus, needs to be removed from the data. To do so, in addition to each sample DHFR transient we acquired, we also acquired a temperature-jump transient from a reference sample of approximately 200 μM tryptophan (Sigma- Aldrich, St. Louis, MO) under the same conditions. This reference transient shows a significant change in fluorescence due to the heating but of a magnitude different from that of the protein samples. We removed any offset difference between the reference and sample by shifting the data so that the early time signal was set to 0. Then, we numerically scaled the reference transient data so that the magnitude of the response to heating was the same as that of the protein sample, and we then subtracted the scaled reference transient from the protein sample transient. This procedure had the effect of removing the contribution to the observed signal from the change in intrinsic tryptophan fluorescence due to heating. To regain a useful scale for comparison, we then shifted the corrected sample transient back to its previous magnitude and normalized the transient to 100 by dividing the entire transient by its initial intensity. These normalized transients are presented as our results.

2.4 Results and Discussion

Equilibrium Fluorescence

The tryptophan fluorescence was characterized for four different complexes: apoenzyme, DHFR·folate, DHFR·$NADP^+$, and DHFR·$NADP^+$·folate. We chose DHFR·$NADP^+$ to represent the holoenzyme complex over the usual choice of DHFR·NADPH for three reasons. First, to use the same cofactor to study both the binary and ternary complexes it was necessary to use $NADP^+$ because the DHFR·NADPH·folate complex reacts slowly and is therefore not stable during the course of the experiment.[34] Second, we hoped to take advantage of the enhanced structural flexibility of DHFR·$NADP^+$ complexes to observe more ligand-related conformational changes. Third, we wanted to minimize additional spectroscopic interactions, such as Förster resonance energy transfer from tryptophan to NADPH, from complicating our interpretation. Although this last point is not an insurmountable problem and might even lead to interesting observations, this study focused on the intrinsic tryptophan fluorescence because it is a probe that does not alter the protein activity and can be examined throughout the entire catalytic reaction.

Upon comparison of relative fluorescence intensities (**Figure 2. 2**), there is very little difference between the apoenzyme and DHFR·$NADP^+$ complex. When folate binds to the apoenzyme, however, there is a significant drop in fluorescence, likely due to the transfer of energy from tryptophan to folate. The fluorescence drops further with the binding of $NADP^+$ to form the tertiary complex. Because the fluorescence does not change much upon binding $NADP^+$, the reduction of fluorescence between DHFR·folate and the tertiary complex can be explained by the different conformation of the enzyme in these two complexes. DHFR·folate is in the occluded

conformation, whereas DHFR·$NADP^+$·folate is in the closed conformation as determined by crystallography studies.[20]

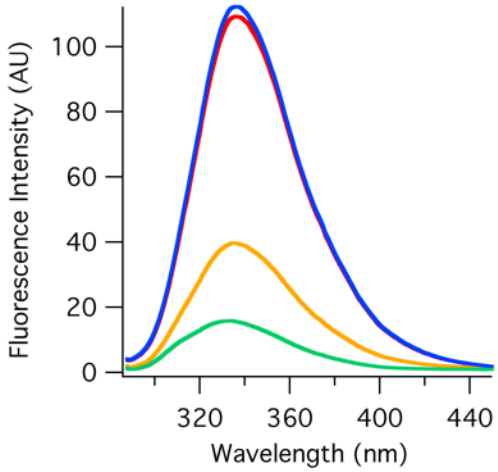

Figure 2. 2 Relative equilibrium tryptophan fluorescence (excitation at 280 nm) of the DHFR apoenzyme (red), DHFR·folate (yellow), DHFR·$NADP^+$ (blue), and DHFR·$NADP^+$·folate (green). These spectra were recorded at 20°C with 3 μM enzyme.

The difference fluorescence spectra of all four complexes were also obtained over a range of temperatures (**Figure 2. 3**). In all four complexes, the fluorescence increases as temperature increases. The fluorescence of the two folate complexes increases dramatically with increasing temperature as compared to that of the apoenzyme or the binary complex with $NADP^+$. This is unsurprising considering that as the temperature increases, the binding affinity decreases, which causes folate to dissociate from the enzyme. Defining a melting temperature for the complexes is not straightforward because DHFR unfolding may include more than two states.[35-37] The addition of ligands to the protein will likely complicate the unfolding mechanism even more. Therefore, we

simply note that the fluorescence response to heating for the apoenzyme and its complexes is consistent with ligand dissociation and this process becomes convolved with unfolding of DHFR above 50°C.[35]

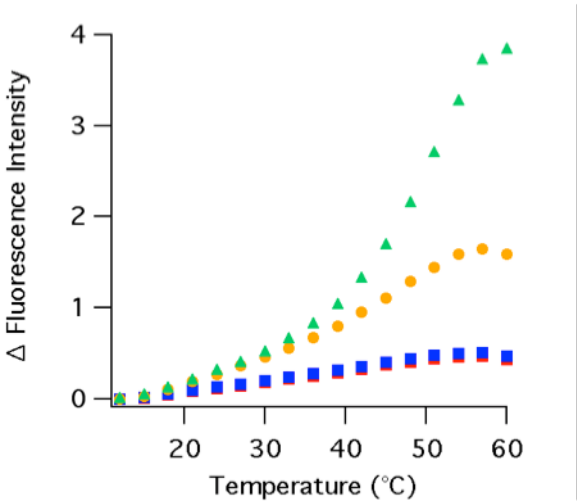

Figure 2. 3 Difference temperature-dependent equilibrium fluorescence (excitation at 280 nm) of the DHFR apoenzyme (red diamonds), DHFR·$NADP^+$ (blue squares), DHFR·folate (yellow circles), and DHFR·$NADP^+$·folate (green triangles) from 12 to 60°C. The tryptophan emission intensity (~340 nm peak maximum) is integrated from 327 to 353 nm. The integrated peak areas are normalized to 1 by the integrated peak area at the lowest temperature studied and corrected for the temperature dependent quantum yield by subtracting the normalized fluorescence of free tryptophan.

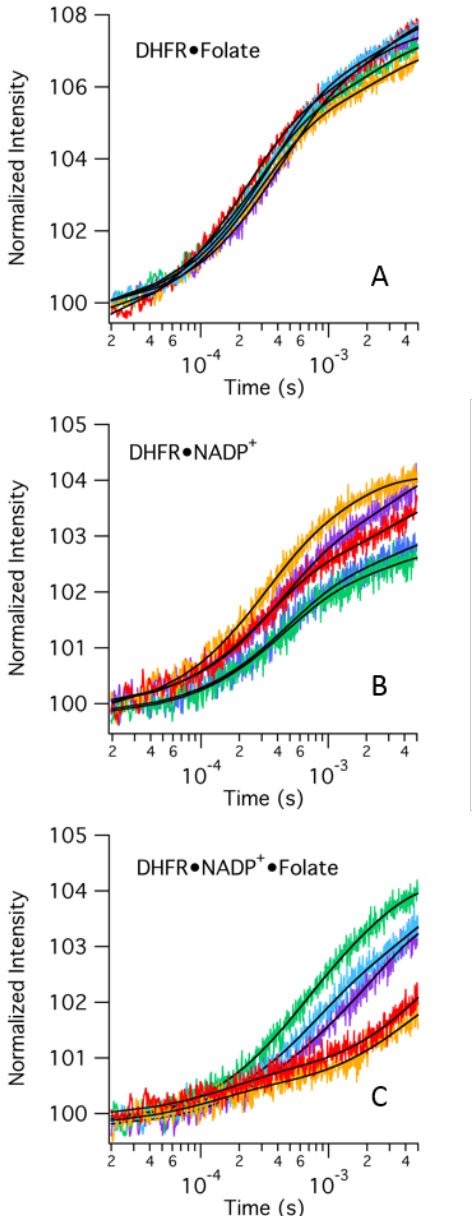

Figure 2. 4 Representative fluorescence temperature-jump transients of three DHFR complexes for a jump from 29 to 36°C. Tryptophan fluorescence is excited at 280 nm and integrated from 327 to 353 nm. Colors refer to either folate or $NADP^+$ concentrations: purple for 100 μM, blue for 125 μM, green for 150 μM, orange for 175 μM, and red for 200 μM: (A) 100 μM DHFR with varying folate concentrations, (B) 100 μM DHFR with varying $NADP^+$ concentrations, and (C) 100 μM DHFR and 1000 μM $NADP^+$ with varying folate concentrations. The black lines indicate the lines of best fit for each transient when fit to a double-exponential curve.

Temperature-Jump Kinetics

Temperature-jump transients of two binary complexes and one tertiary complex were collected with several ligand concentrations (**Figure 2. 4**). The observation time window is from 10 μs to 5 ms. Our temperature-jump system can resolve transients with rise times as short as 10 ns, but we found no significant signals at time scales faster than 10 μs and therefore limited the range to maximize the signal-to-noise ratio. All three complexes show a substantial increase in fluorescence in response to a temperature jump from 29 to 36°C. The increase in fluorescence is consistent with a net dissociation of the substrate at the higher temperature, as seen in **Figure 2. 3**. Interpreting the signal change as dissociation of the ligand due to an increase in temperature is also consistent with the exothermic nature of binding of a ligand to DHFR (**Table 2S. 1**). It is important to note that while ligand dissociation is the direction of the overall change in the equilibrium, the relaxation kinetics of establishing the new equilibrium includes contributions from both the ligand binding and dissociation processes.

With each complex, we observe two events in the temperature-jump transients. There is a faster event with an observed relaxation rate around 2000−4000 s^{-1} and a slower event with an observed relaxation rate around 300−400 s^{-1} (see **Table 2. 1** for example fits at one concentration and **Table 2S. 2** for average data for all concentrations studied). Typical models of DHFR catalysis include loop movement, or more generally conformational rearrangement, as ligands react or bind and dissociate throughout the reaction cycle.[20, 38] Therefore, we first postulated the most likely model for understanding the two observed events in our relaxation transients consisted of sequential ligand binding and conformational rearrangement steps. **Scheme 2. 1** summarizes this model with E indicating a generic enzyme state (i.e., apoenzyme or binary complex with $NADP^+$) and L indicating a ligand. **Scheme 2. 1** also introduces the nomenclature of E* to refer to the enzyme complex

before and after its substrate binding-induced conformational change, without implying a specific loop motion.

Table 2. 1 Example Fit Relaxation Rates and Amplitudes for Temperature-Jump Data

	DHFR•folate[a]	**DHFR•NADP$^+$ [a]**	**DHFR•NADP$^+$•folate[b]**	**DHFR apoenzyme**
Slow Rate (s^{-1})	400 ± 70	300 ± 100	400 ± 100	240 ± 40
Slow Rate Amplitude	2.7 ± 0.3	1.2 ± 0.2	2.4 ± 0.2	2.3 ± 0.5
Fast Rate (s^{-1})	3800 ± 200	2500 ± 91	2200 ± 500	5000 ± 1000
Fast Rate Amplitude	4.9 ± 0.5	2.0 ± 0.2	1.8 ±0.5	0.6 ± 0.08

[a] Reported values are the average of the data taken at [DHFR] = 100 μM and [Ligand] = 150 μM.

[b] Reported values are the average of the data taken at [DHFR] = 100 μM, [$NADP^+$] = 1000 μM and [folate] = 150 μM.

The relationship between the observed relaxation rates and the microscopic rate constants for a kinetic model like **Scheme 2. 1** that includes sequential bimolecular and unimolecular transformations has been previously solved with the assumption that the perturbation is small, a <5% change in equilibrium concentration.[32] The 7°C temperature jump herein induces a change in the equilibrium concentration of <5%. In such cases, the microscopic rate constants can be determined by plotting the sum of the relaxation rates versus the sum of the free concentrations of E and L and plotting the product of the relaxation rates versus the sum of the free concentrations of E and L. The free concentrations indicated are those of the final temperature of the temperature jump. If the data fit this proposed model, each plot should yield a linear relationship. Equations 1−4 display the predicted relationship between the linear fit parameters from these plots and the rate

constants in **Scheme 2. 1**, where m_S and b_S are the slope and intercept of the plot of the sum of rates, respectively, and m_P and b_P are the slope and intercept of the product of the rates, respectively.

Scheme 2. 1

$$E + L \underset{k_{-1}}{\overset{k_1}{\rightleftharpoons}} E{\bullet}L \underset{k_{-2}}{\overset{k_2}{\rightleftharpoons}} E^{*}{\bullet}L$$

$$k_1 = m_s \quad \text{(Eq 1)} \qquad k_{-1} = b_s - \frac{m_p}{m_s} \quad \text{(Eq 2)}$$

$$k_2 = b_s - k_{-1} - k_{-2} \quad \text{(Eq 3)} \qquad k_{-2} = \frac{b_p}{k_{-1}} \quad \text{(Eq 4)}$$

We tested the applicability of the model in **Scheme 2. 1** to our data by making the necessary plots (**Figure 2S. 3**). We solved for the free enzyme and ligand concentrations using thermodynamic equilibrium constants (**Table 2S. 1**) determined previously by isothermal titration calorimetry (ITC) for the interaction of DHFR with folate and DHFR with $NADP^+$.[39] We were unable to find the necessary equilibrium constants for the binding of folate to DHFR·$NADP^+$ in the literature; therefore, we determined this value ourselves using ITC (**Figure 2S. 2** and **Table 2S. 1**).

Upon analyzing the data, we found the model to be inadequate for describing our results. This is most clearly evident from the analysis by the estimation of one negative rate constant for each of the three protein complexes studied (**Table 2S. 3**). As long as the second relaxation phase represents a unimolecular process following the bimolecular event, then the analysis should be valid, even in the extreme case of one the reactions occurring much faster than the other; however, a negative value for a reaction rate is nonsensical and implies our model is incorrect.[32] Both the DHFR·folate and the DHFR· $NADP^+$·folate complexes have a predicted negative value for k_2; the

DHFR·NADP$^+$ complex has a predicted negative value for k−2. Because the negative value was found in the second reaction in all three cases, which would be dominated by the slower relaxation rate, we hypothesized the error in the model had to do with our interpretation of the slower relaxation event.

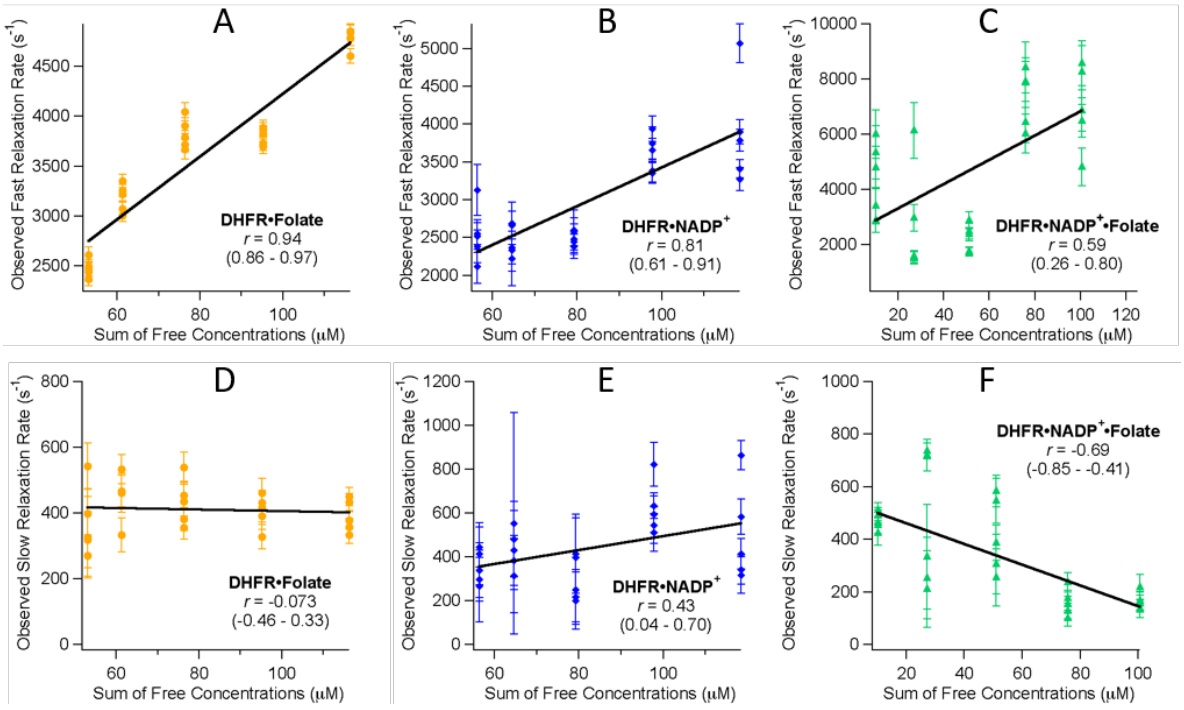

Figure 2. 5 Correlation plots detailing the linear correlation of the observed temperature-jump relaxation rates vs the sum of the free concentrations of enzyme and ligand. Plots A−C show the correlation of the observed faster relaxation rate. Plots D−F show the correlation of the observed slower relaxation rates. The linear correlation coefficient, r, is given in each plot along with the 95% confidence interval for each correlation coefficient given in parentheses.

We can learn more about the nature of each of the observed relaxation events by looking at their concentration dependence. If a relaxation rate is representative of a reaction that is a bimolecular reaction or coupled to a bimolecular reaction, then the relaxation rate should have a

positive linear correlation with the sum of the free concentrations of the bimolecular step.[32] If the fast and slow processes are sequential steps as postulated, we would expect to find some correlation between the sum of the free enzyme and ligand concentrations for both kinetic phases. In addition to the model presented in **Scheme 2. 1**, if we consider the alternative model of the conformational change preceding the binding event, as has been proposed by NMR studies,[19] the stepwise nature of the reaction would still induce a dependence on concentration for both steps, because they are coupled.[32] **Figure 2. 5** shows the correlation plots for both the fast and slow relaxation rates versus the sum of the free concentrations for all three DHFR complexes studied.

The correlation plots in **Figure 2. 5** reveal that all of the fast relaxation rates show a positive correlation with the sum of the free concentrations. The slow rates show a mixture of correlations where the folate binary complex seems to have no correlation, the $NADP^+$ binary complex has a positive correlation, and the tertiary complex has a negative correlation. The strength of the correlation is quantitatively represented by Pearson's product moment correlation coefficient, also known as the linear correlation coefficient r. r ranges from −1.0 to +1.0 and can be tested for significance at a given probability level. The correlation coefficient cutoff value for significance at a 99% confidence level for this data is 0.505 (DF = 23). This means that any r value whose absolute value is above 0.505 displays a significant correlation under this relatively strict standard.[40] The fast relaxation rates of all three complexes show a significant quantitative positive correlation. The entire 95% confidence interval of both of the binary plots meets this significance standard, while the tertiary complex's range does not. This is a strong indication that the faster event is either a bimolecular reaction step or is strongly coupled to one. For the slow rates, only the tertiary complex shows a significant correlation; however, because this r value is negative, it indicates a negative correlation between the relaxation rate and the sum of the free concentrations. A negative correlation is nonsensical and is equivalent to concluding the rates do not depend on the free

concentrations of enzymes and ligand. The correlation analysis gives us more evidence that the fast rate is related to ligand binding and that the slow rate is not. Thus, a kinetic model having sequential ligand binding and conformational rearrangement steps is not consistent with this analysis, regardless of the order of the steps.

While the fast relaxation event can be ascribed to the reversible ligand binding process, the molecular origin of the slow relaxation rate is not clear. Our probe method for this study is intrinsic tryptophan fluorescence. The fluorescence intensity can be altered by several mechanisms such as quenching interactions specific to enzyme conformation, interactions with the substrate, solvent accessibility, and coupling between tryptophans. Additionally, DHFR has five native tryptophans that are spread throughout the enzyme's structure (**Figure 2. 1**). This makes it hard to use this fluorophore to determine the origin of the observed signal change. One possible interpretation of a nonligand binding reaction pathway could be heat-induced protein conformational change. The temperature-jump technique does not necessarily induce a reaction along a reaction cycle-like pathway. Because an increase in temperature favors protein motion, the temperature-jump pulse could be altering the conformational space of the protein in addition to perturbing the ligand binding equilibrium. The heat-induced conformational change is likely not related to protein unfolding because the final temperature of the temperature jump was 36°C for all transients compared to the apoenzyme melting temperature of 49.3°C.[36] Because the binding of substrates tends to increase the thermal stability of the protein, the final temperature jump is even further below the melting temperatures of the protein complexes.[41] We can examine whether the slow event in the transients is related to a noncatalytic protein conformational change by comparison to the temperature-jump transient of the apoenzyme under similar conditions. **Figure 2. 6** shows the results of a temperature jump on the DHFR apoenzyme.

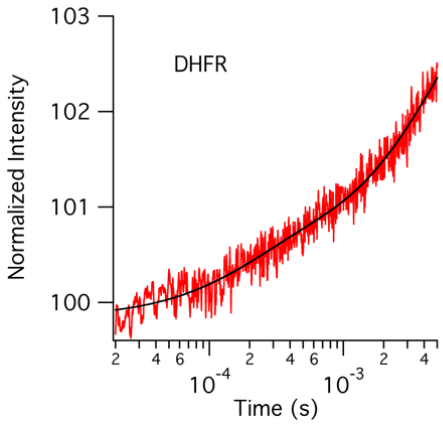

Figure 2. 6 Fluorescence temperature-jump transient of the DHFR apoenzyme. The protein concentration is 100 μM, and the temperature jump is from 29 to 36°C. These conditions mimic those of the enzyme complex transients shown in **Figure 2. 4**.

As can be seen by comparing **Figure 2. 4** and **Figure 2. 6**, the temperature-jump transient of the DHFR apoenzyme is distinct from the transients for the DHFR complexes with respect to both the amplitude and the lifetimes observed. The apoenzyme transient is best fit by a double-exponential curve with a fast rate of 5000 s^{-1} and a slow rate of 200 s^{-1} compared to the rates of 2000−4000 and 300−400 s^{-1} from the enzyme complexes. The temperature jump induces a smaller change in the fluorescence signal in the apoenzyme than in the enzyme complexes. The fast event from the enzyme complex transients has an amplitude change greater than or equal to that of the slower event, further supporting its assignment to ligand binding and dissociation. Conversely, the slower event is the dominant event in the apoenzyme transient. Interestingly, the slower event has a similar amplitude, approximately 2% of the initial intensity, in all four enzyme complexes studied (see **Table 2. 1** and **Table 2S. 2** Average Fit Relaxation Rates and Amplitudes for All Enzyme·Ligand Concentrations). It therefore seems reasonable to assign the slow event in all of the transients to a similar molecular event. The rate of the slower relaxation event depends on the presence and identity of a ligand bound to the enzyme. We therefore conclude that the observed

slower event is due primarily to a conformational rearrangement unrelated to progress along the reaction coordinate as shown in **Scheme 2. 2**.

Scheme 2. 2

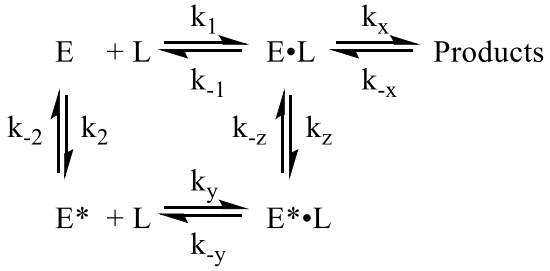

Because the fast rate is related to the ligand binding step and also not directly coupled to the slow rate, we can estimate the rate constants for binding and dissociation of the ligands using a simple two-state model. A linear fit to a plot of the fast rates versus the sum of the free concentrations of enzyme and ligand yields these rate constants. The slope of the line is equivalent to the binding rate constant (k_{on}), and the y-intercept is equivalent to the dissociation rate constant (k_{off}).[32] These plots have already been presented in **Figure 2. 5 A–C**. We present the slopes and y-intercepts as these rate constants in **Table 2. 2**. The values we obtain from this analysis for k_{on} of the two binary complexes is similar to what has been reported in the literature previously (57 ± 5 μM^{-1} s^{-1} for DHFR·folate[34] and 13 μM^{-1} s^{-1} for DHFR·$NADP^+$[42]). We are not aware of a similar measurement for the ternary complex studied here; however, the value of k_{on} for the normal substrate dihydrofolate binding to the holoenzyme complex is reported as 5 μM^{-1} s^{-1}.[42] The order of magnitude difference here might be explained by the difference in cofactor oxidation state and substrate. The k_{off} values are more surprising. k_{off} values for substrates of DHFR have been calculated to be in the range of 1–70 s^{-1}, with the exception being $NADP^+$ having a k_{off} value of

200−300 s^{-1}.[34, 42-43] We observe significantly faster values for k_{off}. This difference may be due to the higher time resolution of the temperature-jump measurement, because previous experiments have relied on stopped-flow mixing and may have been limited by the dead time of the measurement. It may also be due to the model, because it approximates the fast kinetic phase as a two- state reversible binding event. However, the substrate binding/ dissociation relaxation kinetics is convolved with an additional, unresolved loop motion step, which probably affects the observed rate. Additional evidence of this interpretation is the higher k_{off} determined for the ternary complex, for which the Met20 loop motion should have the greatest contribution to the observed relaxation rate. The inability to resolve the loop motion step is not due to the temporal resolution of the temperature-jump experiment but instead is likely due to the insensitivity of the Trp fluorescence to loop conformation. A more specific fluorescence probe would aid in sorting out this interesting observation.

Table 2. 2 Rate Constants for Ligand Binding and Dissociation Determined from Temperature-Jump Measurements

	DHFR•folate	**DHFR•$NADP^+$**	**DHFR•$NADP^+$•folate**
k_{on} **(μM^{-1} s^{-1})**	31 ± 2	26 ± 4	40 ± 10
k_{off} **(s^{-1})**	1100 ± 200	900 ± 300	2400 ± 800

This work was motivated by the question of how conformational rearrangements of DHFR are linked to ligand binding and dissociation. The apoenzyme and the three different enzyme−ligand complexes chosen for this study represent different parts of the DHFR reaction cycle, having different loop conformations. Using time-resolved fluorescence temperature-jump spectroscopy, we

observed two relaxation events. Upon analyzing the fast relaxation rate, we determine that there is likely an additional conformational change that is coupled to ligand association and dissociation. However, a more direct method for probing protein dynamics with specificity that is better than that of intrinsic tryptophan fluorescence will be required to separate the loop motion dynamics from the ligand binding event, to more fully understand the nature of conformational changes in DHFR. For example, the loop conformations could be probed using the reduced cofactor absorbance or fluorescence or by one of the site-specific labeled DHFR variants that have been reported in the literature but have not been applied to kinetics on this time scale.[44-47]

The slow off-pathway conformational rearrangement can be interpreted as evidence of conformational selection as a mechanism for ligand binding. The millisecond conformational fluctuations observed using Trp fluorescence are not coupled to the binding event as would be expected for an induced fit model of ligand binding. The presence of the slow event regardless of ligand state suggests that it corresponds to fluctuations of the protein that would be necessary for the conformational search process. Finally, the dependence of the rate of the slow event on the ligand identity is consistent with a ligand-dependent population shift to a favored conformation, consistent with previous NMR results.[38]

Direct evidence of how loop motions couple to steps along the reaction pathway remains elusive. Our data suggest that there is a conformational rearrangement coupled to the ligand binding steps, but additional kinetic studies are necessary with site-specific probes to confirm these findings. Numerous studies of DHFR mutants or ligand complexes have compared equilibrium structures and their fluctuations using X-ray crystallography, NMR spectroscopy, and molecular dynamics simulations. While these studies are important because they serve to indicate regions of the structure where motions likely play a role in catalysis, they do not directly establish the connection between specific protein motions and progress along the reaction coordinate. We believe the emphasis placed

on the conformational flexibility of key loops in DHFR by these studies is key for understanding the role of enzyme dynamics in DHFR catalysis; however, our data indicate that not all observed motions are due to an effect on the reaction pathway. Thus, our results serve as an additional caution that claims about DHFR flexibility and catalysis need to be supported by direct observation of coupling between specific protein motions and progress along the reaction pathway.

2.5 Supplemental Information

ITC Methods

The association constant, ΔH, and ΔS for folate binding to the binary complex DHFR:$NADP^+$ were determined using isothermal titration calorimetry (ITC) on an VP-ITC microcalorimeter from MicroCal (Northampton, MA). Folate (1.3 mM) was added to the reduced cofactor binary complex (50 μM DHFR , 500 μM $NADP^+$) in 3 μL increments at 25°C. After each injection the system was allowed to equilibrate for 200 seconds. The buffer used was the same as in the equilibrium fluorescence and temperature jump fluorescence experiments (50 mM sodium phosphate, 100 mM NaCl, pH 7). The data was analyzed using the OneSites model in MicroCal's Origin based VP-ITC software (**Figure 2S. 1** and **Figure 2S. 2**).

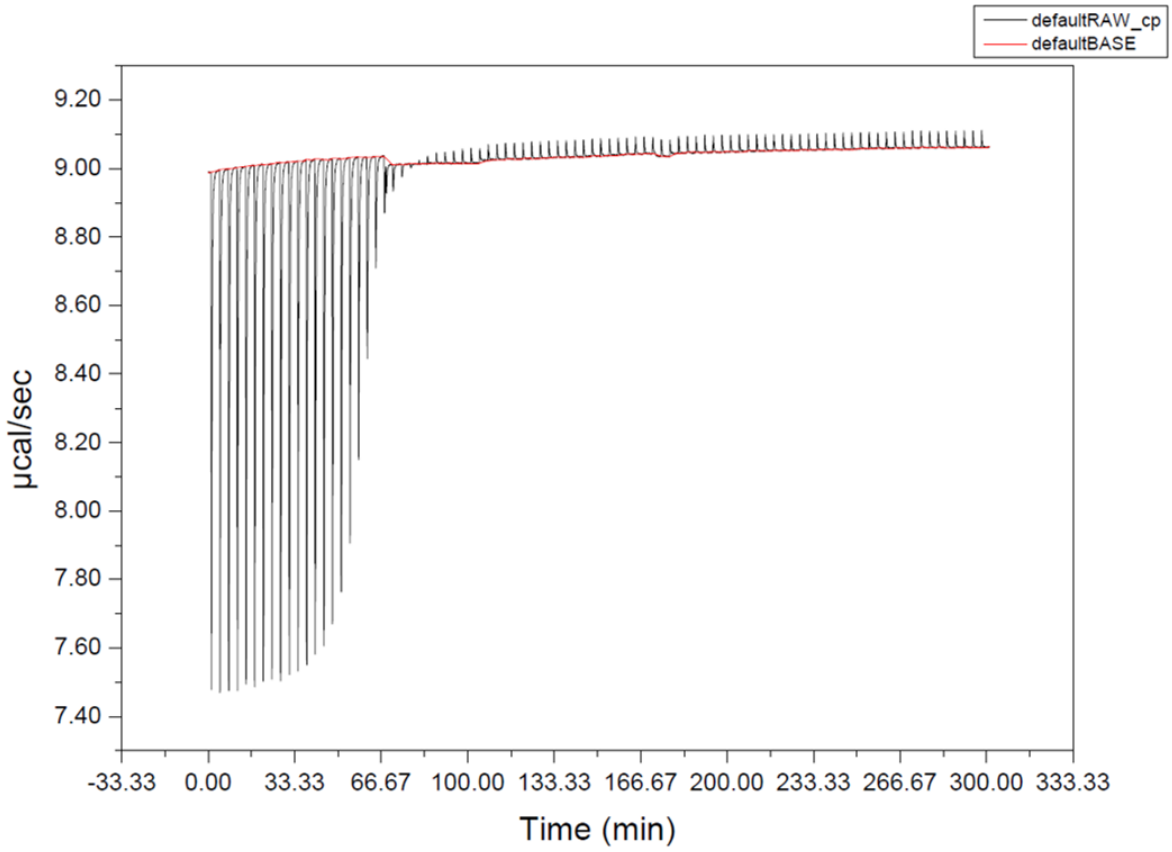

Figure 2S. 1 Raw ITC data for the binding of folate to DHFR•$NADP^+$. Each peak represents a 3 µL injection of a 1.3 mM folate sample into a 1.4 mL sample of initially 50 µM DHFR and 500 µM $NADP^+$.

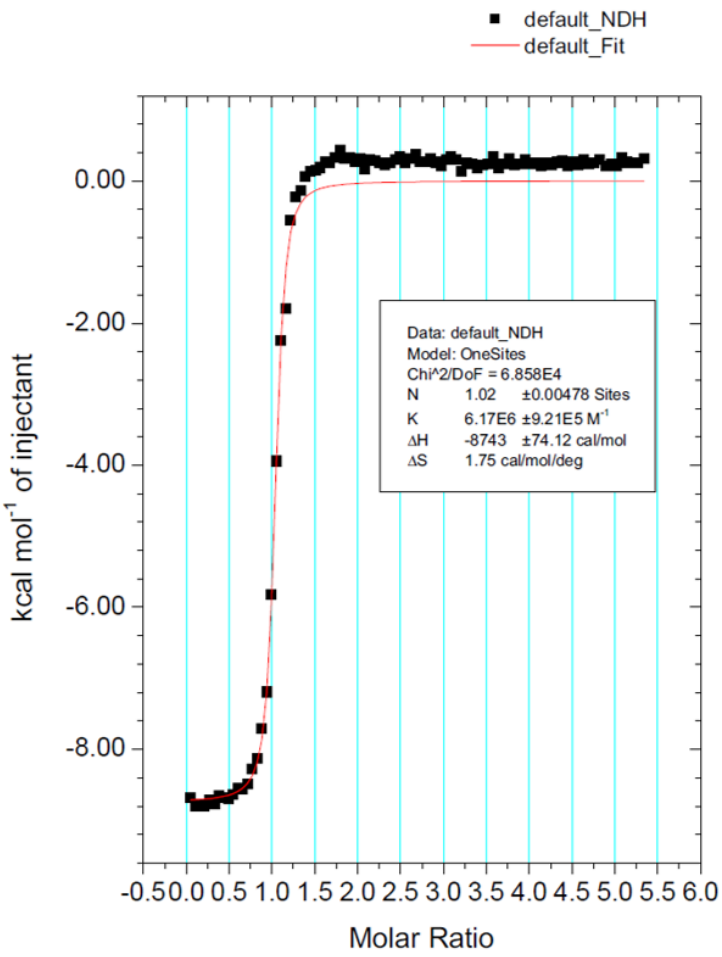

Figure 2S. 2 Processed ITC data for the binding of folate to DHFR·$NADP^+$. Each peak represents a 3 µL injection of a 1.3 mM folate sample into a 1.4 mL sample of initially 50 µM DHFR and 500 µM $NADP^+$. The figure also shows the results of an OneSite model analysis by MicroCal's Origin based VP-ITC software.

Table 2S. 1 Thermodynamic Constants of Ligands Binding to DHFR from Isothermal Titration Calorimetry at 298 K

Complex	**ΔH (kcal/mol)**	**TΔS (kcal/mol)**
Folate binding to DHFR	-11.7[a]	- 4.43[a]
$NADP^+$ binding to DHFR	-20.7[a]	-13.2[a]
Folate binding to DHFR·$NADP^+$	-8.74	0.522

[a] These values came from Grubbs et al. ref 39

Table 2S. 2 Average Fit Relaxation Rates and Amplitudes for All Enzyme·Ligand Concentrations

	Slow Rate (s^{-1})	**Slow Rate Amplitude**	**Fast Rate (s^{-1})**	**Fast Rate Amplitude**
DHFR•folate				
100 μM, 100 μM	400 ± 100	2.2 ± 0.4	2500 ± 90	5 ± 1
100 μM, 125 μM	450 ± 50	2.6 ± 0.2	3200 ± 100	6.3 ± 0.3
100 μM, 150 μM	400 ± 70	2.7 ± 0.3	3800 ± 200	4.9 ± 0.5
100 μM, 175 μM	410 ± 50	2.6 ± 0.2	3800 ± 80	5.2 ± 0.2
100 μM, 200 μM	390 ± 50	3.31 ± 0.09	4800 ± 100	5.5 ± 0.4
DHFR•$NADP^+$				
100 μM, 100 μM	350 ± 80	1.5 ± 0.2	2500 ± 400	1.9 ± 0.5
100 μM, 125 μM	430 ± 90	1.0 ± 0.4	2500 ± 200	1.8 ± 0.4
100 μM, 150 μM	300 ± 100	1.2 ± 0.2	2500 ± 91	2.0 ± 0.2
100 μM, 175 μM	600 ± 100	1.7 ± 0.2	3600 ± 200	2.9 ± 0.2
100 μM, 200 μM	500 ± 200	1.7 ± 0.2	3900 ± 700	2.7 ± 0.3
DHFR•$NADP^+$•folate				
100 μM, 1000 μM, 100 μM	470 ± 30	2.8 ± 0.1	4000 ± 1000	0.6 ± 0.1
100 μM, 1000 μM, 125 μM	500 ± 300	2.5 ± 0.7	3000 ± 2000	1.6 ± 0.7
100 μM, 1000 μM, 150 μM	400 ± 100	2.4 ± 0.2	2200 ± 500	1.8 ±0.5
100 μM, 1000 μM, 175 μM	160 ± 60	3.1 ± 0.8	7000 ± 1000	0.59 ± 0.06
100 μM, 1000 μM, 200 μM	170 ± 30	2.6 ± 0.6	7000 ± 2000	0.62 ± 0.08
DHFR apoenzyme				
100 μM	240 ± 40	2.3 ± 0.5	5000 ± 1000	0.6 ± 0.08

Analysis of Temperature Jump Data Assuming Scheme 1

To analyze the temperature-jump data assuming **Scheme 2. 1**, graphs of the sum of the fast and slow reaction rates versus the sum of the free concentrations and the product of the fast and slow reactions versus the sum of the free concentrations for each of the enzyme complexes studied were made. These plots are given in Figure S3 below. The figure also displays the linear regression line for each data set. The linear fit parameters can be transformed into rate constants for Scheme 1 by the Equations 1-4, from the paper, where m_S and b_S is the slope and intercept of the plot of the sum of rates, and m_P and b_P is the slope and intercept of the product of the rates, respectively. Performing this analysis yields the proposed rate constants given in Table S1. It can be seen by inspection that this analysis is nonsensical because at least one rate constant for each complex is negative. This is one of the reasons we justified rejecting **Scheme 2. 1**.

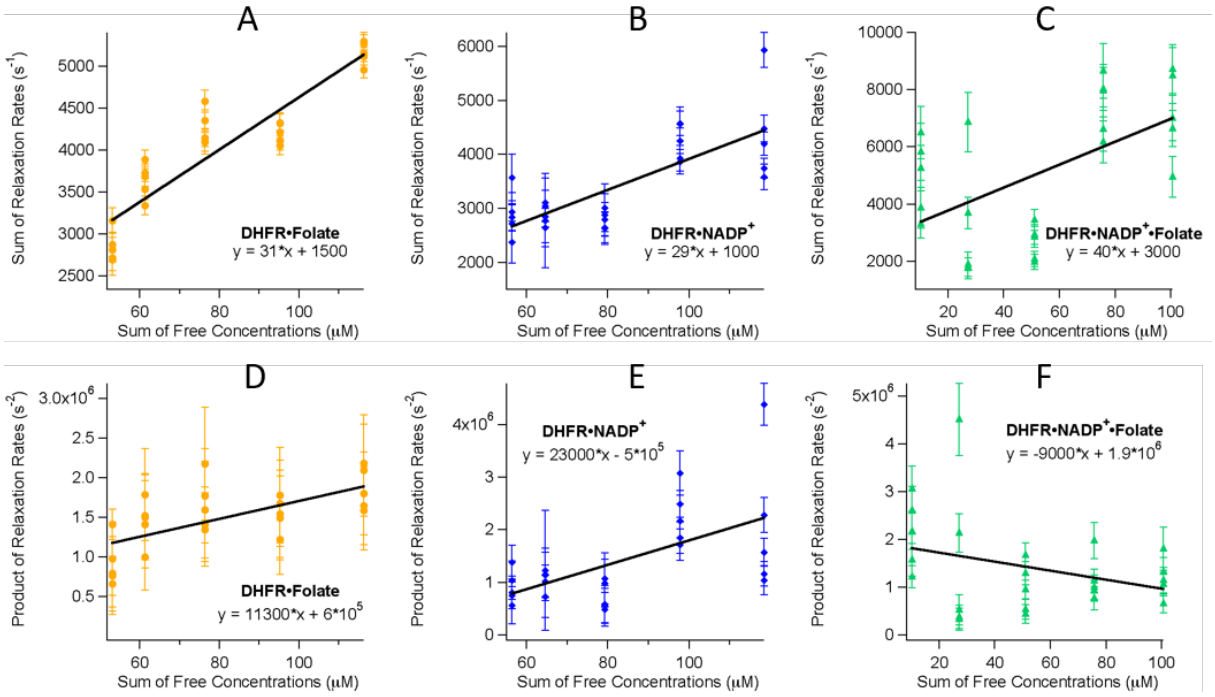

Figure 2S. 3 Graphs for analyzing the temperature-jump transients and the applicability of Scheme 1. Plots A, B, and C show the sum of the observed relaxation rates versus the sum of the free concentrations. Plots D, E, and F show the product of the observed relaxation rates versus the sum of the free concentrations. The linear regression fit is also shown as a black line and its fit equation given.

Table 2S. 3 Proposed Rate Constants for Scheme 1 (When Calculated with Error)

	DHFR•Folate	**DHFR•NADP$^+$**	**DHFR•NADP$^+$•Folate**
k_1 ($M^{-1}s^{-1}$)	31 ± 3	29 ± 5	40 ± 10
k_{-1} (s^{-1})	1100 ± 300	240 ± 500	3200 ± 800
k_2 (s^{-1})	-100 ± 400	3000 ± 5000	-800 ± 1000
k_{-2} (s^{-1})	500 ± 200	-2000 ± 5000	600 ± 200

2.6 References

1. Gulotta, M.; Deng, H.; Deng, H.; Dyer, R. B.; Callender, R. H., Toward an understanding of the role of dynamics on enzymatic catalysis in lactate dehydrogenase. *Biochemistry* **2002,** *41* (10), 3353-63.

2. Callender, R.; Dyer, R. B., The dynamical nature of enzymatic catalysis. *Acc Chem Res* **2015,** *48* (2), 407-13.

3. Bhabha, G.; Lee, J.; Ekiert, D. C.; Gam, J.; Wilson, I. A.; Dyson, H. J.; Benkovic, S. J.; Wright, P. E., A dynamic knockout reveals that conformational fluctuations influence the chemical step of enzyme catalysis. *Science* **2011,** *332* (6026), 234-8.

4. Cameron, C. E.; Benkovic, S. J., Evidence for a functional role of the dynamics of glycine-121 of Escherichia coli dihydrofolate reductase obtained from kinetic analysis of a site-directed mutant. *Biochemistry* **1997,** *36* (50), 15792-800.

5. *Dynamics in Enzyme Catalysis*. 1st ed.; Springer: New York, 2013.

6. Benkovic, S. J.; Hammes-Schiffer, S., A perspective on enzyme catalysis. *Science* **2003,** *301* (5637), 1196-202.

7. Oyen, D.; Fenwick, R. B.; Stanfield, R. L.; Dyson, H. J.; Wright, P. E., Cofactor-Mediated Conformational Dynamics Promote Product Release From Escherichia coli Dihydrofolate Reductase via an Allosteric Pathway. *J Am Chem Soc* **2015,** *137* (29), 9459-68.

8. Klinman, J. P., An integrated model for enzyme catalysis emerges from studies of hydrogen tunneling. *Chem Phys Lett* **2009,** *471* (4-6), 179-193.

9. Klinman, J. P.; Kohen, A., Hydrogen tunneling links protein dynamics to enzyme catalysis. *Annu Rev Biochem* **2013,** *82*, 471-96.

10. Hammes-Schiffer, S.; Benkovic, S. J., Relating protein motion to catalysis. *Annu Rev Biochem* **2006,** *75*, 519-41.

11. Rajagopalan, P. T.; Benkovic, S. J., Preorganization and protein dynamics in enzyme catalysis. *Chem Rec* **2002,** *2* (1), 24-36.

12. Reddish, M. J.; Peng, H. L.; Deng, H.; Panwar, K. S.; Callender, R.; Dyer, R. B., Direct evidence of catalytic heterogeneity in lactate dehydrogenase by temperature jump infrared spectroscopy. *J Phys Chem B* **2014,** *118* (37), 10854-62.

13. Pushie, M. J.; George, G. N., Active-site dynamics and large-scale domain motions of sulfite oxidase: a molecular dynamics study. *J Phys Chem B* **2010,** *114* (9), 3266-75.

14. Bandaria, J. N.; Dutta, S.; Nydegger, M. W.; Rock, W.; Kohen, A.; Cheatum, C. M., Characterizing the dynamics of functionally relevant complexes of formate dehydrogenase. *Proc Natl Acad Sci U S A* **2010,** *107* (42), 17974-9.

15. Eisenmesser, E. Z.; Bosco, D. A.; Akke, M.; Kern, D., Enzyme dynamics during catalysis. *Science* **2002,** *295* (5559), 1520-3.

16. Eisenmesser, E. Z.; Millet, O.; Labeikovsky, W.; Korzhnev, D. M.; Wolf-Watz, M.; Bosco, D. A.; Skalicky, J. J.; Kay, L. E.; Kern, D., Intrinsic dynamics of an enzyme underlies catalysis. *Nature* **2005,** *438* (7064), 117-21.

17. Newby, Z.; Lee, T. T.; Morse, R. J.; Liu, Y.; Liu, L.; Venkatraman, P.; Santi, D. V.; Finer-Moore, J. S.; Stroud, R. M., The role of protein dynamics in thymidylate synthase catalysis: variants of conserved 2'-deoxyuridine 5'-monophosphate (dUMP)-binding Tyr-261. *Biochemistry* **2006,** *45* (24), 7415-28.

18. Liu, C. T.; Wang, L.; Goodey, N. M.; Hanoian, P.; Benkovic, S. J., Temporally overlapped but uncoupled motions in dihydrofolate reductase catalysis. *Biochemistry* **2013,** *52* (32), 5332-4.

19. Boehr, D. D.; Nussinov, R.; Wright, P. E., The role of dynamic conformational ensembles in biomolecular recognition. *Nat Chem Biol* **2009,** *5* (11), 789-96.

20. Sawaya, M. R.; Kraut, J., Loop and subdomain movements in the mechanism of Escherichia coli dihydrofolate reductase: crystallographic evidence. *Biochemistry* **1997,** *36* (3), 586-603.

21. Boekelheide, N.; Salomon-Ferrer, R.; Miller, T. F., 3rd, Dynamics and dissipation in enzyme catalysis. *Proc Natl Acad Sci U S A* **2011,** *108* (39), 16159-63.

22. Oyeyemi, O. A.; Sours, K. M.; Lee, T.; Resing, K. A.; Ahn, N. G.; Klinman, J. P., Temperature dependence of protein motions in a thermophilic dihydrofolate reductase and its relationship to catalytic efficiency. *Proc Natl Acad Sci U S A* **2010,** *107* (22), 10074-9.

23. Alakent, B.; Baskan, S.; Doruker, P., Effect of ligand binding on the intraminimum dynamics of proteins. *J Comput Chem* **2011,** *32* (3), 483-96.

24. Fan, Y.; Cembran, A.; Ma, S.; Gao, J., Connecting protein conformational dynamics with catalytic function as illustrated in dihydrofolate reductase. *Biochemistry* **2013,** *52* (12), 2036-49.

25. Tuttle, L. M.; Dyson, H. J.; Wright, P. E., Side-chain conformational heterogeneity of intermediates in the Escherichia coli dihydrofolate reductase catalytic cycle. *Biochemistry* **2013,** *52* (20), 3464-77.

26. Radkiewicz, J. L.; Brooks, C. L., Protein Dynamics in Enzymatic Catalysis: Exploration of Dihydrofolate Reductase. *Journal of the American Chemical Society* **2000,** *122* (2), 225-231.

27. Cammarata, M. B.; Thyer, R.; Rosenberg, J.; Ellington, A.; Brodbelt, J. S., Structural Characterization of Dihydrofolate Reductase Complexes by Top-Down Ultraviolet Photodissociation Mass Spectrometry. *J Am Chem Soc* **2015,** *137* (28), 9128-35.

28. Mauldin, R. V.; Lee, A. L., Nuclear magnetic resonance study of the role of M42 in the solution dynamics of Escherichia coli dihydrofolate reductase. *Biochemistry* **2010,** *49* (8), 1606-15.

29. Lamb, K. M.; N, G. D.; Wright, D. L.; Anderson, A. C., Elucidating features that drive the design of selective antifolates using crystal structures of human dihydrofolate reductase. *Biochemistry* **2013,** *52* (41), 7318-26.

30. Feeney, J.; Birdsall, B.; Kovalevskaya, N. V.; Smurnyy, Y. D.; Navarro Peran, E. M.; Polshakov, V. I., NMR structures of apo L. casei dihydrofolate reductase and its complexes with trimethoprim and NADPH: contributions to positive cooperative binding from ligand-induced refolding, conformational changes, and interligand hydrophobic interactions. *Biochemistry* **2011,** *50* (18), 3609-20.

31. Callender, R.; Dyer, R. B., Advances in time-resolved approaches to characterize the dynamical nature of enzymatic catalysis. *Chem Rev* **2006,** *106* (8), 3031-42.

32. Bernasconi, C. F., *Relaxation Kinetics*. Academic Press: New York, 1976.

33. Davis, C. M.; Dyer, R. B., WW domain folding complexity revealed by infrared spectroscopy. *Biochemistry* **2014,** *53* (34), 5476-84.

34. Posner, B. A.; Li, L.; Bethell, R.; Tsuji, T.; Benkovic, S. J., Engineering specificity for folate into dihydrofolate reductase from Escherichia coli. *Biochemistry* **1996,** *35* (5), 1653-63.

35. Ohmae, E.; Kurumiya, T.; Makino, S.; Gekko, K., Acid and thermal unfolding of Escherichia coli dihydrofolate reductase. *J Biochem* **1996,** *120* (5), 946-53.

36. Gekko, K.; Yamagami, K.; Kunori, Y.; Ichihara, S.; Kodama, M.; Iwakura, M., Effects of point mutation in a flexible loop on the stability and enzymatic function of Escherichia coli dihydrofolate reductase. *J Biochem* **1993,** *113* (1), 74-80.

37. Ionescu, R. M.; Smith, V. F.; O'Neill, J. C., Jr.; Matthews, C. R., Multistate equilibrium unfolding of Escherichia coli dihydrofolate reductase: thermodynamic and spectroscopic description of the native, intermediate, and unfolded ensembles. *Biochemistry* **2000,** *39* (31), 9540-50.

38. Boehr, D. D.; McElheny, D.; Dyson, H. J.; Wright, P. E., The dynamic energy landscape of dihydrofolate reductase catalysis. *Science* **2006,** *313* (5793), 1638-42.

39. Grubbs, J.; Rahmanian, S.; DeLuca, A.; Padmashali, C.; Jackson, M.; Duff, M. R., Jr.; Howell, E. E., Thermodynamics and solvent effects on substrate and cofactor binding in Escherichia coli chromosomal dihydrofolate reductase. *Biochemistry* **2011,** *50* (18), 3673-85.

40. Kobayashi, K., *A Handbook of Applied Statistics in Pharmacology*. CRC Press/Taylor Francis Group: Boca Raton, FL, 2012.

41. Sasso, S.; Protasevich, I.; Gilli, R.; Makarov, A.; Briand, C., Thermal denaturation of bacterial and bovine dihydrofolate reductases and their complexes with NADPH, trimethoprim and methotrexate. *J Biomol Struct Dyn* **1995,** *12* (5), 1023-32.

42. Fierke, C. A.; Johnson, K. A.; Benkovic, S. J., Construction and evaluation of the kinetic scheme associated with dihydrofolate reductase from Escherichia coli. *Biochemistry* **1987,** *26* (13), 4085-92.

43. Cayley, P. J.; Dunn, S. M.; King, R. W., Kinetics of substrate, coenzyme, and inhibitor binding to Escherichia coli dihydrofolate reductase. *Biochemistry* **1981,** *20* (4), 874-9.

44. Chen, S.; Wang, L.; Fahmi, N. E.; Benkovic, S. J.; Hecht, S. M., Two pyrenylalanines in dihydrofolate reductase form an excimer enabling the study of protein dynamics. *J Am Chem Soc* **2012,** *134* (46), 18883-5.

45. Chen, S.; Fahmi, N. E.; Wang, L.; Bhattacharya, C.; Benkovic, S. J.; Hecht, S. M., Detection of dihydrofolate reductase conformational change by FRET using two fluorescent amino acids. *J Am Chem Soc* **2013,** *135* (35), 12924-7.

46. Antikainen, N. M.; Smiley, R. D.; Benkovic, S. J.; Hammes, G. G., Conformation coupled enzyme catalysis: single-molecule and transient kinetics investigation of dihydrofolate reductase. *Biochemistry* **2005,** *44* (51), 16835-43.

47. Liu, C. T.; Layfield, J. P.; Stewart, R. J., 3rd; French, J. B.; Hanoian, P.; Asbury, J. B.; Hammes-Schiffer, S.; Benkovic, S. J., Probing the electrostatics of active site microenvironments along the catalytic cycle for Escherichia coli dihydrofolate reductase. *J Am Chem Soc* **2014,** *136* (29), 10349-60.

Chapter 3:

Site-specific Tryptophan Labels Reveal Local Millisecond Motions of Dihydrofolate Reductase

Vaughn, M. B., Biren, C., Li, Q. and Dyer, R. B.

3.1 Abstract

Escherichia coli dihydrofolate reductase (DHFR) is a small, flexible enzyme that is often used as an model system for understanding enzyme dynamics. Recently, native tryptophan fluorescence was used as a probe to study micro- to millisecond dynamics of DHFR. Consequently, the origin of the observed conformational changes could not be assigned to a specific region within the enzyme. Here, we use DHFR mutants, each with a single tryptophan as a probe for temperature jump fluorescence spectroscopy, to further inform our understanding of DHFR dynamics. The equilibrium tryptophan fluorescence of the mutants shows that each tryptophan is in a different environment and that wildtype DHFR fluorescence is not a simple summation of all the individual tryptophan fluorescence signatures, likely due to excimer coupling between two of the tryptophan residues. Additionally, each mutant exhibits a slow conformational change that is independent of ligand association and dissociation, similar to the wildtype enzyme. However, the relaxation rate depends on the location of the tryptophan within the enzyme, supporting the conclusion that the tryptophan fluorescence dynamics do not originate from a single collective motion, but instead report on local motions throughout the enzyme.

3.2 Introduction

Enzyme dynamics across all timescales are important for enzymatic catalysis. Conformational changes and protein motions have been implicated in every step of catalysis from crossing the barrier of the chemistry step on the femtosecond timescale to rotating whole domains on the order of milliseconds.[1] Dihydrofolate reductase (DHFR) is a classic model for studying enzyme dynamics and remains an active area of research.[2-7] DHFR is a small flexible enzyme with multiple mobile loops. The Met20 loop changes conformation throughout the catalytic cycle: closed in the substrate bound complexes and occluded in the product bound complexes.[8]

Figure 3. 1 Crystal structure (PDB: 1RX2) of wildtype *E. coli* DHFR (blue) with $NADP^+$ cofactor (yellow) and folate (green). The five native tryptophans are labeled and shown in magenta.

While documenting the Met20 loop conformations and interpreting the purpose of those conformational changes has been a subject of great scrutiny,[2, 5, 7, 9-10] other conformational changes

have been recently observed using temperature jump (T-jump) fluorescence spectroscopy.[11] These motions are uncoupled to ligand binding processes and were observed on the millisecond timescale using native tryptophan (trp) fluorescence as a probe. *E. coli* DHFR has five native tryptophans (W22, W30, W47, W74, W133) located throughout the enzyme, as shown in **Figure 3. 1**. W22 is located on the Met20 loop, W133 is located on the FG loop, W30 is near the substrate binding site, and W47 and W74 are close together but removed from the active site. Because wildtype DHFR (wt-DHFR) has multiple tryptophans, the previous study could not identify the origin of the observed slow conformational change.

Here, we characterize the equilibrium fluorescence and T-jump dynamics of DHFR mutants, each with a single tryptophan residue (denoted as midW mutants). We found that all midW mutants exhibited biphasic relaxation rates similar to wt-DHFR with a concentration dependent fast relaxation rate and a concentration independent slow relaxation rate. Notably, the slow relaxation rate of the midW mutants differs based on the location of the trp probe within the enzyme and are generally faster than the slow event observed in wt-DHFR. This evidence supports the conclusion that the observed relaxation rate in wt-DHFR likely arises from conformational changes that modulate the tryptophan interactions and that individual tryptophan residues report on local motions.

3.3 Experimental Methods

Mutant DHFR plasmid generation, protein expression, and purification

C-terminal six histidine-tagged DHFR midW mutant plasmids were generated via the Custom Cloning Division within the Emory Integrated Genomics Core. In each midW mutant all but one of the native tryptophans were mutated to phenylalanine. The prefix "mid" is old English for with; thus, midW22 is the DHFR mutant containing W22 with all other tryptophans mutated to phenylalanine. The midW mutants were expressed and purified as described for wildtype DHFR in

the previous chapter.[11] Briefly, BL21 (DE3) *E. coli* competent cells were transformed with the midW mutant plasmids, grown with 100 μg/mL ampicillin, induced with 1 mM isopropyl β-D-thiogalactopyranoside (IPTG) overnight, and harvested by centrifugation. The pelleted cells were lysed by sonication and the insoluble debris was removed by centrifugation. The supernatant was purified by loading on a HisPrep affinity column and washed to remove protein contaminants as well as endogenous NADPH. Finally, the midW protein was eluted with 500 mM imidazole, buffer exchanged, concentrated, and stored at -80°C. Protein concentration was determined by absorbance at 280 nm with a predicted molar extinction coefficient[12] of 10,810 M^{-1} cm^{-1}. MidW mutants retained 20 – 90% of the wildtype activity as shown in the supplemental information section.

Equilibrium Fluorescence

Equilibrium fluorescence measurements of wt-DHFR apoenzyme and the midW mutants with their corresponding complexes (apoenzyme, E·Folate, E·$NADP^+$, and E·$NADP^+$·Folate) were taken on a Horiba (Japan) Dual-Fl spectrofluorometer. Spectra were obtained by exciting with 280 nm light, corresponding to tryptophan absorbance. Each sample contained 3 μM of enzyme in phosphate buffer (50 mM sodium phosphate, 100 mM NaCl, pH 7). Samples included 6 μM of the appropriate ligands for the two binary complexes. For the tertiary complex, both 6 μM folate and $NADP^+$ were present. Spectra were collected in triplicate and were averaged together. To compare changes in fluorescence intensities between complexes, the entirety of the trp fluorescence peaks were integrated. The integrated intensities of the enzyme·ligand complexes of each mutant are reported as a percentage of the corresponding apoenzyme fluorescence intensity. Additionally, temperature dependent fluorescence spectra were collected from 12°C to 45°C in increments of 3°C. The trp fluorescence was integrated between 327 nm and 353 nm, which corresponds to the

bandpass filter used in the temperature jump experiments. The resulting intensities were normalized to 1 with respect to the lowest temperature measured and the intrinsic temperature dependence of tryptophan was subtracted. These results are presented as change in fluorescence intensity.

Temperature Jump Fluorescence Spectroscopy

Temperature jump fluorescence transients were collected and analyzed as described in the previous chapter.[11] Briefly, the temperature jump was induced via a 2.09 μm, ~10 ns laser pulse at 12.5 Hz. The changes in trp fluorescence were probed by exciting the sample with 280 nm light, focusing the emission through a bandpass filter (327 nm – 353 nm), and measuring the intensity with a photomultiplier tube. The temperature jumps reported here are from 29°C to 36°C, well below the melting temperatures of the midW mutants which range from 42°C to 49°C (data not shown). The phosphate buffer that was used for the equilibrium fluorescence experiments was D_2O exchanged for T-jump use. The samples all contained 100 μM enzyme with varying concentrations of folate, up to 200 μM. The intrinsic temperature dependence of tryptophan was subtracted from each transient using approximately 200 μM free tryptophan as a reference. Then, the corrected fluorescence transients were normalized to 100 by dividing the entire transient by its initial fluorescence intensity, effectively reporting percent change in fluorescence intensity over time.

3.4 Results and Discussion

The tryptophan fluorescence spectra of all five midW mutants were measured for four different enzyme·ligand complexes: apoenzyme, E·Folate, E·$NADP^+$, and E·$NADP^+$·Folate. The fluorescence intensity of each midW mutant was much less than the wildtype enzyme, as expected since the midW mutants each contain only one tryptophan whereas wt-DHFR contains 5 tryptophans. As shown in **Figure 3. 2 A**, the intensity of trp fluorescence of each midW mutant

differs, with midW74 exhibiting the greatest fluorescence intensity, followed by midW30, midW47, midW133, and midW22 with the lowest fluorescence intensity. Additionally, the shift in trp fluorescence between midW mutants shows that the trp in each mutant is in a different environment. Typically, a blue shift indicates a more hydrophobic environment and tends to be concomitant with an increase in fluorescence intensity. A red shift indicates a more hydrophilic environment, which usually corresponds with a decrease in fluorescence intensity. Interestingly, the trp fluorescence of the midW mutants does not necessarily follow these trends. For example, midW47 and midW133 are blue shifted compared to midW74 and midW30, yet midW47 and midW133 display lower fluorescence intensities. This indicates that there must be some quenching interactions with W47 and W133 in the apoenzyme. Additionally, there are likely quenching interactions at position 22, given that midW22 exhibits a similar shift compared to midW74 and midW30. The similar shift suggests a similar environment; however, midW22 trp fluorescence is drastically reduced.

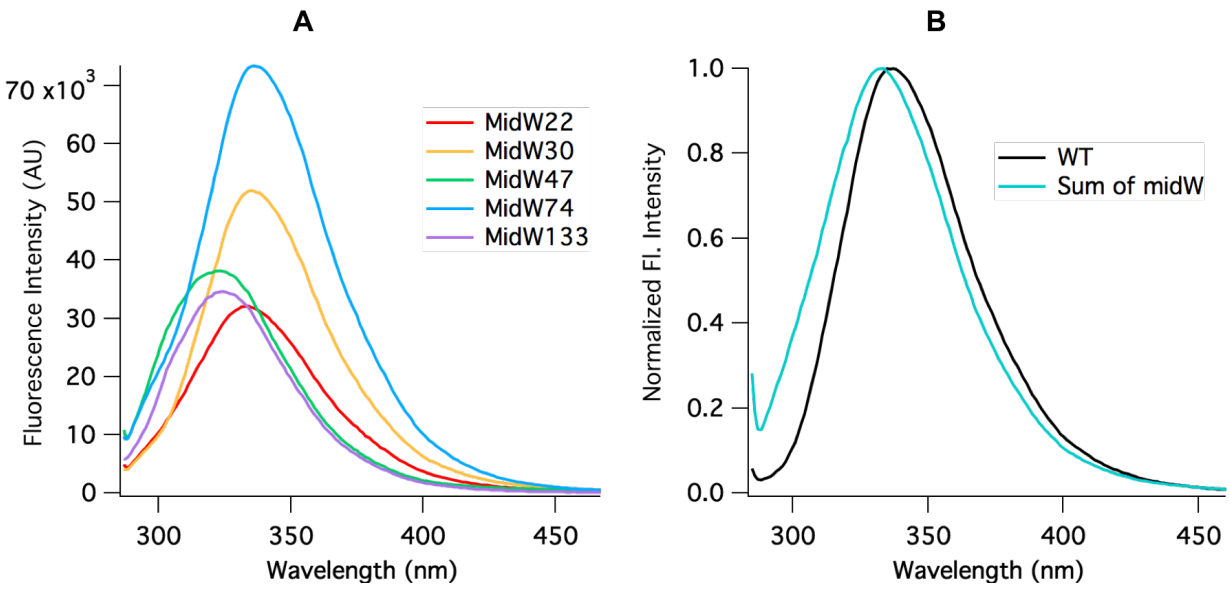

Figure 3. 2 A) Trp fluorescence of the apoenzymes of the five midW mutants. Differences in fluorescence intensity and shift indicate that each tryptophan is in a unique environment. **B)** Wt-DHFR trp fluorescence spectrum and the summation of the midW mutants' fluorescence spectra. Wt-DHFR has a much greater fluorescence intensity than the individual midW mutants combined. The intensities have been normalized to 1 here to better demonstrate the blue shift of the summed spectra compared to the wildtype spectrum. This data shows that the wt-DHFR trp fluorescence is not a simple linear combination of each individual tryptophan's fluorescence.

Figure 3. 2 B compares the wt-DHFR trp fluorescence spectrum to the sum of the trp fluorescence spectra of the midW mutants. The intensities have been normalized to 1 to better demonstrate the difference in lambda max between the two spectra. The difference in the spectra shows that the wt-DHFR trp fluorescence is not a simple linear combination of the individual tryptophans' fluorescence. This has been observed previously, albeit in a less direct manner by Ohmae et al. where a single tryptophan was mutated to various hydrophobic residues.[13] They

observed that the trp fluorescence decreased in varying amounts depending on which tryptophan was mutated. In this way, they came to the same conclusion as stated above. Furthermore, W47 and W74 are known to form an excimer pair.[13] Typically, the emission of the excimer is red shifted compared to the emission of the fluorescent monomers, which may contribute to the observed red shift of the wildtype DHFR fluorescence compared to the sum of the midW mutants' fluorescence.

Two patterns emerge when the trp fluorescence of the midW mutant ligand complexes are compared. **Figure 3. 3 A** shows the midW22 mutant complexes, which exhibits the same trend as all the other mutants except midW47, which is shown in panel B. **Table 3. 1** shows the integrated fluorescence intensity of each complex as a percentage of the apoenzyme fluorescence intensity. MidW22 and the other three midW mutants (midW30, midW74, and midW133) show very little change upon binding $NADP^+$ compared to the apoenzyme and show a significant change compared to apoenzyme for the binary complex with folate and the tertiary complex. Importantly, there is only a small difference in the trp fluorescence intensity between the E·Folate and E·$NADP^+$·Folate complexes which exist in the occluded and closed conformations, respectively. This indicates that W22, W30, W74, and W133 are not particularly sensitive to the conformational state of the Met20 loop and are instead primarily sensitive to the presence of folate. Conversely, the trp fluorescence of midW47 (**Figure 3. 3 B**) decreases by different amounts based on which ligands are bound. There is a small decrease upon binding $NADP^+$ and a larger decrease upon binding folate, which decreases further in the tertiary complex. However, the decrease in fluorescence intensity of binding folate and $NADP^+$ combined are less than the observed decrease in fluorescence intensity of the tertiary complex. This means that the decrease in fluorescence intensity observed in the tertiary complex is not simply due to quenching of the trp fluorescence from the presence of ligands; there is also a contribution from the conformation of the enzyme. Thus, midW47 is more sensitive to changes in the enzyme conformation compared to the other midW mutants.

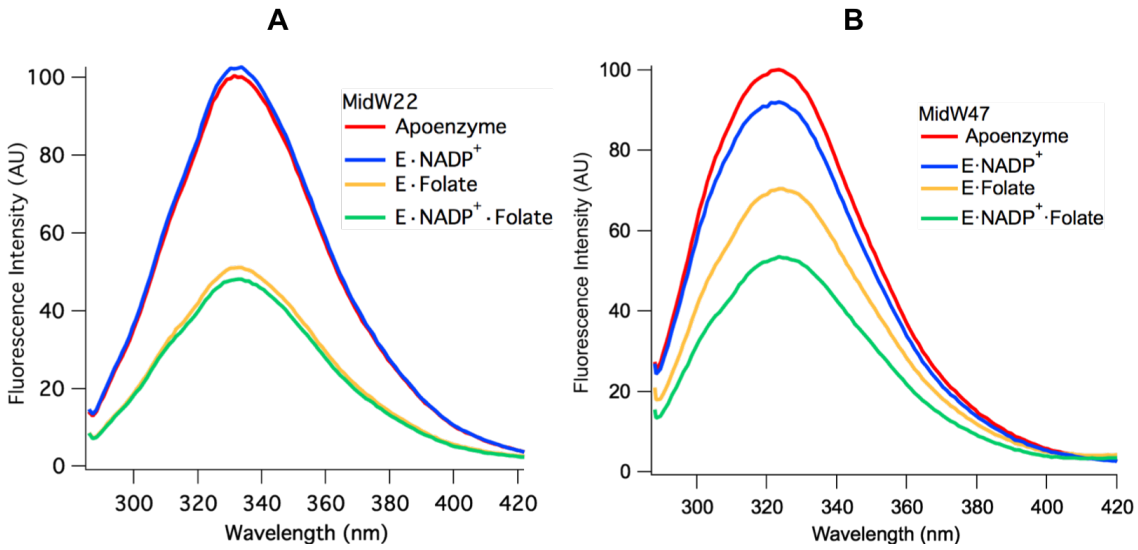

Figure 3. 3 Equilibrium trp fluorescence of midW22 (**A**) and midW47 (**B**) and their ligand complexes. The trp fluorescence of midW22 appears to be primarily modulated by the presence of folate, whereas the trp fluorescence of midW47 changes with each ligand complex.

Table 3. 1 Integrated trp fluorescence intensity of the enzyme·ligand complexes as a percentage of the integrated trp fluorescence intensity of the apoenzyme.

	E·NADP$^+$	**E·Folate**	**E·NADP$^+$·Folate**
Wildtype	93%	36%	24%
midW22	102%	52%	49%
midW30	106%	42%	40%
midW47	92%	71%	54%
midW74	98%	64%	61%
midW133	93%	64%	63%

The temperature dependent trp fluorescence of the midW mutants, corrected for the intrinsic temperature dependence of tryptophan fluorescence, follows the same trend as the wildtype enzyme: an increase in fluorescence intensity with increasing temperature, due primarily to ligand

dissociation. Each of the midW mutants follows the trend as expected based on their change in trp fluorescence with different ligands bound. **Figure 3. 4** shows the change in fluorescence intensity for midW22 and midW47 as representative data.

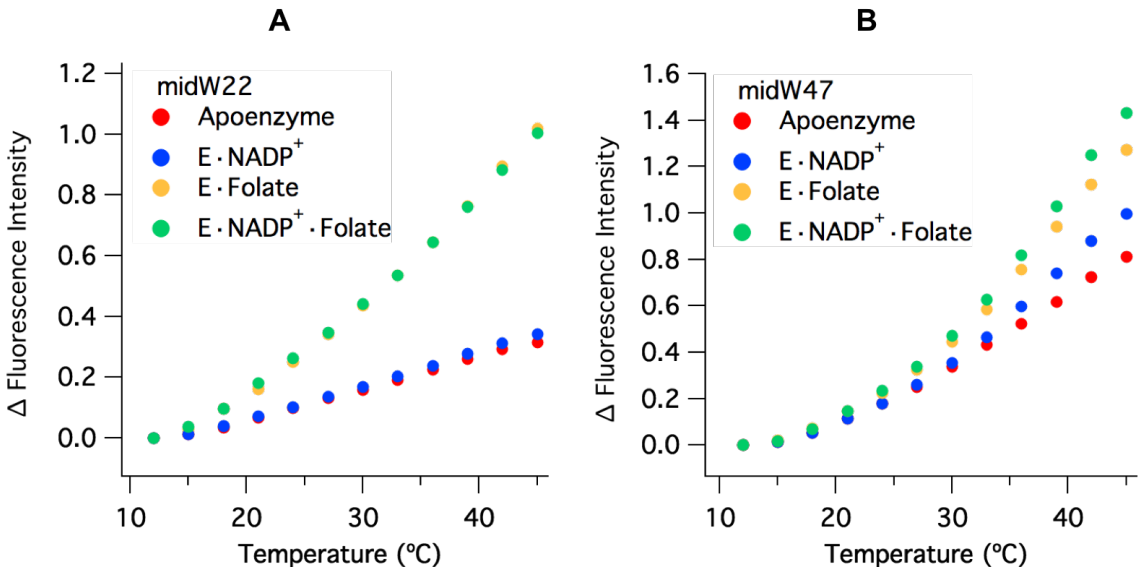

Figure 3. 4 Change in fluorescence intensity versus temperature, corrected for the intrinsic temperature dependence of trp fluorescence, of midW22 (**A**) and midW47 (**B**). All complexes demonstrate an increase in fluorescence with increasing temperature. The change in intensity for the binary complex with $NADP^+$ and apoenzyme compared to the two folate bound complexes is similar for midW22, which is expected based on the similarities in the spectra of apoenzyme/E·$NADP^+$ and E·Folate/E·$NADP^+$·Folate. Conversely, each midW47 complex has a slightly different temperature dependence, reflecting the difference in trp fluorescence intensity for the different ligand bound states.

The T-jump transients for all five midW mutants with folate share a few key characteristics. They all fit to double exponentials with two distinct phases that follow the behavior of the wildtype relaxation profile. The fast relaxation rate of all midW mutants is strongly concentration dependent with an average linear correlation coefficient, r, value of 0.90 ± 0.03, indicating that the fast rate is

convolved with ligand binding/unbinding and any associated loop motions . The slow relaxation rate is not concentration dependent, as demonstrated by a low average r value of -0.2 ± 0.3. **Figure 3. 5** shows T-jump transients of midW47 and the concentration dependent plots. Although all five mutants show similar behavior with respect to concentration, the relaxation rates of the slow phase vary based on the position of the tryptophan, as shown in **Table 3. 2.** W47 and W74 are spatially close together, located at the top of DHFR when orientated as in **Figure 3. 1**. MidW47 and midW74 have close average slow relaxation rates of ~730 s^{-1}. MidW22 and midW30 have substantially faster slow phase relaxation rates, in excess of 1000 s^{-1} and are within one standard deviation of one another. Similarly, W22 and W30 are close together spatially, located near the substrate binding site. Lastly, W133 is located on the distal FG loop and midW133 has the slowest average slow phase relaxation rate of 370 s^{-1}. The differing rates indicate that the tryptophans are reporting on local motions. The binary complex of wt-DHFR with folate has a slow concentration independent relaxation rate of 400 s^{-1}. This is slower than the majority of the concentration independent rates observed in the midW mutants. Even an average of the rates weighted by the relative fluorescence intensities of the midW mutants would be faster than what is observed in the wildtype enzyme. Thus, similar to the equilibrium fluorescence, the T-jump dynamics of the wildtype enzyme are not a simple combination of the midW mutant dynamics. Again, this may be explained in part by the coupling of W47 and W74. The fluorescence of wt-DHFR has contributions from both the individual tryptophans and the interaction of tryptophan residues with each other. Local motions that change the environment of the individual tryptophans are reported by the midW mutants and are a component of the wt-DHFR fluorescence signal. Global motions that modulate the distances or orientation of the trp-trp interactions are not observed in the midW mutants but do impact the transients observed in wt-DHFR.

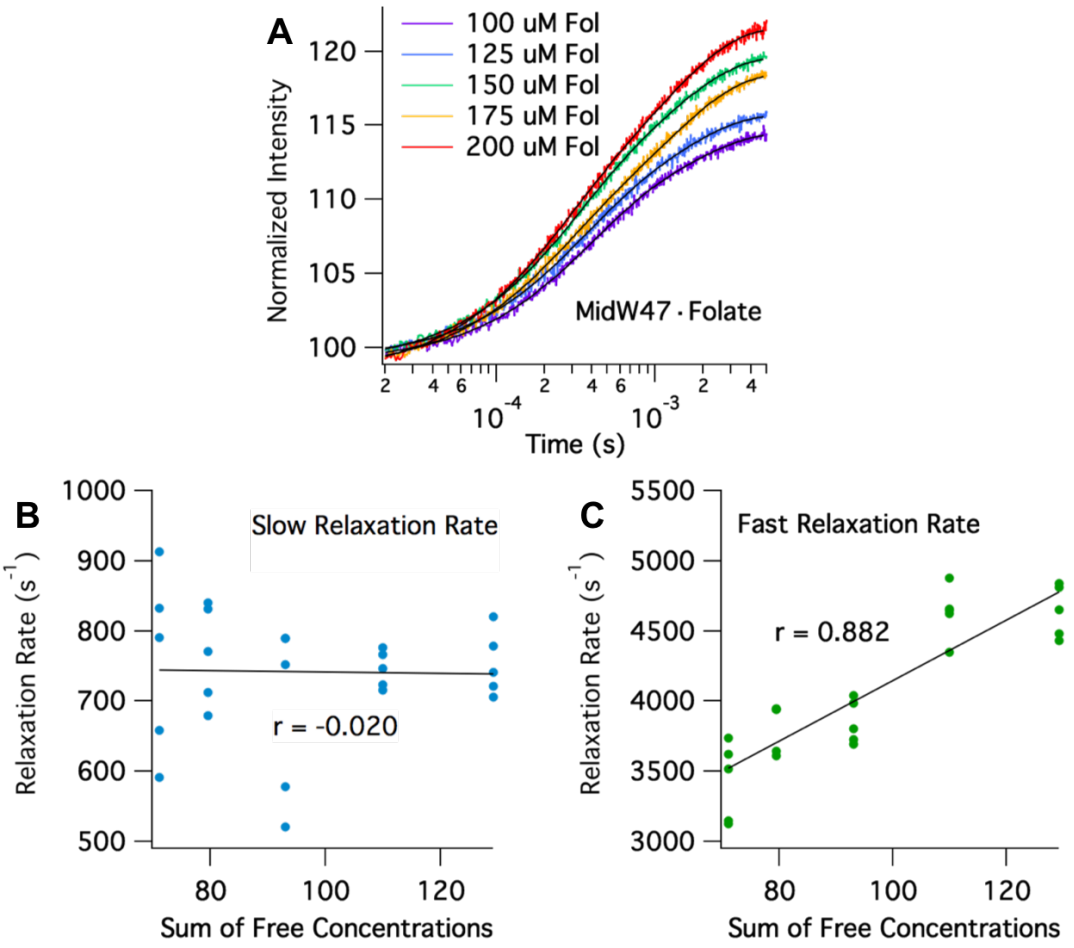

Figure 3. 5 A) T-jump trp fluorescence transients of midW47·Folate with varying concentrations of folate. The black traces are double exponential fits. **B)** Correlation plot for the slow relaxation rates of midW47·Folate versus the sum of the concentration of free enzyme and free ligand. The slow relaxation rate is concentration independent, as shown by the low r value. **C)** Correlation plot for the fast relaxation rates of midW47·Folate versus the sum of free concentrations. The r value close to one confirms that the fast relaxation rate is strongly concentration dependent.

Table 3. 2 Average relaxation rates of the slow phase for the binary folate complexes of all five midW mutants.

Enzyme	midW22	midW30	midW47	midW74	midW133
Average Slow Rate (s^{-1})	2700 ± 900	1800 ± 960	740 ± 90	720 ± 180	370 ± 90

3.5 Conclusion

In this study, we characterized the equilibrium trp fluorescence and T-jump dynamics of five DHFR mutants, each with a single tryptophan residue. The equilibrium fluorescence confirms that each tryptophan residue is in a unique environment and that there are local quenching interactions. The wt-DHFR trp fluorescence is not a simple combination of the individual tryptophans' fluorescence, likely due to excimer formation with W47 and W74. The T-jump dynamics demonstrate that all of the tryptophan residues are sensitive to ligand binding and dissociation. Furthermore, the flexibility of DHFR is highlighted by the presence of slow millisecond conformational changes throughout the enzyme that are not coupled to ligand association/dissociation processes relating to progress along the catalytic cycle. These globally-experienced fluctuations do not originate from a single collective motion, but instead arise from local motions with slightly different relaxation rates. Some of the relaxation rates are quite slow and likely do not impact catalysis. However, some relaxation rates, such as those observed in midW22 and midW30, are fast compared to the steady state turnover rate of DHFR, and thus, could be involved in conformational sampling and the search for reactive conformations. Beyond gaining insight about the enzyme dynamics of DHFR, this research has shown the utility of site specific labels in conjunction with T-jump methodologies in studying enzyme dynamics on the microsecond to millisecond timescale.

3.6 Supplemental Information

Relative Activity Assay

The relative activities of the midW mutants compared to wildtype DHFR were measured as previously described.[14] Briefly, 20 μL of 2.5 mM DHF were added to 980 μL of pre-equilibrated 10 nM DHFR and 51 μM NADPH in phosphate buffer (50 mM sodium phosphate, 100 mM NaCl, 5 mM 2-mercaptoethanol, pH 7). The rate of reaction was measured by monitoring the disappearance of the 340 nm absorbance band as NADPH was oxidized. The initial rates are reported in **Table 3S. 1** as a percentage of the initial rate of wildtype DHFR. Notably, midW22 retains 90% of the wildtype activity, while the other midW mutants have much lower activity. W22 is important for catalysis; it participates in a hydrogen bonding network with D27, T113, and the substrate DHF.[15] However, the other tryptophans appear to have little importance in catalysis because the midW22 mutant, in which W30, W47, W74, and W133 are replaced with phenylalanine, shows only a modest decrease in activity.

Table 3S. 1 Relative activity of the midW mutants compared to wildtype DHFR

Enzyme	wildtype	midW22	midW30	midW47	midW74	midW133
Relative Activity	100%	90%	33%	20%	20%	22%

Isothermal Calorimetry

The dissociation constant and thermodynamic parameters of folate binding to the midW mutants at 25°C were determined using isothermal calorimetry (ITC) on a MicroCal Auto-iTC200 from Malvern Panalytical (United Kingdom). The samples contained 350 μL of 100 μM enzyme and were injected with 2.4 μL of 1 mM folate (buffer: 50 mM sodium phosphate, 100 mM NaCl, pH 7). The system was allowed to equilibrate for 150 seconds between injections. Representative ITC data

are shown in **Figure 3S. 1**. The ITC data were analyzed using the MicroCal ITC-ORIGIN Analysis Software. The resulting K_d, ΔH, and ΔS of ligand binding were used to calculate the sum of free concentrations, which were used to the determine the concentration dependence of the temperature jump relaxation rates.

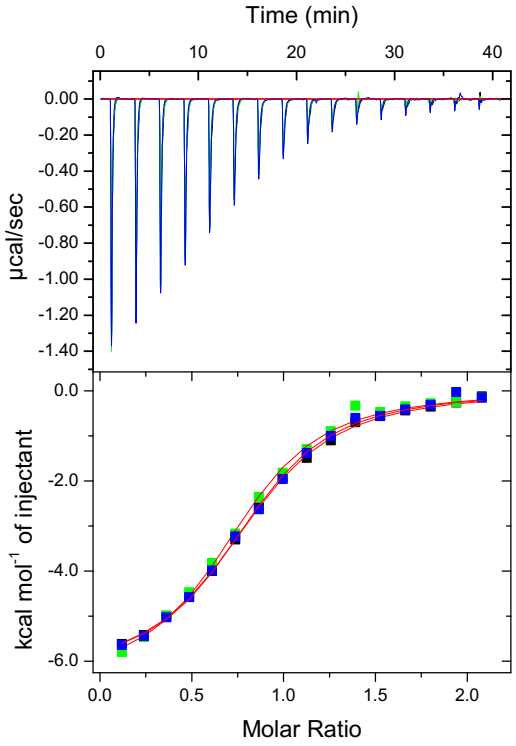

Figure 3S. 1 Raw ITC data for folate binding to midW74 in triplicate (top). Processed ITC data for folate binding to midW74 in triplicate (bottom). The curves represent fits using the OneSite model in the MicroCal ITC-ORIGIN Analysis Software.

Table 3S. 2 Dissociation and thermodynamic constants for the binding of folate to the five midW mutants.

midW mutant	**K_d** (μM)	**ΔH** (kcal/mol)	**ΔS** (cal/mol/K)
midW22	3.7	-7.78	-1.26
midW30	4.5	-5.04	7.55
midW47	12	-7.03	-1.16
midW74	8.4	-6.34	1.98
midW133	9.4	-5.70	3.85

3.7 References

1. Henzler-Wildman, K.; Kern, D., Dynamic personalities of proteins. *Nature* **2007,** *450* (7172), 964-72.

2. Mhashal, A. R.; Vardi-Kilshtain, A.; Kohen, A.; Major, D. T., The role of the Met(20) loop in the hydride transfer in Escherichia coli dihydrofolate reductase. *J Biol Chem* **2017,** *292* (34), 14229-14239.

3. Huang, Q.; Rodgers, J. M.; Hemley, R. J.; Ichiye, T., Extreme biophysics: Enzymes under pressure. *J Comput Chem* **2017,** *38* (15), 1174-1182.

4. Wang, Z.; Antoniou, D.; Schwartz, S. D.; Schramm, V. L., Hydride Transfer in DHFR by Transition Path Sampling, Kinetic Isotope Effects, and Heavy Enzyme Studies. *Biochemistry* **2016,** *55* (1), 157-66.

5. Oyen, D.; Fenwick, R. B.; Stanfield, R. L.; Dyson, H. J.; Wright, P. E., Cofactor-Mediated Conformational Dynamics Promote Product Release From Escherichia coli Dihydrofolate Reductase via an Allosteric Pathway. *J Am Chem Soc* **2015,** *137* (29), 9459-68.

6. Singh, P.; Francis, K.; Kohen, A., Network of remote and local protein dynamics in dihydrofolate reductase catalysis. *ACS Catal* **2015,** *5* (5), 3067-3073.

7. Hughes, R. L.; Johnson, L. A.; Behiry, E. M.; Loveridge, E. J.; Allemann, R. K., A Rapid Analysis of Variations in Conformational Behavior during Dihydrofolate Reductase Catalysis. *Biochemistry* **2017,** *56* (15), 2126-2133.

8. Sawaya, M. R.; Kraut, J., Loop and subdomain movements in the mechanism of Escherichia coli dihydrofolate reductase: crystallographic evidence. *Biochemistry* **1997,** *36* (3), 586-603.

9. Boehr, D. D.; Schnell, J. R.; McElheny, D.; Bae, S. H.; Duggan, B. M.; Benkovic, S. J.; Dyson, H. J.; Wright, P. E., A distal mutation perturbs dynamic amino acid networks in dihydrofolate reductase. *Biochemistry* **2013,** *52* (27), 4605-19.

10. Bhabha, G.; Lee, J.; Ekiert, D. C.; Gam, J.; Wilson, I. A.; Dyson, H. J.; Benkovic, S. J.; Wright, P. E., A dynamic knockout reveals that conformational fluctuations influence the chemical step of enzyme catalysis. *Science* **2011,** *332* (6026), 234-8.

11. Reddish, M. J.; Vaughn, M. B.; Fu, R.; Dyer, R. B., Ligand-Dependent Conformational Dynamics of Dihydrofolate Reductase. *Biochemistry* **2016,** *55* (10), 1485-93.

12. Gill, S. C.; von Hippel, P. H., Calculation of protein extinction coefficients from amino acid sequence data. *Anal Biochem* **1989,** *182* (2), 319-26.

13. Ohmae, E.; Sasaki, Y.; Gekko, K., Effects of five-tryptophan mutations on structure, stability and function of Escherichia coli dihydrofolate reductase. *J Biochem* **2001,** *130* (3), 439-47.

14. Chen, S.; Fahmi, N. E.; Wang, L.; Bhattacharya, C.; Benkovic, S. J.; Hecht, S. M., Detection of dihydrofolate reductase conformational change by FRET using two fluorescent amino acids. *J Am Chem Soc* **2013,** *135* (35), 12924-7.

15. Agarwal, P. K.; Billeter, S. R.; Rajagopalan, P. T.; Benkovic, S. J.; Hammes-Schiffer, S., Network of coupled promoting motions in enzyme catalysis. *Proc Natl Acad Sci U S A* **2002,** *99* (5), 2794-9.

Chapter 4:

Viscosity Dependent Met20 Loop Motions of Dihydrofolate Reductase

Vaughn, M. B.; Biren, C.; Li, Q.; and Dyer, R. B.

4.1 Abstract

Dihydrofolate reductase (DHFR) is a classic model for studying enzyme dynamics. DHFR is well known for the conformational change of the Met20 loop during its catalytic cycle. Met20 loop motions are important for catalysis and are predicted to play a role in product release. However, the rate of the loop motions has not been directly observed. Here, we site-specifically incorporate a small naphthalene-derived, environmentally sensitive BADAN (6-bromoacetyl-2-dimethylaminonaphthalene) fluorophore on the Met20 loop to study DHFR loop dynamics on the microsecond timescale using temperature jump fluorescence spectroscopy. We measured the relaxation rates of the closed-open, occluded-open, and closed-occluded transitions which have not been directly measured before. The closed-occluded transition includes two steps. One of the relaxation events occurs at approximately double the rate compared to the closed-open or occluded-open transitions in the binary complexes (E·NADPH and E·Folate). Another relaxation event occurs at a rate that is an order of magnitude faster. We used sucrose, a viscogen, to modulate loop motions, demonstrating that temperature jump fluorescence spectroscopy is sensitive to changes in the rate of loop motions. Therefore, this technique could be used to identify other loop motion modifiers such as distal mutations and small molecule inhibitors.

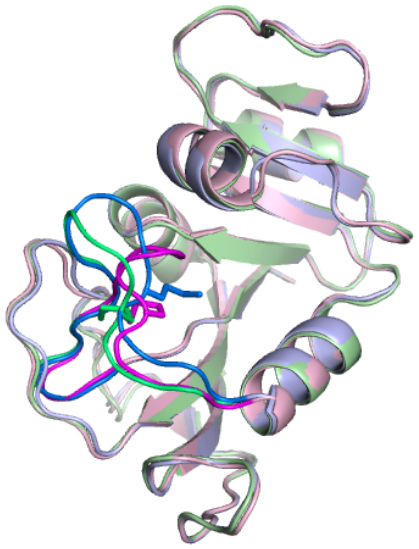

Figure 4. 1 Crystal structure of wildtype DHFR. The Met20 loop is highlighted in the three conformations: open (green, PBD 1RA9), closed (blue, PDB 1RX2), and occluded (pink, 1RX7). The sidechain of residue M20 is shown as well.

4.2 Introduction

Dihydrofolate reductase (DHFR) is a small ubiquitous enzyme that catalyzes the NADPH mediated reduction of dihydrofolate (DHF) to tetrahydrofolate (THF). Because of its role in nucleic acid biosynthesis, DHFR has been a target for anticancer, antibacterial, and antifungal agents.[1] DHFR has several flexible loops that are important for catalysis. In particular, the Met20 loop (residues 9-24) changes conformation throughout the catalytic cycle. The three conformations are shown in **Figure 4. 1**. The Met20 loop is closed over the active site in the reactant bound states and exists in the occluded conformation, protruding into the active site preventing the nicotinamide ring of the cofactor from binding in the THF bound states. The third conformation is a disordered open state and is observed in the apoenzyme as well as a variety of DHFR·ligand complexes.[2] Met20 loop motions are important for catalysis. Mutations that change the flexibility of the Met20 loop can

decrease k_{cat} by approximately 80%[3] and decrease the rate of hydride transfer from NADPH to substrate by 400-fold.[4] Measuring loop motions presents a challenge because they are predicted to occur on the microsecond timescale,[5] which is difficult to access with techniques commonly used to study enzymes such as stopped-flow and quench-flow.

As discussed in the previous two chapters, temperature jump (T-jump) fluorescence spectroscopy has been used to study the enzyme dynamics of DHFR on the microsecond timescale.[6] However, these studies used native tryptophan fluorescence, which provided limited information about the loop motions. Here, we incorporate a small, environmentally sensitive BADAN (6-bromoacetyl-2-dimethylaminonaphthalene) fluorophore at residue 20 (M20-BADAN) and characterize the fluorescence spectra of M20-BADAN as well as several enzyme·ligand complexes. Relaxation rates of conformational changes within the Met20 loop were measured using T-jump fluorescence spectroscopy; sucrose was used to change the viscosity of the solution and modulate the observed conformational changes. Notably, we found that the transition from closed to occluded comprises two steps that could be due to a sequential loop and ligand conformational change or could arise from an intermediate loop position, which may be the open conformation.

4.3 Experimental Methods

Protein Preparation and Labeling

The mutant *E. coli* DHFR plasmid (DHFR-M20C/C85A/C152S) was made by the Custom Cloning Division within the Emory Integrated Genomics Core. The two native cysteines, C152 and C85, were mutated to serine and alanine as described previously by Liu et al.[7] M20 was mutated to cysteine so that the thiol-reactive BADAN fluorophore could be incorporated on the Met20 loop. *E. coli* competent cells were transformed with the plasmid and the mutant protein was expressed and

purified by affinity chromatography as previously described for wt-DHFR[6] and single tryptophan mutants in Chapters 2 and 3.

The purified enzyme was labeled with BADAN using the procedure provided by the manufacturer (Life Technologies). A 15-fold excess of BADAN was dissolved in acetonitrile and added drop-wise to 50 μM enzyme in aqueous buffer (50 mM sodium phosphate, 100 mM NaCl, 5 mM TCEP, pH 7). The reaction mixture was allowed to stir at room temperature for 4 hours. The labeled protein was separated from excess fluorophore using an Econo-Pac DG10 desalting column. The labeling efficiency (83 ± 3%) was calculated by determining the concentration of enzyme and BADAN using the UV-vis absorbance and molar extinction coefficients at 280 nm (31,100 $M^{-1}cm^{-1}$) and 387 nm (14,950 $M^{-1}cm^{-1}$), respectively. Unlabeled enzyme does not contribute to the fluorescence signal, so it does not interfere with the equilibrium and temperature jump fluorescence experiments.

Equilibrium Fluorescence

Fluorescence spectra of M20-BADAN apoenzyme and ligand complexes were measured with a Horiba Dual-Fl spectrofluorometer (Japan) in triplicate. Samples contained 3 μM enzyme or Glutathione-BADAN adduct (GB) and 9 μM of the appropriate ligands (folate, $NADP^+$, and NADPH) in aqueous buffer (50 mM sodium phosphate, 100 mM NaCl, pH 7) with 0%, 20%, and 40% sucrose by weight. Samples were excited at 405 nm. **Figure 4. 2 A** and **Figure 4. 3** show spectra collected at room temperature. The intensities of the peaks in the sucrose series were normalized, setting the intensity of the BADAN fluorescence of each 0% sucrose sample to 100 (**Figure 4. 3**). Additionally, temperature dependent spectra were collected from 12°C to 45°C in increments of 3°C. The BADAN peaks were integrated, the intrinsic temperature dependence of

BADAN was subtracted, and the intensities were normalized to the lowest temperature (**Figure 4. 3 B**).

Temperature Jump Fluorescence Spectroscopy

Laser induced temperature-jump fluorescence spectroscopy was used to investigate the dynamics of M20-BADAN apoenzyme, E·Folate, E·NADPH, and E·$NADP^+$·Folate. The methodology is described in detail in Chapter 2. Briefly, a temperature jump of ~15°C (final temperature 35 ± 1°C) was generated by a 10 ns laser pulse of 2.09 μm light at a rate of 12.5 hertz. The BADAN fluorescence was probed by excitation at 405 nm. The emission light was focused on a photomultiplier tube after passing through a bandpass filter (518 nm – 574 nm). The data was collected, averaged (5000 shots), and digitized on an oscilloscope. The buffer used for the equilibrium fluorescence measurements was D_2O exchanged for temperature jump use. All samples contained 100 μM enzyme and 100 μM glutathione-BADAN adduct was used as the reference. In addition to enzyme, the binary complex samples contained 200 μM folate or NADPH. The sample of the tertiary complex contained 200 μM $NADP^+$ and 1 mM folate. Differing concentrations of sucrose (0% to 40% by weight) were used to vary the viscosity of the sample and reference solution. The intrinsic temperature dependence of BADAN was subtracted from each transient, which is reported here as a percentage of the sample's original fluorescence signal.

4.4 Results and Discussion

The equilibrium fluorescence of M20-BADAN reveals different fluorescent signatures for different ligand-bound states (**Figure 4. 2**). The apoenzyme has the highest fluorescence intensity with a peak max at ~510 nm. The fluorescence intensity of the binary complex with $NADP^+$ is decreased compared to the apoenzyme and is very slightly blue shifted. Similarly, the binary complex

with NADPH fluorescence is also slightly blue shifted, although the intensity is drastically reduced. The binary complex with folate and the tertiary complex with folate and $NADP^+$ are red shifted compared to the apoenzyme, with lambda max at ~520 nm, though the tertiary complex has a lower intensity than the binary complex.

The shift of the fluorescence spectra appears to report on which ligands are present. The oxidized and reduced cofactor slightly blue shift the BADAN fluorescence, whereas folate in the binary and tertiary complex causes about a 10 nm red shift. A possible explanation is that in the absence of folate, the BADAN fluorophore occupies the substrate binding pocket, making the BADAN partially solvent protected. Upon binding folate, the BADAN leaves the binding pocket and becomes more solvent exposed. This is consistent with the observed red shift. The fluorescence intensity seems indicative of the conformation of the Met20 loop. In the apoenzyme, the Met20 loop is disordered in the open conformation and has the highest fluorescence intensity. The binary complex with folate is in the occluded conformation and the BADAN fluorescence is quenched by about 20%. The conformation with the lowest fluorescence intensity is the closed conformation. Both the tertiary complex and the binary complex with NADPH are in the closed conformation. Interestingly, E·NADPH has a lower fluorescence intensity than E·$NADP^+$·Folate. This may be due to slight differences within the closed conformation, i.e. the binary complex may be more "tightly" closed, or it could be due to a different population distribution of states between the two classically described closed complexes. In the binary complex with $NADP^+$, the Met20 loop is ascribed as mostly open vis crystallography,[2] with a few crystal structures showing closed-like conformations. Hence, the fluorescence intensity of E·$NADP^+$ is close to that of the apoenzyme, albeit slightly lower due to a small population of enzyme in the closed conformation.

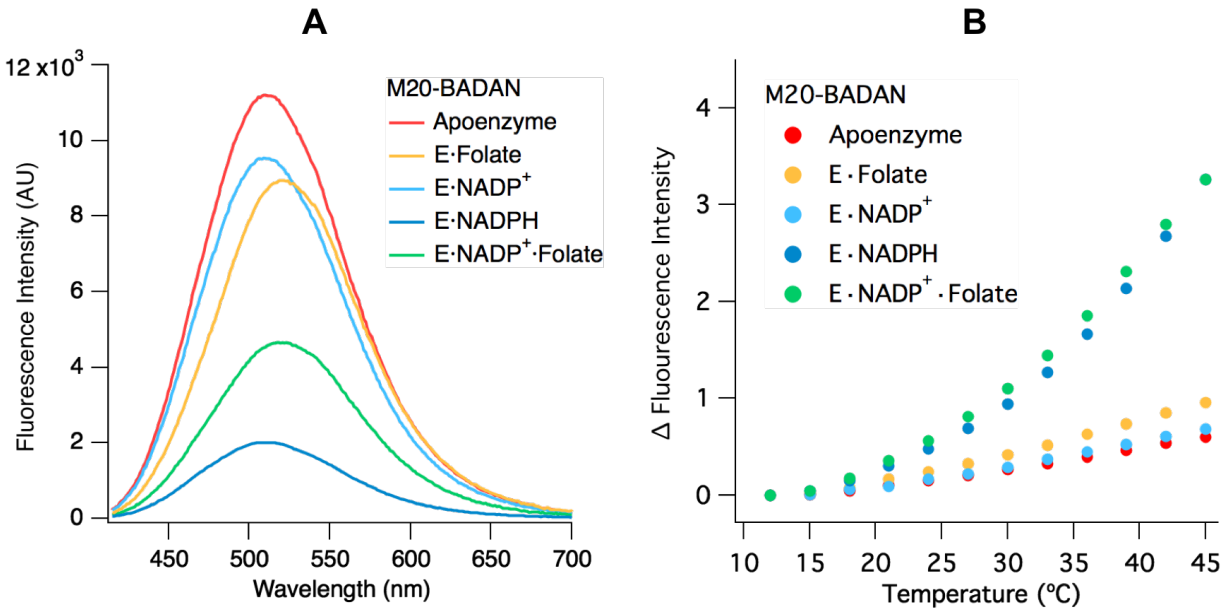

Figure 4. 2 A) Fluorescence spectra of five M20-BADAN complexes, excited at 405 nm. The fluorescence intensity is indicative of the Met20 loop conformation, whereas lambda max depends on the presence of cofactor and folate. B) Temperature dependent M20-BADAN fluorescence intensity, integrated and corrected for the intrinsic temperature dependence of BADAN fluorescence. The fluorescence intensity of all complexes increase with temperature, primarily due to ligand dissociation. Thus, the complexes with the greatest increase of intensity correspond to the complexes with the most quenching in the ligand-bound state.

Figure 4. 2 B shows the temperature dependent fluorescence intensity of each ligand complex, normalized to the intensity of the lowest temperature and corrected for the intrinsic temperature dependence of BADAN fluorescence (**Figure 4S. 1**). As expected, the fluorescence intensity increases with increasing temperature due to ligand dissociation. The most drastic increase in intensity is seen in the E·NADPH and the tertiary complex, which are the two samples that showed the greatest difference between the apoenzyme and the ligand-bound state. Similarly, the E·Folate complex increases in fluorescence less than the two closed complexes, but more than the

E·NADP$^+$ complex. The apoenzyme shows a slight increase in fluorescence, which may be due to increased disorder of the Met20 loop.

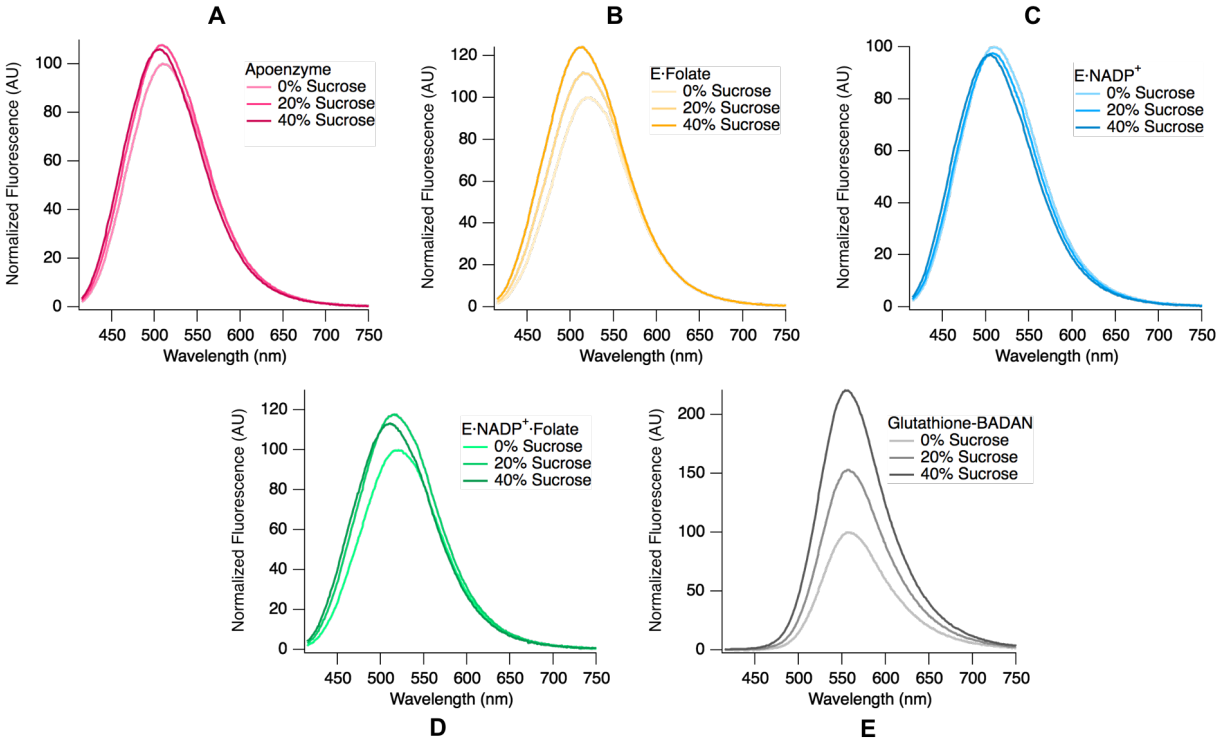

Figure 4. 3 BADAN fluorescence spectra for the apoenzyme (A), E·Folate (B), E·NADP$^+$ (C), E·NADP$^+$·Folate (D), and the Glutathione-BADAN adduct (E) with 0%, 20%, and 40% sucrose. Each set of spectra have been scaled to 100 based on the fluorescence intensity at 0% sucrose.

One method for modulating loop motions is to change the viscosity of the enzyme solution. This has been used previously as an indirect method of modulating LDH activity by slowing down loop closure over the active site by adding sucrose to the solution.[8] The fluorescence spectra of M20-BADAN, several ligand complexes, and the water soluble glutathione-BADAN adduct (GB) are shown in **Figure 4. 3** at three sucrose concentrations: 0%, 20%, and 40% by weight, which correspond to viscosities of 0.72, 1.4, and 3.8 cP. As expected, the GB behaves as a typical solvent exposed fluorophore. The fluorescence intensity of GB increases with increasing concentrations of sucrose and the peak max of the 40% sucrose sample is blue shifted ~5 nm compared to 0%

sucrose. Similarly, the fluorescence of the apoenzyme and E·NADP$^+$ are blue shifted ~5 nm; yet, they do not follow a simple trend of increasing fluorescence intensity. The binary complex with folate increase in intensity with increasing sucrose concentration, but is blue shifted ~10 nm. The tertiary complex is also blue shifted ~10 nm, yet the trend in its fluorescence intensity is similar to that of the apoenzyme. The BADAN fluorescence response to sucrose provides information about each of the complexes and the fluorophore's environment, but the interpretation is not necessarily straightforward. For example, the BADAN fluorophore in the E·Folate complex is likely exposed in part to the solvent, given the increase in fluorescence with increased concentrations of sucrose. However, the shift in λ_{max} for E·Folate is larger than what is observed for the free GB, indicating that sucrose may also impact the protein environment with regards to the folate. Additionally, a larger shift is observed for high sucrose concentrations with E·NADP$^+$·Folate. The anomalous trend in intensity for the apoenzyme, E·NADP$^+$, and E·NADP$^+$·Folate complexes may indicate that the BADAN fluorophore in these complexes is less solvent exposed and more sensitive to changes within the protein. Furthermore, the presence of sucrose may shift the binding equilibria of the cofactor and substrate as well as the population distribution of the closed, open, and occluded states.

Temperature jump fluorescence spectroscopy was used to study the Met20 loop dynamics of M20-BADAN apoenzyme, the binary complex with folate, the binary complex with NADPH, and the tertiary complex with NADP$^+$ and folate. Transients of the apoenzyme fit best to double exponentials (**Figure 4. 4**). Apoenzyme with 0% sucrose has a slow relaxation rate of 532 s^{-1} and a fast relaxation rate of 13,000 s^{-1} (**Table 4. 1**). The slow relaxation rate is a few hundred per second, which is similar to that of wt-DHFR.[6] The fast relaxation rate is several thousand times per second faster than what has been reported for wt-DHFR or mutants site-specifically labeled with tryptophan. Both relaxation rates decrease with viscosity, though the slow relaxation rate stalls at

~200 s^{-1}, compared to the fast relaxation rate which continues to decrease over the viscosity range measured here.

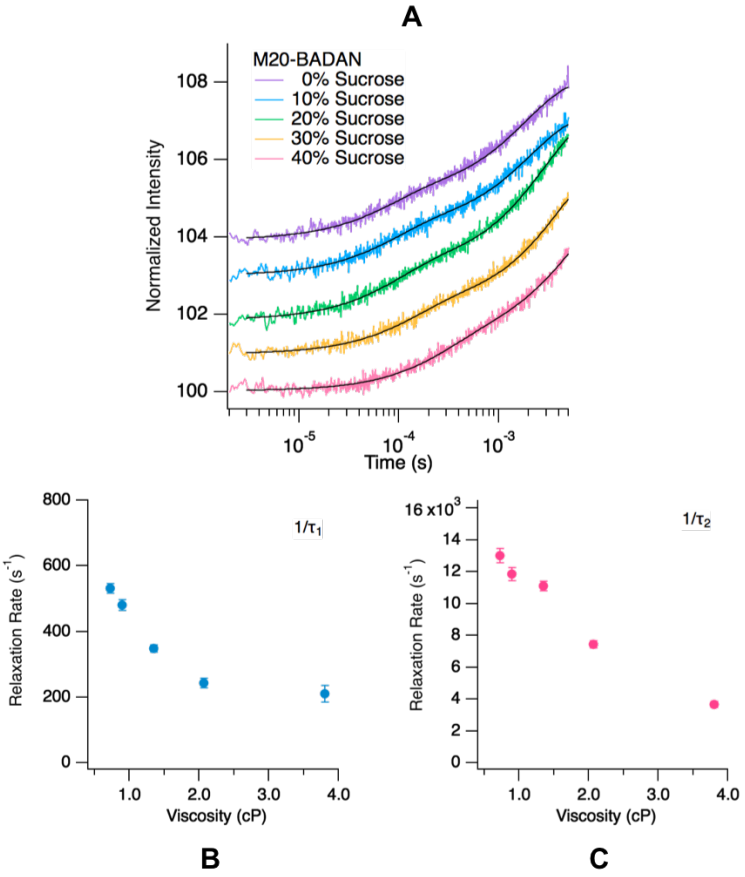

Figure 4. 4 A) T-jump transients of apoenzyme M20-BADAN at sucrose concentrations from 0% to 40%. The black trace shows the double exponential fit for each transient. B) The slow relaxation rate versus viscosity. C) The fast relaxation rate versus viscosity.

Table 4. 1 Relaxation rates for M20-BADAN apoenzyme double exponential fits with respect to sucrose concentration.

Sucrose Concentration	$1/\tau_1$ (s^{-1})	$1/\tau_2$ (s^{-1})
0%	532 ± 15	13,000 ± 440
10%	481 ± 17	11,800 ± 420
20%	349 ± 11	11,100 ± 310
30%	243 ± 14	7,500 ± 230
40%	210 ± 26	3,700 ± 170

T-jump transients of M20-BADAN·Folate are shown in **Figure 4. 5**. Samples with 0%, 10% and 20% sucrose fit best to triple exponentials and samples with 30% and 40% sucrose fit best to double exponentials. This is likely not due to the disappearance of a relaxation phase, but is instead due to the difficulties of exponential data fitting. **Figure 4. 5 C** shows relaxation rates 2 and 3 versus viscosity. At 1.35 cP (20% sucrose), relaxation rate 2 ($1/\tau_2$) is higher than expected given the trend of decreasing rate with increasing viscosity. It is artificially augmented due to the faster $1/\tau_3$. At higher viscosities, there is insufficient amplitude change to separate the two faster relaxation rates and thus, they converge. Similar to wt-DHFR and M20-BADAN apoenzyme, the slowest relaxation rate of E·Folate is several hundred per second. The second relaxation rate is similar to what has been reported for ligand association/dissociation for wt-DHFR. The fastest relaxation rate ($1/\tau_3$) is ~2.3 times faster than what is observed for the M20-BADAN apoenzyme. In the binary complex with folate, the Met20 loop is in the occluded conformation; in the apoenzyme the Met20 loop is disordered and in the open conformation. The dissociation of folate triggered by the temperature jump induces the Met20 loop to change from the occluded conformation to the open conformation. This third phase is likely due to this transition.

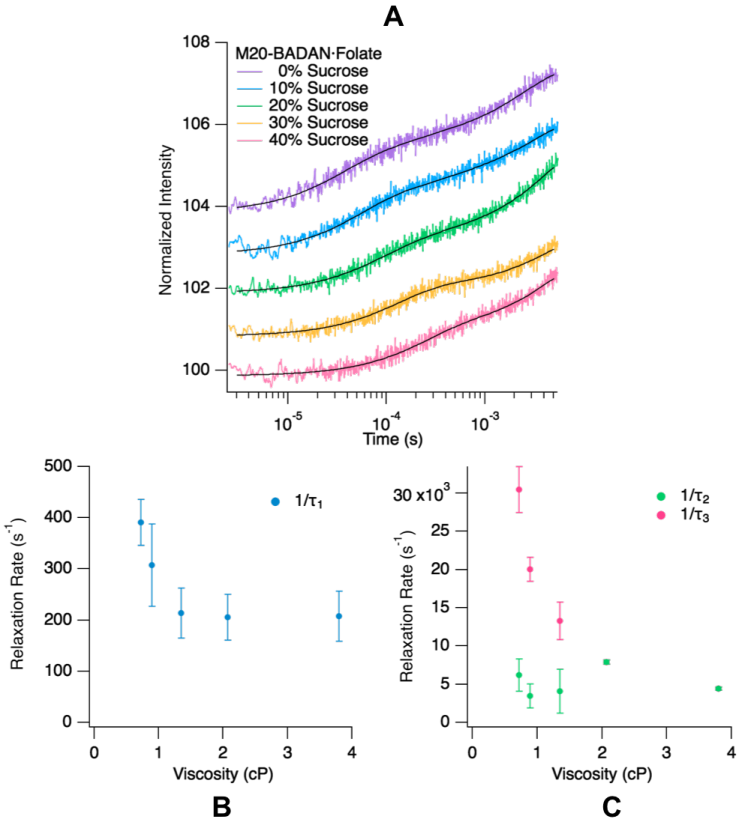

Figure 4. 5 A) T-jump transients of M20-BADAN·Folate at sucrose concentrations from 0% to 40%. The samples with 0%, 10% and 20% sucrose fit best to triple exponentials, whereas samples with 30% and 40% sucrose fit best to double exponentials. B) and C) show the relaxation rates derived from the exponential fits versus viscosity.

Table 4. 2 Relaxation rates for M20-BADAN·Folate double and triple exponential fits with respect to sucrose concentration.

Sucrose Concentration	$1/\tau_1$ (s^{-1})	$1/\tau_2$ (s^{-1})	$1/\tau_3$ (s^{-1})
0%	391 ± 45	6,200 ± 2,100	30,500 ± 3,000
10%	308 ± 80	3,500 ± 1,600	20,100 ± 1,600
20%	214 ± 49	4,100 ± 2,800	13,300 ± 2,400
30%	206 ± 45	7,940 ± 290	
40%	207 ± 49	4,400 ± 230	

Temperature jump transients of M20-BADAN·NADPH from 0% to 30% sucrose fit best to triple exponentials (**Figure 4. 6** and **Table 4. 3**). All three relaxation rates decrease with respect to increasing viscosity. The slowest relaxation rate (1,370 s^{-1}) is faster than what is observed for the apoenzyme or E·Folate; however, it is similar to slow concentration independent rates observed in single tryptophan DHFR mutants as discussed in the previous chapter. Furthermore, it is unsurprising that the slow relaxation rate varies depending on the enzyme·ligand complex as this was also observed by tryptophan fluorescence in wt-DHFR. The second relaxation rate is 5,380 s^{-1} and is similar to the second relaxation rate of E·Folate as well as a previously observed concentration dependent relaxation rate for DHFR·ligand complexes corresponding to ligand association/dissociation. Contrary to E·Folate, the binary complex with NADPH shows a clean separation of all relaxation rates, likely due to the larger total amplitude change which allows for better exponential fitting. The fastest relaxation rate for E·NADPH is 23,900 s^{-1}, which is slightly slower than what is observed for the binary complex with folate. The Met20 loop is in the closed conformation in E·NADPH; thus, the temperature jump triggers the closed to open transition. Comparatively, this transition is slower than the occluded to open transition observed in E·Folate.

Table 4. 3 Relaxation rates for M20-BADAN·NADPH with respect to sucrose concentrations.

Sucrose Concentration	$1/\tau_1$ (s^{-1})	$1/\tau_2$ (s^{-1})	$1/\tau_3$ (s^{-1})
0%	1,310 ± 70	5,380 ± 350	23,900 ± 1,300
10%	1,090 ± 110	3,890 ± 410	16,000 ± 1,000
20%	800 ± 280	2,520 ± 430	10,200 ± 700
30%	230 ± 470	1,590 ± 460	6,300 ± 700

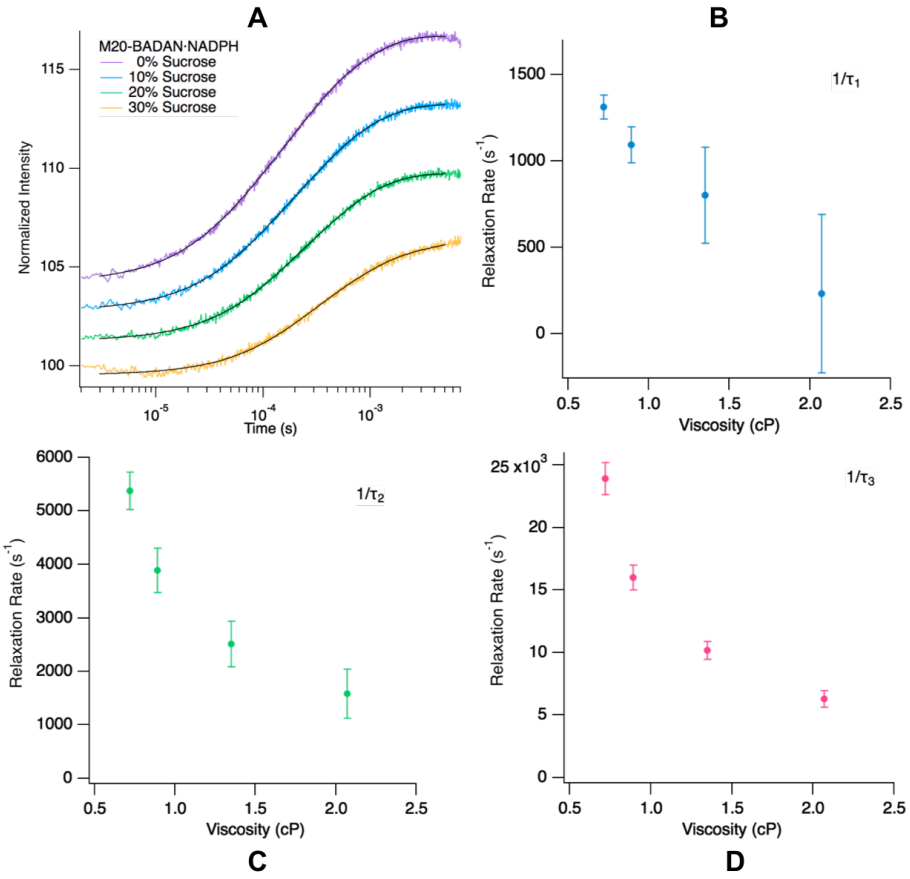

Figure 4. 6 A) T-jump transients for M20-BADAN·NADPH at sucrose concentrations from 0% to 30% fit to triple exponential fits. B, C, D) Relaxation rates from the exponential fits versus viscosity.

The transients of the M20-BADAN·NADP$^+$·folate complex fit best to a summation of four exponentials (**Figure 4. 7** and **Table 4. 4**). The slowest relaxation event is close to that of E·NADPH. The second relaxation rate is slightly faster than what is observed for the binary complexes, which were assigned to ligand association/dissociation. As such, the higher rate corresponds to the higher concentration of ligands used in the tertiary complex. Indeed, the second relaxation rate observed for the M20-BADAN·NADP$^+$·folate complex is close to the concentration dependent relaxation rate observed for the tertiary complex of wt-DHFR in which higher ligand

concentrations were also used. The third and fourth relaxation rates are both faster than the fastest relaxation observed in the two binary complexes by a factor of two and an order of magnitude, respectively. In the tertiary complex, the Met20 loop is in the closed conformation; however, the binary complex with folate is in the occluded conformation. By using an excess of folate, the system is poised for the closed to occluded transition. Here, we observe two phases, indicating that there are two steps involved. The two steps could be a loop motion and a conformational rearrangement of the ligand, such as the nicotinamide ring of the cofactor swinging out of the binding pocket. Alternatively, there could be an intermediate loop position between closed and occluded, or the Met20 loop could sample the open conformation, proceeding from closed to open to occluded. The relaxation rates in the tertiary complex are much faster that what is observed for the occluded to open and closed to open transitions in the binary complexes; however, Fan et al. report wt-DHFR accessing open-like conformations near the transition state of hydride transfer,[9] which supports the idea that the transition from closed to occluded includes the open conformation as an intermediate.

Table 4. 4 Relaxation rates for M20-BADAN·$NADP^+$·Folate with respect to sucrose concentrations.

Sucrose Concentration	$1/\tau_1$ (s^{-1})	$1/\tau_2$ (s^{-1})	$1/\tau_3$ (s^{-1})	$1/\tau_4$ (s^{-1})
0%	1485 ± 17	10,250 ± 410	64,800 ± 7,100	832,000 ± 70,000
10%	1653 ± 20	11,480 ± 340	108,300 ± 12,000	788,000 ± 67,000
30%	573 ± 11	6,290 ± 160	58,500 ± 3,500	563,000 ± 27,000
40%	475 ± 17	5,030 ± 170	40,500 ± 2,600	300,000 ± 9,000

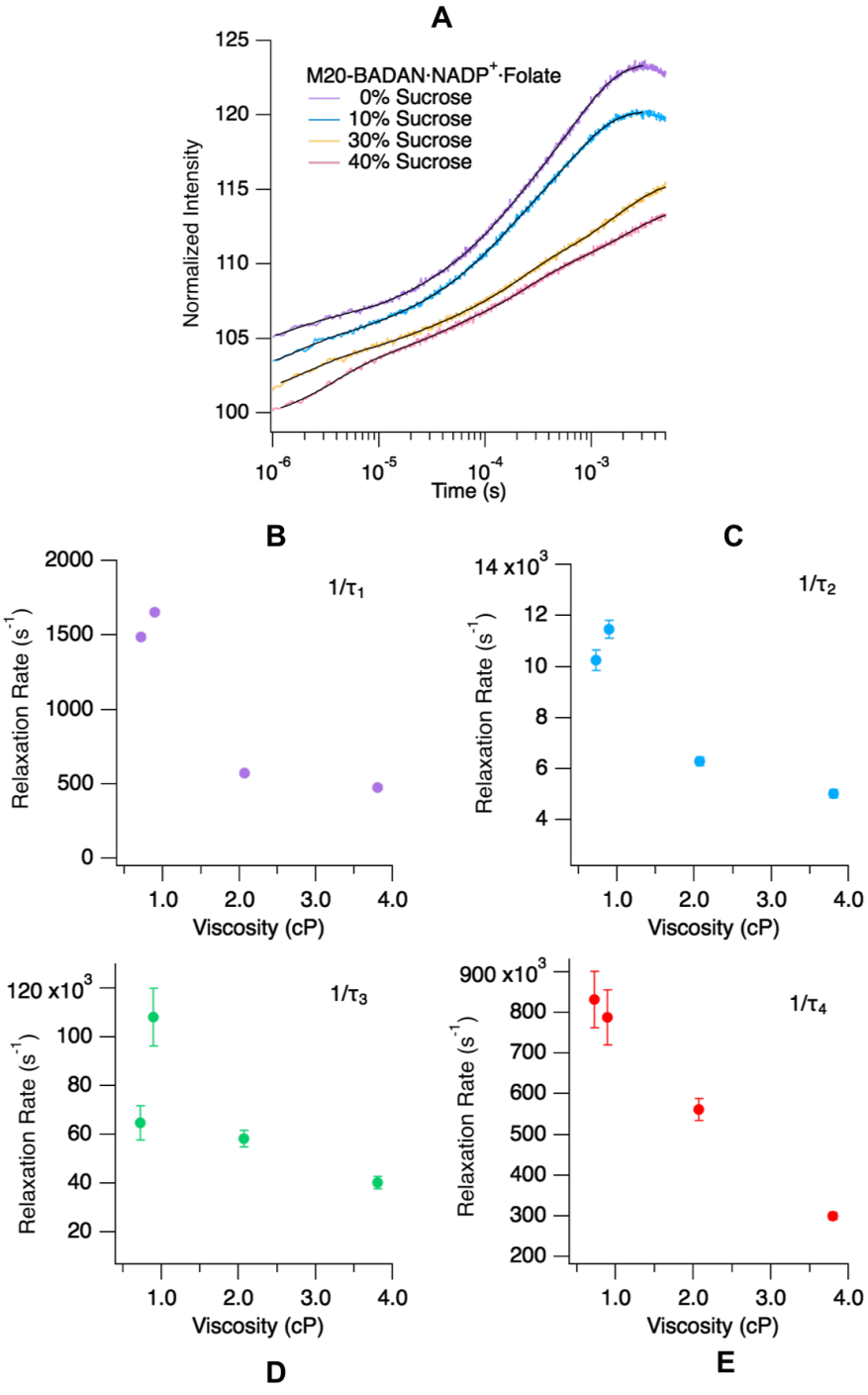

Figure 4. 7 A) T-jump transients for M20-BADAN·NADP$^+$·Folate with sucrose concentrations from 0% to 40% fit to a summation of four exponentials. B, C, D, E) Relaxation rates versus viscosity.

In all of the enzyme complexes studied here, the relaxation rates demonstrate an inverse relationship with respect to viscosity. The only exception to this trend is the second relaxation rate in E·Folate, which as discussed before, is an artifact due to the limitations of exponential data fitting. The inverse relationship with viscosity indicates that each event depends on interaction with the solvent, either a conformational change in which protein-solvent interactions are important or ligand binding in which diffusion through solvent plays a role in the rate. Interestingly, the viscosity dependence does differ from what has been observed previously for protein conformational changes.[10] Typically, under low viscosity conditions, the rate of conformational change is relatively insensitive to changes in viscosity. Conversely, under higher viscosity conditions, the rate decreases with increasing viscosity. The difference in behavior between high and low viscosity regimes is attributed to the internal friction of the protein. At low viscosity, the internal friction dominates the barrier, which is reflected in the rate. At sufficiently high viscosity, the solvent or external friction is greater than the internal friction; thus, the external friction dominates and a dependence on viscosity is observed. The relaxation rates for the T-jump transients of the M20-BADAN complexes do not follow this trend. A few of them such as $1/\tau_2$ of the apoenzyme and $1/\tau_4$ of the tertiary complex appear to be fairly linear over the viscosity range studied here. However, the majority of the relaxation rates appear to be less sensitive to viscosity at the higher viscosities, contrary to what is predicted to happen based on the interplay between internal and external friction. Due to the viscosity dependent nature of the relaxation rates at low viscosity, we can conclude that the internal friction of DHFR in the absence of sucrose is low. However, not only does sucrose increase the viscosity of the solution, it can also cause proteins to become more compact.[11] Compact stages of protein folding have shown to have increased internal friction.[12] An analogous response in enzymes would explain the viscosity dependent behavior observed in DHFR; the more compact the enzyme

structure the more internal friction is generated. At high sucrose concentrations, the relaxation rates of M20-BADAN are insensitive to viscosity, which is indicative of high internal friction.

4.5 Conclusion

In summary, we directly measured Met20 loop motions on the microsecond timescale, which has not been accomplished previously. We detected two temporally distinct steps involved in the closed to occluded transition, which could be due to intermediate loop positions or a sequential loop motion and ligand conformational rearrangement. Importantly, we have established the presence of enzyme loop motions on the low microsecond timescale. Recent advancements in computational capabilities allow for microsecond long simulations,[13] so Met20 loop motions should be accessible by extended simulations. Additionally, we have shown that Met20 loop motions along with other conformational changes within DHFR can be modulated by viscosity. Loveridge et al. tested the activity of DHFR in a variety of co-solvents to vary the viscosity and dielectric constant.[14] They report that k_{cat} is decreases with increasing viscosity, but the hydride transfer rate is unaffected. Conformational changes, such as loop motions, are modulated by viscosity including the loop motion involved with product release, which is the rate limiting step of DHFR catalysis. We observe that the rates of all conformational changes measured here vary with viscosity. The viscosity dependence of the loop motions demonstrates that temperature jump fluorescence spectroscopy is a useful method for studying loop motion modulation. NMR and computational studies have predicted that the FG and Met20 loop motions are coupled.[9, 15] The methodology described here combined with strategic mutations, such as G121V and N23PP mutations that have been shown to decrease loop flexibility, could determine the relationship between the FG and Met20 loop motions.

4.6 Supplemental Information

Glutathione-BADAN Adduct Synthesis

BADAN is not water soluble, which is problematic for use in aqueous buffers. Therefore, a water soluble glutathione-BADAN adduct was synthesized. BADAN (5 mg) was dissolved in acetonitrile and added to a buffered solution (50 mM sodium phosphate, 100 mM NaCl, pH 7) of 15-fold excess glutathione. The mixture was allowed to stir are room temperature for 4 hours, protected from light. Rotary evaporation was used to remove acetonitrile before lyophilization. The lyophilized powder was dissolved in 5% acetonitrile, 95% water, filtered, and loaded on a C18 HPLC column. The glutathione-BADAN adduct was eluted with a constant gradient from 5% to 100% acetonitrile over 50 minutes with a flow rate of 1 mL/min. The molar mass of the glutathione-BADAN adduct was confirmed by mass spectroscopy and the molar extinction coefficient at 387 nm in buffer was determined (14,950 $M^{-1}cm^{-1}$).

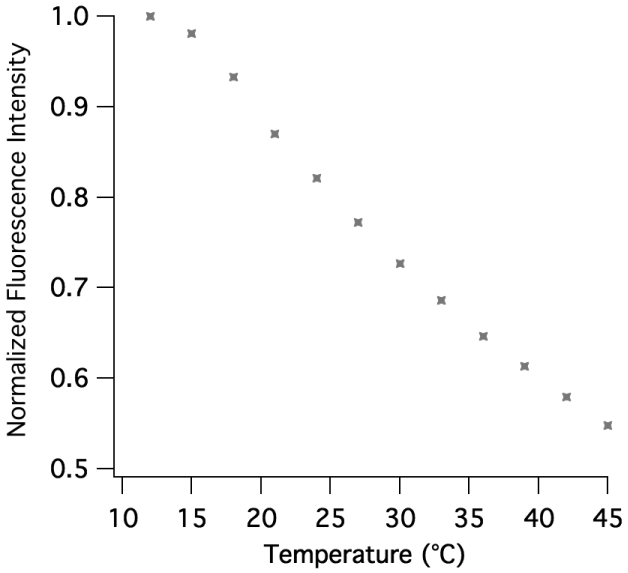

Figure 4S. 1 Integrated fluorescence intensity of glutathione-BADAN adduct versus temperature. The intensity was normalized to 1 at the lowest temperature.

Activity of Labeled mutant

Relative activity of the M20-BADAN enzyme compared to wt-DHFR was determined as described in the literature[16] and in the previous chapter. Briefly, 20 μL of 2.5 mM DHF were added to 980 μL of pre-equilibrated 10 nM DHFR and 51 μM NADPH in phosphate buffer (50 mM sodium phosphate, 100 mM NaCl, 5 mM 2-mercaptoethanol, pH 7). Cofactor absorbance was monitored at 340 nm to determine the rate of the reaction. The labeled mutant retained 50% of the wildtype activity.

4.7 References

1. Schweitzer, B. I.; Dicker, A. P.; Bertino, J. R., Dihydrofolate reductase as a therapeutic target. *FASEB J* **1990,** *4* (8), 2441-52.

2. Sawaya, M. R.; Kraut, J., Loop and subdomain movements in the mechanism of Escherichia coli dihydrofolate reductase: crystallographic evidence. *Biochemistry* **1997,** *36* (3), 586-603.

3. Bhabha, G.; Lee, J.; Ekiert, D. C.; Gam, J.; Wilson, I. A.; Dyson, H. J.; Benkovic, S. J.; Wright, P. E., A dynamic knockout reveals that conformational fluctuations influence the chemical step of enzyme catalysis. *Science* **2011,** *332* (6026), 234-8.

4. Li, L.; Falzone, C. J.; Wright, P. E.; Benkovic, S. J., Functional role of a mobile loop of Escherichia coli dihydrofolate reductase in transition-state stabilization. *Biochemistry* **1992,** *31* (34), 7826-33.

5. Henzler-Wildman, K.; Kern, D., Dynamic personalities of proteins. *Nature* **2007,** *450* (7172), 964-72.

6. Reddish, M. J.; Vaughn, M. B.; Fu, R.; Dyer, R. B., Ligand-Dependent Conformational Dynamics of Dihydrofolate Reductase. *Biochemistry* **2016,** *55* (10), 1485-93.

7. Liu, C. T.; Layfield, J. P.; Stewart, R. J., 3rd; French, J. B.; Hanoian, P.; Asbury, J. B.; Hammes-Schiffer, S.; Benkovic, S. J., Probing the electrostatics of active site microenvironments along the catalytic cycle for Escherichia coli dihydrofolate reductase. *J Am Chem Soc* **2014,** *136* (29), 10349-60.

8. Hernandez-Meza, J. M.; Sampedro, J. G., Trehalose Mediated Inhibition of Lactate Dehydrogenase from Rabbit Muscle. The Application of Kramers' Theory in Enzyme Catalysis. *J Phys Chem B* **2018,** *122* (15), 4309-4317.

9. Fan, Y.; Cembran, A.; Ma, S.; Gao, J., Connecting protein conformational dynamics with catalytic function as illustrated in dihydrofolate reductase. *Biochemistry* **2013,** *52* (12), 2036-49.

10. Ansari, A.; Jones, C. M.; Henry, E. R.; Hofrichter, J.; Eaton, W. A., The role of solvent viscosity in the dynamics of protein conformational changes. *Science* **1992,** *256* (5065), 1796-8.

11. Kim, Y. S.; Jones, L. S.; Dong, A.; Kendrick, B. S.; Chang, B. S.; Manning, M. C.; Randolph, T. W.; Carpenter, J. F., Effects of sucrose on conformational equilibria and fluctuations within the native-state ensemble of proteins. *Protein Sci* **2003,** *12* (6), 1252-61.

12. Pabit, S. A.; Roder, H.; Hagen, S. J., Internal friction controls the speed of protein folding from a compact configuration. *Biochemistry* **2004,** *43* (39), 12532-8.

13. Rodriguez-Bussey, I.; Yao, X. Q.; Shouaib, A. D.; Lopez, J.; Hamelberg, D., Decoding Allosteric Communication Pathways in Cyclophilin A with a Comparative Analysis of Perturbed Conformational Ensembles. *J Phys Chem B* **2018,** *122* (25), 6528-6535.

14. Loveridge, E. J.; Tey, L. H.; Allemann, R. K., Solvent effects on catalysis by Escherichia coli dihydrofolate reductase. *J Am Chem Soc* **2010,** *132* (3), 1137-43.

15. Boehr, D. D.; Schnell, J. R.; McElheny, D.; Bae, S. H.; Duggan, B. M.; Benkovic, S. J.; Dyson, H. J.; Wright, P. E., A distal mutation perturbs dynamic amino acid networks in dihydrofolate reductase. *Biochemistry* **2013,** *52* (27), 4605-19.

16. Chen, S.; Fahmi, N. E.; Wang, L.; Bhattacharya, C.; Benkovic, S. J.; Hecht, S. M., Detection of dihydrofolate reductase conformational change by FRET using two fluorescent amino acids. *J Am Chem Soc* **2013,** *135* (35), 12924-7.

Chapter 5:

Activity-Related Microsecond Dynamics Revealed by Temperature-Jump Förster Resonance Energy Transfer Measurements on Thermophilic Alcohol Dehydrogenase

Reproduced with permission from

Vaughn, M. B.; Zhang, J.; Spiro, T. G.; Dyer, R. B.; Klinman, J. P., Activity-Related Microsecond Dynamics Revealed by Temperature-Jump Forster Resonance Energy Transfer Measurements on Thermophilic Alcohol Dehydrogenase. *J. Am. Chem. Soc.* **2018,** *140* (3), 900-903.

Copyright 2018 American Chemical Society

5.1 Abstract

Previous studies of a thermophilic alcohol dehydrogenase (ht-ADH) demonstrated a range of discontinuous transitions at 30°C that include catalysis, kinetic isotope effects, protein hydrogen−deuterium exchange rates, and intrinsic fluorescence properties. Using the Förster resonance energy transfer response from a Trp-NADH donor−acceptor pair in T-jump studies of ht-ADH, we now report microsecond protein motions that can be directly related to active site chemistry. Two distinctive transients are observed: a slow, kinetic process lacking a temperature break, together with a faster transient that is only detectable above 30°C. The latter establishes a link between enzyme activity and micro-second protein motions near the cofactor binding site, in a region distinct from a previously detected protein network that communicates with the substrate binding site. Though evidence of direct dynamical links between microsecond protein motions and active site bond cleavage events is extremely rare, these studies highlight the potential of T-jump measurements to uncover such properties.

5.2 Introduction

Increasingly, the dynamical sampling of protein conformational substates is expected to play an important role in controlling the rate of enzyme catalyzed reactions.[1-7] Stochastic sampling of states may involve motions that range from picoseconds to milliseconds,[8] and the microsecond time regime has been predicted to be an especially key component in the creation of productive conformations.[9] The microsecond regime can be difficult to access, as it is typically too long for routine molecular dynamics simulations and NMR is not suitable for large protein systems such as the tetrameric thermophilic alcohol dehydrogenase from *B. stearothermophilus* (ht-ADH), an archetypic system for relating changes in protein dynamics to active site chemistry.

Previous studies of ht-ADH demonstrated numerous anomalous breaks in behavior as the temperature is reduced below 30°C, which include an increase in the enthalpy of activation for the millisecond chemical (hydride transfer) step,[10] an increase in the temperature dependence of the kinetic isotope effect (KIE) on hydride transfer,[10] and a change in the pattern of time averaged hydrogen−deuterium exchange (HDX) within the substrate binding domain.[11] These aggregate behaviors can be explained by active conformational sampling at the elevated, physiologically relevant temperatures of *B. stearothermophilus*, that becomes reduced below the 30 °C break point. In the present study, we follow the protein dynamics of the ternary complex of ht-ADH with NADH and the substrate analog isobutyramide, via time-resolved temperature-jump Förster resonance energy transfer (FRET) spectroscopy. We observe two relaxation rates, the faster of which disappears below 30°C. We attribute the absence of the faster rate below 30 °C to a "freezing out" of collective motions that modulate the FRET efficiency. We conclude that these same motions are important in the search for reactive conformations in the Michaelis complex.

5.3 Results and Discussion

Fluorescence spectroscopy is a useful probe for studying enzyme motions because it is environmentally sensitive. Ht-ADH contains three tryptophans (Trp): W87 that resides behind bound substrate, W49 that is proximal to bound cofactor, and W167 located on the protein surface far from the active site (**Figure 5. 1**). In this work, we focus on W87F, a variant having W87 alone substituted by phenylalanine. Control experiments with W167in show that W167 does not participate in FRET with the cofactor (**Figure 5S. 1**), which simplifies assignment of the FRET signal origin to energy transfer between W49 and NADH.[12-13] Furthermore, W87F and wildtype ht-ADH exhibit similar kinetic properties and a break in behavior at 30°C,[13] making W87F a suitable surrogate for studying site-specific protein motions.

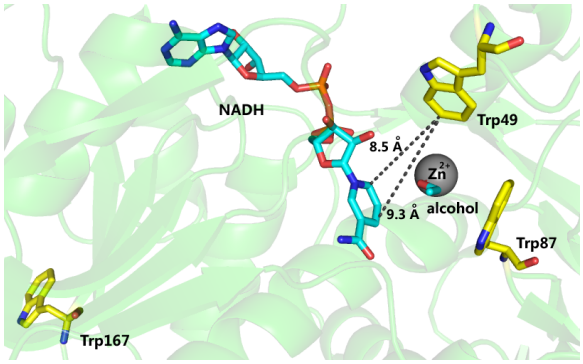

Figure 5. 1 Structure of ht-ADH in green with NADH and alcohol in cyan. The three tryptophan residues are yellow. This structure was created from an overlap of PDB: 1RJW and 3MEQ.

The steady state tryptophan fluorescence of W87F is modulated by ligand binding (**Figure 5. 2A**). Compared to apoenzyme, the binary complex of ht-ADH with isobutyramide shows a slight increase in Trp fluorescence (~330 nm). Binding NADH to the apoenzyme quenches the Trp fluorescence, while inducing NADH fluorescence (~435 nm), due to Förster energy transfer from W49 to NADH. The FRET signal depends on the distance and relative orientation of the donor and

acceptor transition dipoles,[14] with W49 expected to lie within ca. 9Å of the nicotinamide ring of cofactor (**Figure 5. 1**) well within 23.4 Å, the Forster radius of this FRET pair.[14]

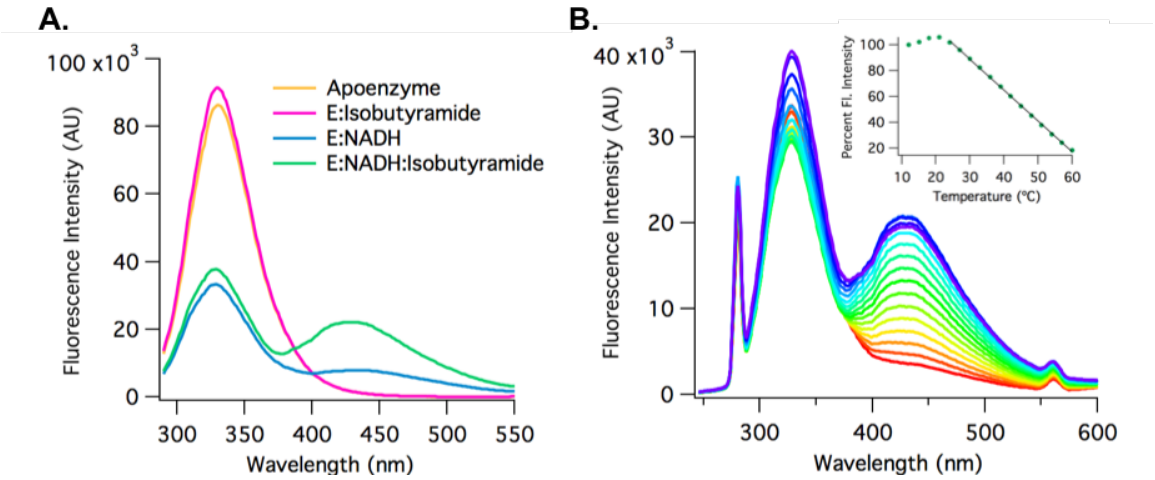

Figure 5. 2 (A) Equilibrium fluorescence spectra of ht-ADH W87F (2 μM) with ligands NADH (20 μM) and isobutyramide (100 mM) in potassium phosphate buffer (50 mM, pH 7) excited at 280 nm. FRET between W49 and NADH is strongest in the ternary complex. (B) Temperature dependent fluorescence spectra of ht-ADH W87F:NADH:isobutyramide. The inset shows the integrated NADH emission (420−460 nm) vs temperature.

The ht-ADH W87F·NADH·isobutyramide ternary complex shows a much stronger FRET signal (**Figure 5. 2A**), indicating that binding of the substrate analog alters the enzyme conformation and brings W49 into better alignment with NADH. Temperature dependent fluorescence spectra show that the FRET signal of the tertiary complex is nearly temperature independent below 30°C (**Figure 5. 2B**). The decrease in FRET intensity at higher temperatures may be attributed to an increase in flexibility of W87F ADH allowing for fluctuations that lead to possible changes in the relative orientation of the donor−acceptor transition dipole moments as well as some increase in the average distance between W49 and the nicotinamide ring of the cofactor.

T-jump fluorescence spectroscopy was used to interrogate conformational fluctuations of the W87F ternary complex on the ns to μs time scale. T-jumps of 9°C were generated by laser heating with a range of final temperatures between 22 and 50°C (**Figure 5S. 2**). The resulting FRET transients display distinct behaviors as a function of temperature (**Figure 5. 3A**). In no instance were these found to exhibit a concentration dependence with respect to NADH or isobutyramide, indicating relaxation events that are independent of ligand association/dissociation processes (**Figure 5S. 3**). A number of fits to the experimental traces were tested via a combination of single and/or two exponential decays across the experimental temperature regime. A best fit was identified that corresponds to two exponentials above 30°C together with a single decay process below this point (**Table 5S. 1**). It is striking that the slow relaxation shows continuity across the full temperature range, whereas the fast process has been slowed to such an extent below 30 °C that it no longer contributes to the observed transients. These changes in rate constants are mirrored in their amplitudes, with the slow rate being characterized by a constant amplitude (within the noise of the measurement) whereas the fast rate shows a linear increase above 30°C (**Figure 5S. 4**). The Arrhenius plot (**Figure 5. 3B**) shows the dramatic decrease in the rate of the fast process with decreasing temperature and its disappearance at 30°C. Moreover, its activation energy 10.4 ± 1.3 kcal/mol is close to the enthalpy of activation, 11.0 ± 0.6 kcal/mol for the hydride transfer step above 30°C,[13] whereas that of the slow process is weakly temperature dependent with an activation energy of 3.0 ± 0.9 kcal/mol. Thus, the T-jump FRET response, which is sensitive to motions along the reaction coordinate (**Figure 5. 1**), provides direct support for the view that catalysis is enabled by protein motions that become activated above 30°C. These are likely collective motions involved in the search for a reactive conformation. Further insight as to the origin of the two phases comes from the temperature dependence of fluorescence anisotropy of the tertiary complex (**Figure 5S. 5**). Below 30°C, the anisotropy decreases with increasing temperature, indicating the relative orientation

of the donor and acceptor transition dipole moments is changing with temperature. Therefore, the slow T-jump FRET response observed in this temperature regime is due to a reorientation of the donor and acceptor with respect to one another. The combined anisotropy and temperature jump FRET results lead to assignment of the slow phase to a local motion that predominately changes the orientation of the dipole moments. Above 30°C, the fluorescence anisotropy is relatively temperature independent, either because the dipole orientation is no longer changing, or more likely, the average dipole orientation factor is 2/3 due to conformational sampling. Thus, the trend in the fast T-jump FRET, dominant above 30°C, corresponds to collective motions that modulate the distance between the FRET pair.

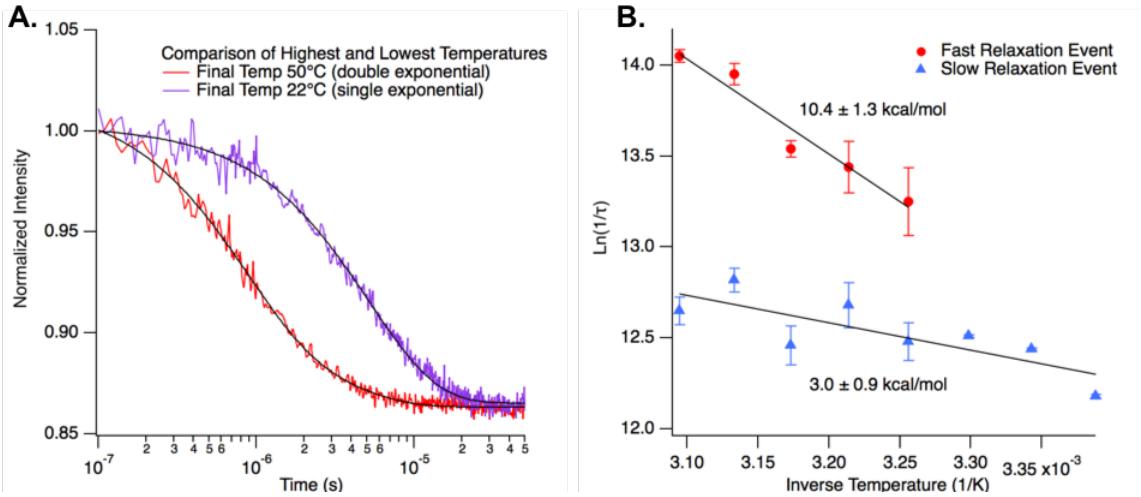

Figure 5. 3 (A) Temperature-jump (ΔT = 9°C) FRET transients of the highest and lowest final temperatures. The transients are shown as normalized FRET intensity to highlight the difference in shape. The highest temperature fits best to a double exponential and the lowest temperature fits best to a single exponential. (B) Arrhenius plot of observed relaxation rates. The slower relaxation rate is present at all temperatures (2.6×10^5 s^{-1} at 34°C) and appears to be slightly temperature dependent. Conversely, the faster rate (5.7×10^5 s^{-1} at 34°C) is present only at temperatures above 30 °C and is strongly temperature dependent.

The disappearance of the fast process below 30°C is suggestive of a glass transition, and it has been hypothesized that thermophilic enzymes may have much higher glass transition temperatures than mesophilic enzymes.[15] Ht-ADH catalysis still occurs below this temperature, but the activation enthalpy is much higher, 17.0 ± 0.4 kcal/mol,[10, 13] which has been previously attributed to an impairment of the facilitating protein motions.[16] The rate of catalysis for a related dehydrogenase, lactate dehydrogenase (LDH), has also been shown to be controlled by the search for a reactive conformation in the formation of binary and ternary complexes through collective motions.[1, 9] Fast and slow kinetics have been observed for LDH on similar time scale as observed here for ADH.[17] It has been shown that psychrophilic, mesophilic, and thermophilic LDH have the same enzymatic efficiency at the host organism's optimal growth temperature.[10] Furthermore, pig heart LDH demonstrates a structural change and similar break in enzyme activity around 35°C, indicating that elevated glass transitions may not be restricted to thermophilic enzymes.[18]

Previous studies of ht-ADH show strong structural anisotropy with regard to a network of protein motions that connects a solvent exposed dimer (Interface I, **Figure 5S. 6**) with the substrate binding pocket ca. 17 Å from W87.[19] This interface connects subunits in which the primary contact is a Tyr25−Tyr25 stacking interaction that has been correlated with temperature breaks in k_{cat}, the kinetic isotope effect, and the fluorescent lifetime of W87in.[12, 19] The structure of ADH is a dimer of dimers, generating both the symmetrical dimer Interface I, and a second asymmetrical Interface, II, characterized by a contact between W49 and Phe272 from the adjacent subunit (**Figure 5S. 6**). A T-jump study of apoW78F showed microsecond fluorescence transients, which were attributed to opening and closing of this contact; the apoprotein does not adopt the structure of the ternary complex, and no 30°C break was observed in the rates.[13]

The remarkable T-jump results reported here implicate a second network of motions within ht-ADH that arises at Interface II and modulates the relative position of the reactive nicotinamide ring of the cofactor, as reported by FRET. Thus, positioning of the hydride donor and acceptor for reaction, as well as other key residues that engage in the stabilization of dipolar and electrostatic changes accompanying the net hydride transfer reaction, appears to be facilitated by two structurally orthogonal networks, directed at the cofactor on one hand and the substrate on the other (**Figure 5S. 6**).

A general theory for hydrogen transfer in enzymatic C−H cleavage reactions has emerged in which hydrogen transfer occurs via a tunneling reaction dictated by protein motions that create both reactant−product ground state degeneracies and close hydrogen donor−acceptor distances.[20-21] This process has been represented by k_{tun} within a full rate equation that incorporates a prior protein conformational search for catalytically relevant protein substates defined as F_{conf}:[22]

$$k_{obs} = F_{conf} k_{tun}$$

As discussed, the enthalpic barrier for C−H cleavage reactions that occur via tunneling will be comprised of a combination of local rapid protein motions (ps−ns) together with slower more remote motions (μs−ms) that can be considered to arise primarily from F_{conf} and the outer sphere reorganization term, λ_{out}, in k_{tun}. Independent of time scale, all of the motions that precede the tunneling event are considered to be equilibrated, stochastic processes.[1, 23]

In a recently completed study of the enzyme soybean lipoxygenase, the enthalpic barriers for rates of hydrogen− deuterium exchange (HDX) within a remote loop at the protein surface were found to correlate with mutation-induced trends in the enthalpic barriers for the rate of H-tunneling at the active site.[22] The physical picture that emerged involves a well-defined motional network that connects the SLO protein− solvent interface with the active site ca. 15−30 Å away. For this earlier

study, the absolute magnitude of the enthalpies from HDX and catalysis were distinct, as anticipated from the different physical processes controlling a thermally averaged HDX vs the chemical hydride transfer step. In contrast, the present T-jump study of ht-ADH provides a microsecond time constant and activation energy for protein reorganization that can be directly compared to k_{cat}. Of note, although the time scales for k_{cat} and FRET in ht-ADH differ by 3 orders of magnitude, the energies of activation are almost identical. Though the latter could be fortuitous, the data strongly implicate a link between thermally equilibrated, microsecond protein motions and the creation of active site configurations that support hydrogen transfer via tunneling. Although evidence for such direct dynamical links between microsecond protein motions and active site bond cleavage events is extremely rare, T-jump measurements appear ideally suited both to the detection of such motions and to the resolution of their relationship to networks for motional communication between protein−solvent interfaces and enzyme active sites.

5.4 Supplemental Information

Expression and Purification of ht-ADH-W87F

The W87F, W87in, W49in, W167in mutants were generated from the wild-type *B. stearothermophilus* htADH gene previously cloned into the *E. coli* pET-24b(+) expression vector as described in previously.[11-13] Recombinant *ht*-ADHs were transformed and expressed in *Escherichia coli* BL21 (DE3) cells (Stratagene). Transformed BL21 (DE3) cells were grown in LB medium containing kanamycin (30 mg/L) and 0.25 mM $ZnSO_4$. When the absorbance at 600 nm was around 0.6, cells were induced with 0.2mM IPTG (isopropyl β-D-1-thiogalactopyranoside) and grown at 37°C overnight while shaking at 200 rpm. The cells were harvested via centrifugation at 5,000 x g for 20 min at 4°C. The cell pellets were re-suspended in lysis buffer [25 mM potassium

phosphate, 0.2 mM DTT (pH 7.2)] with lysozyme (1 mg/ml). After lysis, the cells were centrifuged at 20,000 x g for 20min at 4°C. The clear supernatant was heated at 60°C for 15 min and then was centrifuged at 20,000 x g for 15 min. The resulted supernatant was loaded onto a DEAE column, which was pre-equilibrated with lysis buffer. The ht-ADH was collected by using elution buffer (25 mM potassium phosphate (pH 7.2) 0.2 mM DTT, 0.25M NaCl) and dialysis against lysis buffer. The concentrated *ht*-ADH was loaded onto Blue Sepharose 6 fast flow affinity column and washed by lysis buffer. After that, 5 mM 5'-adenosine monophoshate was used to elute the *ht*-ADH. Finally, the protein was concentrated and stored at -80°C until further use. Protein concentrations were calculated using the Bradford assay. UV-vis spectra were recorded on a Cary 50 Biospectrophotometer.

Equilibrium Fluorescence Characterization

Fluorescence spectra were obtained using a Dual-Fl Fluorometer (Horiba Scientific, Edison, New Jersey) via a 280 nm excitation for four complexes: htADH-W87 apoenzyme, E:NADH, E:Isobutyramide, and E:NADH:Isobutyramide. The samples were prepared using the follow concentrations: 2 μM enzyme, 20 μM NADH, and 100 mM isobutyramide in potassium phosphate buffer (50 mM, pH 7). Temperature dependent spectra were obtained for the ternary complex from 12°C to 60°C in increments of 3°C using a peltier temperature controller. The NADH fluorescence peak was integrated between 420 – 460 nm and plotted versus temperature. Similarly, FRET anisotropy of the ternary complex was determined using the integrated intensity of parallel and perpendicularly polarized emission.

Temperature-Jump Fluorescence Spectroscopy

Temperature-jump fluorescence relaxation experiments were performed on a custom built instrument as previously described. Briefly, a Q-switched Ho:YAG laser (AQS-Ho-YAG, IPG

Phototonics Corp., Oxford, MA) is used to generate a temperature jump of approximately 9°C. Temperature jumps are generated with deuterium exchanged samples rather than H_2O to take advantage of the difference in absorbance bands in the far IR. H_2O absorbs too strongly, whereas D_2O absorbs enough for a 9°C jump. Change in fluorescence is probed by ~280 nm excitation generated by frequency-tripled Ti:Sapphire (845 nm) pumped by a Verdi V12 laser (Coherent, Santa Clara, CA). Sample emission is focused through an appropriate bandpass filter and is measured by a Hamamatsu R7518 photomultiplier tube (Hamamatsu Pho- tonics K. K., Hamamatsu, Japan). The signal is digitized and averaged (5000 shots) by a using a Wavesurfer 62Xs-B oscilloscope (Teledyne LeCroy, Chestnut Ridge, NY). Temperature-jump experiments were performed on the ternary complex (100 μM enzyme, 500 μM NADH, and 100 mM isobutyramide) in 50 mM potassium phosphate D_2O buffer at pD 7. Tryptophan (100 μM) was used as a reference to determine the size of the temperature jump as well as subtract out the inherent temperature dependence of tryptophan fluorescence. The intensity of the transients are normalized and are reported as a percent of initial fluorescence intensities.

Construction of Figure 1

The structure of ht-ADH with NADH and alcohol shown in Figure 1 was created by PyMOL. Here, only the chain A of ht-ADH was displayed. PDB: 1RJW contains the structure of ht-ADH, alcohol and metal $Zn2^+$, but not NADH. The position of NADH was added into Figure 1 by performing the structure alignment between 1RJW (chain A) and 3MEQ (chain A).

Figures and Charts

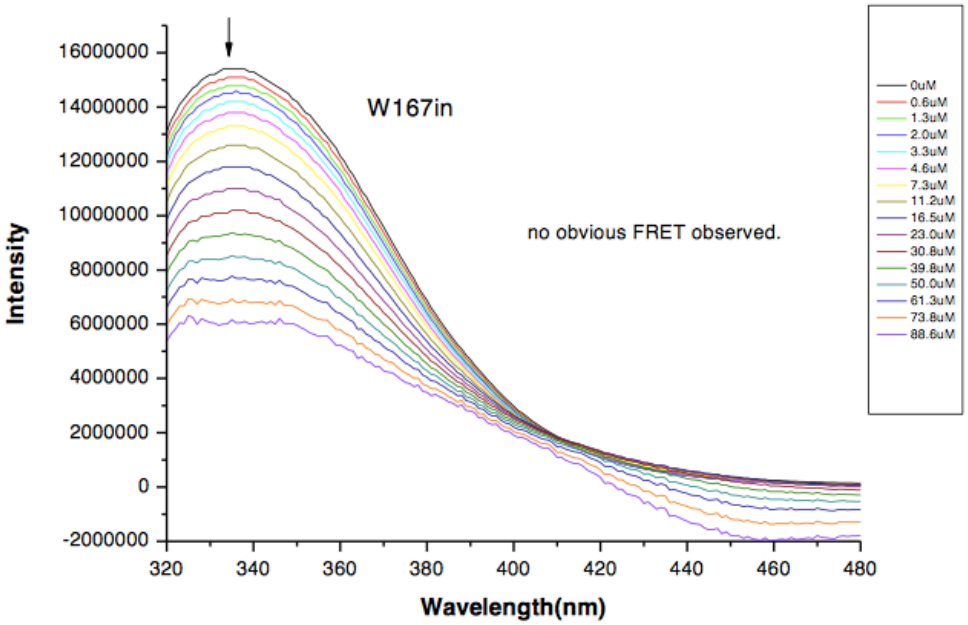

Figure 5S. 1 Fluorescence spectra of ht-ADH W167in (2 μM) with the titration of different concentrations of NADH in the present of 100mM isobutyramide. The spectra are corrected with the NADH fluorescence background.

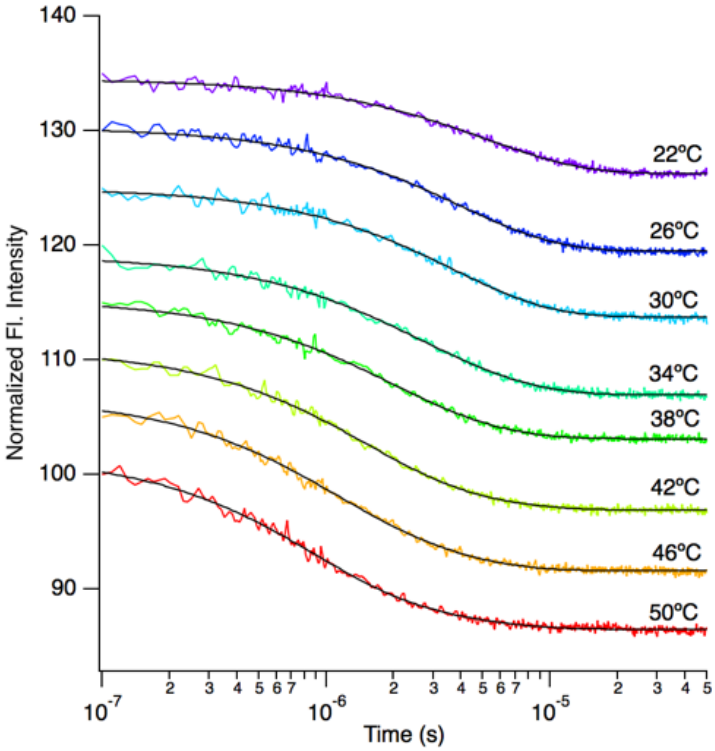

Figure 5S. 2 Temperature jump (Δ9°C) transients of ht-ADH W87F·NADH·isobutyramide (100 μM enzyme, 500 μM NADH, and 100 mM isobutyramide in deuterium exchanged 50 mM potassium phosphate, pH 7) monitoring FRET between W49 and NADH. Transients with final temperatures above 30°C fit best to double exponentials whereas transients at and below 30°C fit best to single exponentials.

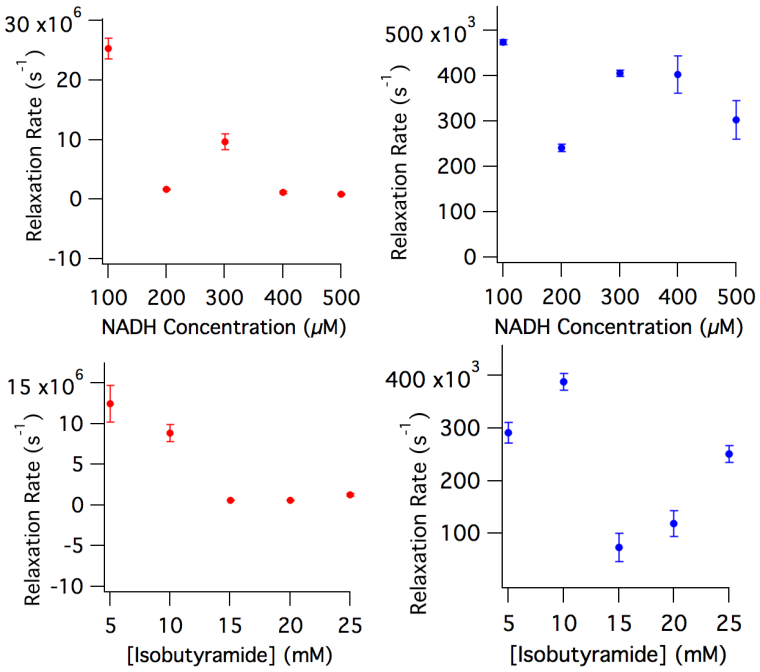

Figure 5S. 3 Temperature jump FRET relaxation rates (left - fast phase, right - slow phase) versus ligand concentration. Transients were generated from an 8°C jump, with a final temperature of 38°C. Samples with a range of ligand concentrations were prepared. (A. 100 μM enzyme, 100 mM isobutyramide, 100 – 500 μM NADH and B. 100 μM enzyme, 400 μM NADH, 5 – 25 mM isobutyramide). Temperature jump spectroscopy reports on relaxation kinetics; hence, information is obtained about both the forward and reverse processes. Ligand association is a bimolecular process. If the active site occupancy were changing due to the temperature jump, the relaxation rates would be concentration dependent. However, no dependence was observed with either NADH or isobutyramide at the concentration range employed in the T-jump assays (100 μM enzyme, 500 μM NADH and 100 mM isobutyramide).

Table 5S. 1 Each transient from **Figure 5S. 2** was fit to both a single exponential function and a double exponential function. Reported in the chart is the percentage that χ^2 decreased when comparing the single exponential fits to double exponential fits. At and below 30°C the χ^2 value decreases by a negligible amount; thus, the transients are best fit to single exponentials. Conversely, above 30°C the χ^2 value decreases upon fitting to a double exponential, so these transients are fit to double exponentials.

Final Temperature	Decrease in χ^2
22	3%
26	5%
30	3%
34	10%
38	11%
42	30%
46	38%
50	45%

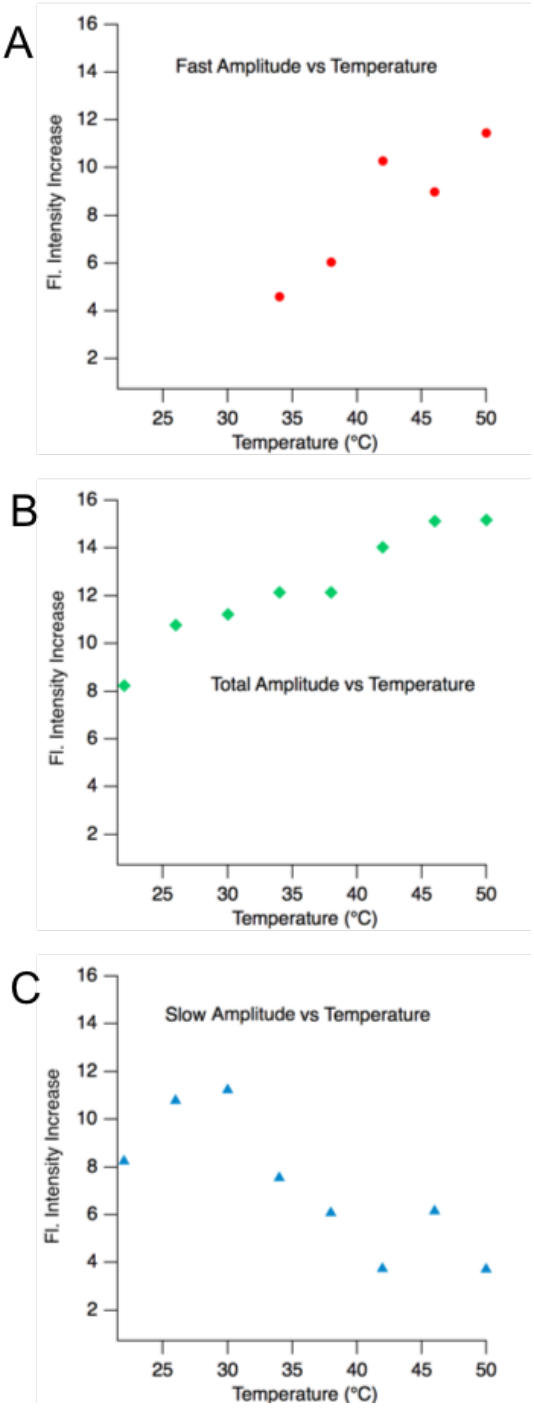

Figure 5S. 4 Amplitudes of transients from **Figure 5S. 2**: A) fast phase, B) total amplitude change, and C) slow phase. The fast phase amplitude increases with temperature, which accounts for the majority of the total increase in amplitude with temperature. The slow phase amplitude shows no distinct trend with temperature.

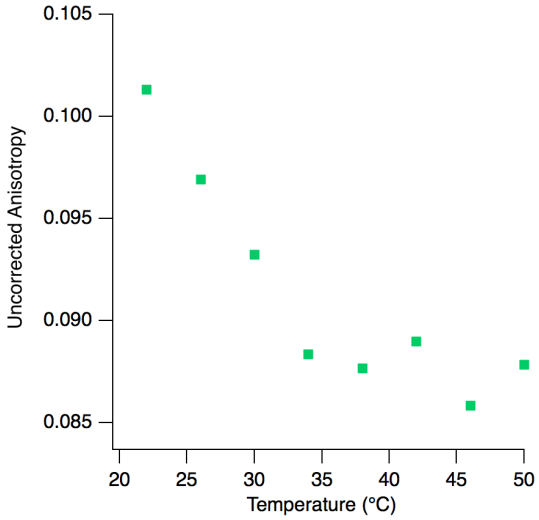

Figure 5S. 5 Fluorescence anisotropy for the tertiary complex (uncorrected for instrument response) versus temperature. Below 30°C, the anisotropy decreases with temperature, compared to above 30°C where the anisotropy shows little correlation with temperature.

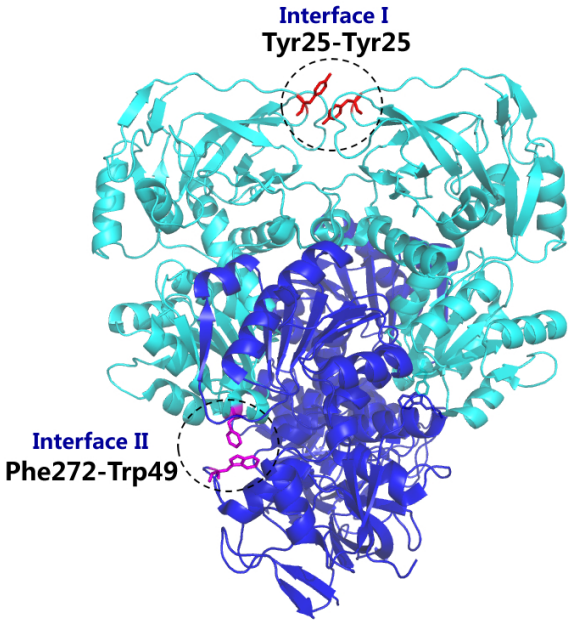

Figure 5S. 6 The topology of the ht-ADH structure (composed of four identical subunits) generates two types of dimer interfaces, labelled I and II, respectively. Interface I is characterized by a Tyr25-Tyr25 π stacking interaction that links to the bound substrate ca. 17 Å away. Interface II shows the interaction of Trp49, ca. 9 Å from the nicotinamide ring of cofactor, with Phe 272 on an opposing subunit.

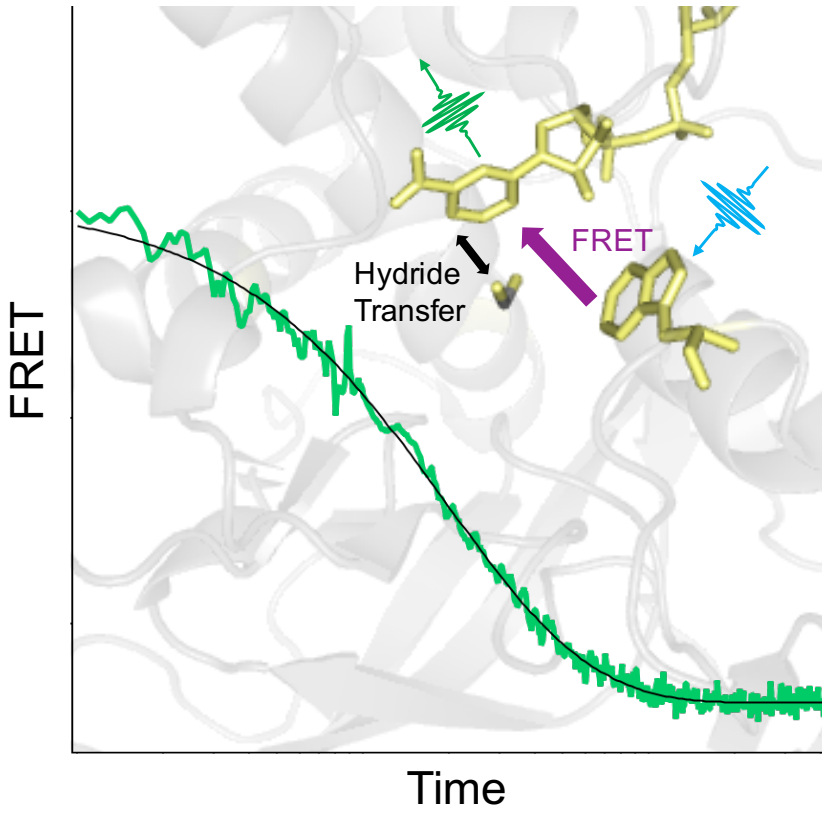

Figure 5S. 7 Conceptual schematic showing change in FRET versus time as well as the alignment of the hydride transfer and FRET axes.

5.5 References

1. Klinman, J. P.; Kohen, A., Hydrogen tunneling links protein dynamics to enzyme catalysis. *Annu Rev Biochem* **2013,** *82*, 471-96.

2. Callender, R.; Dyer, R. B., The dynamical nature of enzymatic catalysis. *Acc Chem Res* **2015,** *48* (2), 407-13.

3. Nashine, V. C.; Hammes-Schiffer, S.; Benkovic, S. J., Coupled motions in enzyme catalysis. *Curr Opin Chem Biol* **2010,** *14* (5), 644-51.

4. Hay, S.; Scrutton, N. S., Good vibrations in enzyme-catalysed reactions. *Nat Chem* **2012,** *4* (3), 161-8.

5. Luk, L. Y.; Loveridge, E. J.; Allemann, R. K., Protein motions and dynamic effects in enzyme catalysis. *Phys Chem Chem Phys* **2015,** *17* (46), 30817-27.

6. Fraser, J. S.; Clarkson, M. W.; Degnan, S. C.; Erion, R.; Kern, D.; Alber, T., Hidden alternative structures of proline isomerase essential for catalysis. *Nature* **2009,** *462* (7273), 669-73.

7. Motlagh, H. N.; Wrabl, J. O.; Li, J.; Hilser, V. J., The ensemble nature of allostery. *Nature* **2014,** *508* (7496), 331-9.

8. Henzler-Wildman, K.; Kern, D., Dynamic personalities of proteins. *Nature* **2007,** *450* (7172), 964-72.

9. Reddish, M. J.; Peng, H. L.; Deng, H.; Panwar, K. S.; Callender, R.; Dyer, R. B., Direct evidence of catalytic heterogeneity in lactate dehydrogenase by temperature jump infrared spectroscopy. *J Phys Chem B* **2014,** *118* (37), 10854-62.

10. Kohen, A.; Cannio, R.; Bartolucci, S.; Klinman, J. P., Enzyme dynamics and hydrogen tunnelling in a thermophilic alcohol dehydrogenase. *Nature* **1999,** *399* (6735), 496-9.

11. Liang, Z. X.; Lee, T.; Resing, K. A.; Ahn, N. G.; Klinman, J. P., Thermal-activated protein mobility and its correlation with catalysis in thermophilic alcohol dehydrogenase. *Proc Natl Acad Sci U S A* **2004,** *101* (26), 9556-61.

12. Meadows, C. W.; Ou, R.; Klinman, J. P., Picosecond-resolved fluorescent probes at functionally distinct tryptophans within a thermophilic alcohol dehydrogenase: relationship of temperature-dependent changes in fluorescence to catalysis. *J Phys Chem B* **2014,** *118* (23), 6049-61.

13. Meadows, C. W.; Balakrishnan, G.; Kier, B. L.; Spiro, T. G.; Klinman, J. P., Temperature-Jump Fluorescence Provides Evidence for Fully Reversible Microsecond Dynamics in a Thermophilic Alcohol Dehydrogenase. *J Am Chem Soc* **2015,** *137* (32), 10060-3.

14. Lakowicz, J. R., *Principles of Fluorescence Spectroscopy*. 3rd. ed.; Springer: US, New York, 2006.

15. Ringe, D.; Petsko, G. A., The 'glass transition' in protein dynamics: what it is, why it occurs, and how to exploit it. *Biophys Chem* **2003,** *105* (2-3), 667-80.

16. Nagel, Z. D.; Dong, M.; Bahnson, B. J.; Klinman, J. P., Impaired protein conformational landscapes as revealed in anomalous Arrhenius prefactors. *Proc Natl Acad Sci U S A* **2011,** *108* (26), 10520-5.

17. Clarke, A. R. W., A. D. B.; Hart, K. W.; Holbrook, J. J., *Biochim. Biophys. Acta, Protein Struct. Mol. Enzymol.* **1985,** *829*, 397− 407.

18. Khrapunov, S.; Chang, E.; Callender, R. H., Thermodynamic and Structural Adaptation Differences between the Mesophilic and Psychrophilic Lactate Dehydrogenases. *Biochemistry* **2017,** *56* (28), 3587-3595.

19. Nagel, Z. D.; Cun, S.; Klinman, J. P., Identification of a long-range protein network that modulates active site dynamics in extremophilic alcohol dehydrogenases. *J Biol Chem* **2013,** *288* (20), 14087-97.

20. Knapp, M. J.; Klinman, J. P., Environmentally coupled hydrogen tunneling. Linking catalysis to dynamics. *Eur J Biochem* **2002,** *269* (13), 3113-21.

21. Hammes-Schiffer, S., Hydrogen tunneling and protein motion in enzyme reactions. *Acc Chem Res* **2006,** *39* (2), 93-100.

22. Offenbacher, A. R.; Hu, S.; Poss, E. M.; Carr, C. A. M.; Scouras, A. D.; Prigozhin, D. M.; Iavarone, A. T.; Palla, A.; Alber, T.; Fraser, J. S.; Klinman, J. P., Hydrogen-Deuterium Exchange of Lipoxygenase Uncovers a Relationship between Distal, Solvent Exposed Protein Motions and the Thermal Activation Barrier for Catalytic Proton-Coupled Electron Tunneling. *ACS Cent Sci* **2017,** *3* (6), 570-579.

23. Soudackov, A. V.; Hammes-Schiffer, S., Proton-coupled electron transfer reactions: analytical rate constants and case study of kinetic isotope effects in lipoxygenase. *Faraday Discuss* **2016,** *195*, 171-189.

Chapter 6:

Conclusions and Future Directions

Morgan Bair Vaughn

6.1 Alcohol Dehydrogenase

Previous studies of thermophilic alcohol dehydrogenase (ADH) observed anomalous behavior at temperatures below 30°C. The activation energy of catalysis increases,[1] the KIE becomes more temperature dependent,[1] and the pattern of hydrogen-deuterium exchange rates change in the substrate binding pocket.[2] In this body of work, temperature jump (T-jump) Förster Resonance Energy Transfer (FRET) spectroscopy was used to study the dynamic sampling of a thermophilic alcohol dehydrogenase (ADH) on the nanosecond to microsecond timescale. We observed collective motions that modulate distances along the hydride transfer donor-acceptor axis that are present above 30°C and absent below 30°C. Notably, the activation energies of the collective motions and catalysis above 30°C are within error of each other, implying a link between collective motions on the nano- to microsecond timescale and catalysis on the millisecond timescale. Hydride transfer, particularly in the case of tunneling, depends heavily on the donor-acceptor distance. Therefore, collective motions that modulate the donor-acceptor distance are important for the search for reactive conformations.

Uncovering the "freezing-out" of collective motions along the hydride transfer axis in thermophilic ADH leads to the question of whether or not other enzymes experience a similar phenomenon. Do collective motions in other enzymes aid in the search for the reactive conformation? Do they also "freeze out" and if so, at what temperature? Is this unique to hydride transfer enzymes that utilize tunneling since the donor-acceptor distance plays a vital role in these enzymes? Schwartz and Schramm have found that some enzyme systems such as purine nucleoside phosphorylase (PNP) and lactate dehydrogenase (LDH) exhibit promoting vibrations – fast motions

that facilitate barrier crossing.[3] However, these motions are much faster than what we report here, on the femtosecond timescale rather than nanoseconds to microseconds. Previous reports of LDH ascertained that collective motions are important for the search for reactive conformations and that there are actually several active conformations with differing reactivity.[4] A recent study examined substrate binding and activity of homologous LDH from pig heart (mesophile) and mackerel icefish (psychrophile).[5] Interestingly, the pig heart LDH demonstrated an increase in activation energy below 35°C, reminiscent of the increase in activation energy of ADH below 30°C. This raises the question, are the collective motions of pig heart LDH abrogated below 35°C, similar to ADH? If so, this would indicate that such transitions are not limited to thermophiles and can even occur at higher temperatures despite the fact that pig heart LDH is a mesophile.

Temperature jump FRET spectroscopy could be used to study collective motions in pig heart LDH and any other enzymes that demonstrate anomalous temperature dependent behaviors. In particular, hydride transfer enzymes may be amendable to this strategy because they often use NADH or NADPH as a cofactor which is a FRET pair with tryptophan, thereby making incorporation of a probe fairly simple. By studying several enzyme systems, we can determine whether or not temperature-mediated collective motions are a motif across hydride transfer enzymes that employ tunneling, or perhaps are characteristic of an even wider class of enzymes.

6.2 Dihydrofolate Reductase

It is well established that conformational changes within *E. coli* DHFR are important for catalysis.[6-10] However, there are still questions about what dynamics occur within DHFR and how they are connected to the catalytic cycle. Here, we used temperature jump fluorescence spectroscopy to investigate enzyme dynamics of DHFR on the microsecond timescale. With native tryptophan fluorescence as a probe, we found that DHFR exhibits a relaxation lifetime of several hundred microseconds that is coupled to ligand dissociation/association as well as a slow motion with a

lifetime of several milliseconds that is uncoupled to ligand binding. Because the slow relation rate is concentration independent, it is difficult to assign a function to the conformational change; albeit, the slow relaxation rate does vary based on which ligand is present. This difference indicates that the conformational change is sensitive to the state of the enzyme. To investigate the dynamics of DHFR further, we created midW mutants – mutants in which four out of the five native tryptophans have been mutated to phenylalanine, leaving a single tryptophan as a site-specific fluorescence probe. In all of the midW mutants we observed dynamics similar to wildtype DHFR (wt-DHFR): a fast concentration dependent relaxation rate coupled to ligand association/dissociation and a slow concentration independent relaxation rate. Interestingly, the relaxation rate on the millisecond timescale differed based on the location of the probe, with tryptophans in similar regions of the enzyme exhibiting similar relaxation rates. However, all but one of the slow relaxation rates of the midW mutants were faster than what we observed in the wildtype enzyme, leading us to conclude that the individual tryptophans were reporting on local motions, whereas in wt-DHFR the tryptophan fluorescence is reporting on global conformational changes sensed by the interaction of the tryptophans with each other. Lastly, we explored loop motions of DHFR by incorporating a site-specific label on the Met20 loop. We measured the relaxation rates of the closed-open, occluded-open, and closed-occluded transitions, which has not been accomplished before. Importantly, we established that the closed to occluded transition occurs on the low microsecond timescale. The closed to occluded conformational change is a hallmark of DHFR catalysis; the Met20 loop changes conformation from closed to occluded at some point during the transition from reactants to products. In the future, this transition could be studied in more detail by computational methods, given the recent advancements in microsecond simulations. Additionally, the closed to occluded transition includes two relaxation phases, indicative of a two-step process. Fan et al. report that the Met20 loop accesses the open conformation near the transition state of the hydride transfer. Our

evidence supports that the transition from closed to occluded does not follow a two state model but instead requires an intermediate, which could be the open conformation.

In this body of work, we have demonstrated the utility of temperature jump fluorescence spectroscopy to map the dynamics of DHFR. Future studies could use this technique to study if and how enzyme motions are modulated by mutations and inhibitors. For example, the FG loop in DHFR crystal structures does not show an obvious conformational change for different ligand-bound states,[11] but NMR backbone chemical shifts change dramatically between the closed and occluded conformations, indicating that there is at least an environmental change.[12] The flexibility of the FG loop is important for catalysis; when G121, a residue within the FG loop, is mutated to valine, the hydride transfer rate is decreased 400-fold.[13] Furthermore, it is hypothesized that the FG and Met20 loop motions are coupled. Boehr et al. observed dampening of both the FG and Met20 backbone motions on the picosecond to nanosecond timescale in the G121V mutant.[13] Fan et al. report computational studies that show two hydrogen bond interactions of Q18 between the FG loop and Met20 loop in the closed conformation.[14] At the transition state, these hydrogen bonds break, allowing the Met20 loop to adopt an open conformation. DHFR mutants with substitutions that impair the flexibility of the FG loop form an additional hydrogen bond between the FG and Met20 loop, stabilizing the closed conformation. To determine if the FG and Met20 loop motions are coupled on the microsecond timescale, the loop dynamics of each knockout mutant could be studied with T-jump fluorescence spectroscopy using mutants with site-specific labels in the FG and Met20 loops. Presumably, if FG loop flexibility is decreased, we would observe a corresponding change in the Met20 loop dynamics and vice versa.

A strategy similar to the one described above could be employed to study the effects of allosteric inhibitors on enzyme dynamics. The mechanism of allosteric inhibition is not well understood, particularly when binding an allosteric effector does not induce a structural change at

the active site. It is hypothesized that dynamics are the link between allosteric effectors and active site chemistry. Recently, several allosteric inhibitors have been identified for DHFR and have shown to be active against variants with resistance to all known classes of clinical DHFR inhibitors.[15] One of the identified allosteric binding pockets is located below the FG loop. Given the hypothesis that the FG and Met20 loop motions are coupled, it seems reasonable that the mechanism by which the inhibitor shuts down activity is by disrupting the loop motions. Again, site-specific labeling of the loops coupled with T-jump fluorescence spectroscopy could be used to determine if the proposed mechanism is correct. Allosteric regulation is an exciting avenue for drugs in part because, like the recently discovered DHFR allosteric inhibitors, they have been shown to be effective against mutants that have developed resistance to competitive inhibitors. Understanding how allosteric effectors communicate with the active site can assist in identifying alternative effector binding sites and improve rational drug design.

6.3 Perspective

The work presented here has demonstrated the capability of temperature jump fluorescence spectroscopy to elucidate enzyme dynamics. We studied two model enzymes and increased our knowledge of these systems in hopes that what we learned will be broadly applicable to other enzymes. The ultimate goal is to understand how enzymes function, with a focus on dynamics as a missing puzzle piece. Identifying and measuring motions along with characterizing dynamic-function paradigms is a necessary step to building a robust mathematical model of enzymes. Although there have been many improvements, current models are still lacking, as revealed by limited de novo enzyme genesis and rational drug design. Having a complete understand of enzyme function will allow scientists to harness the potential of enzymes to solve many problems that plague our society,

such producing net-zero carbon fuels, combating antibiotic resistance, and facilitating green industrial processes.

6.4 References

1. Kohen, A.; Cannio, R.; Bartolucci, S.; Klinman, J. P., Enzyme dynamics and hydrogen tunnelling in a thermophilic alcohol dehydrogenase. *Nature* **1999,** *399* (6735), 496-9.

2. Liang, Z. X.; Lee, T.; Resing, K. A.; Ahn, N. G.; Klinman, J. P., Thermal-activated protein mobility and its correlation with catalysis in thermophilic alcohol dehydrogenase. *Proc Natl Acad Sci U S A* **2004,** *101* (26), 9556-61.

3. Schramm, V. L.; Schwartz, S. D., Promoting Vibrations and the Function of Enzymes. Emerging Theoretical and Experimental Convergence. *Biochemistry* **2018,** *57* (24), 3299-3308.

4. Reddish, M. J.; Peng, H. L.; Deng, H.; Panwar, K. S.; Callender, R.; Dyer, R. B., Direct evidence of catalytic heterogeneity in lactate dehydrogenase by temperature jump infrared spectroscopy. *J Phys Chem B* **2014,** *118* (37), 10854-62.

5. Khrapunov, S.; Chang, E.; Callender, R. H., Thermodynamic and Structural Adaptation Differences between the Mesophilic and Psychrophilic Lactate Dehydrogenases. *Biochemistry* **2017,** *56* (28), 3587-3595.

6. Bhabha, G.; Biel, J. T.; Fraser, J. S., Keep on moving: discovering and perturbing the conformational dynamics of enzymes. *Acc Chem Res* **2015,** *48* (2), 423-30.

7. Hanoian, P.; Liu, C. T.; Hammes-Schiffer, S.; Benkovic, S., Perspectives on electrostatics and conformational motions in enzyme catalysis. *Acc Chem Res* **2015,** *48* (2), 482-9.

8. Singh, P.; Abeysinghe, T.; Kohen, A., Linking protein motion to enzyme catalysis. *Molecules* **2015,** *20* (1), 1192-209.

9. Hammes-Schiffer, S.; Benkovic, S. J., Relating protein motion to catalysis. *Annu Rev Biochem* **2006,** *75*, 519-41.

10. Ramanathan, A.; Savol, A.; Burger, V.; Chennubhotla, C. S.; Agarwal, P. K., Protein conformational populations and functionally relevant substates. *Acc Chem Res* **2014,** *47* (1), 149-56.

11. Sawaya, M. R.; Kraut, J., Loop and subdomain movements in the mechanism of Escherichia coli dihydrofolate reductase: crystallographic evidence. *Biochemistry* **1997,** *36* (3), 586-603.

12. Osborne, M. J.; Venkitakrishnan, R. P.; Dyson, H. J.; Wright, P. E., Diagnostic chemical shift markers for loop conformation and substrate and cofactor binding in dihydrofolate reductase complexes. *Protein Sci* **2003,** *12* (10), 2230-8.

13. Boehr, D. D.; Schnell, J. R.; McElheny, D.; Bae, S. H.; Duggan, B. M.; Benkovic, S. J.; Dyson, H. J.; Wright, P. E., A distal mutation perturbs dynamic amino acid networks in dihydrofolate reductase. *Biochemistry* **2013,** *52* (27), 4605-19.

14. Fan, Y.; Cembran, A.; Ma, S.; Gao, J., Connecting protein conformational dynamics with catalytic function as illustrated in dihydrofolate reductase. *Biochemistry* **2013,** *52* (12), 2036-49.

15. Srinivasan, B.; Rodrigues, J. V.; Tonddast-Navaei, S.; Shakhnovich, E.; Skolnick, J., Rational Design of Novel Allosteric Dihydrofolate Reductase Inhibitors Showing Antibacterial Effects on Drug-Resistant Escherichia coli Escape Variants. *ACS Chem Biol* **2017,** *12* (7), 1848-1857.